A Finite Element approach to understanding constitutive elasto-plastic, visco-plastic behaviour in lead free micro-electronic BGA structures

Caroline Graham BEng (Hons)

Submitted for the degree of Doctor of Philosophy

Heriot-Watt University

Engineering and Physical Science / Institute of Manufacturing Process and Energy Engineering

December 2015

ABSTRACT

This work investigates the non-linear elasto-plastic and visco-plastic behaviour of lead free solder material and soldered joints. Specifically, Finite Element (FE) tools were used to better understand the deformations within Ball Grid Array solder joints (BGA), and numerical and analytical methods were developed to quantify the identified constituent deformations. FE material models were based on the same empirical constitutive models (elastic, plastic and creep) used in analytical calculations. The current work recognises the large number of factors influencing material behaviour which has led to a wide range of published material properties for near eutectic SnAgCu alloys.

The work discovered that the deformation within the BGA was more complex than is generally assumed in the literature. It was shown that shear deformation of the solder ball could account for less than 5% of total measured displacement in BGA samples. Shear displacement and rotation of the solder balls relative to the substrate are sensitive to the substrate orthotropic properties and substrate geometry (relative to solder volume and array pattern). The FE modelling was used to derive orthotropic FR4 properties independently using published data. An elastic modulus for Sn3.8Ag0.7Cu was measured using homologous temperatures below 0.3. Suggested values of Abaqus-specific creep parameters *m* and *f* (not found in literature) for Sn3.8Ag0.7Cu have been validated with published data.

Basic verification against simple analytical calculations has given a better understanding of the components of overall specimen displacement that is normally missing from empirical validation alone. A combined approach of numerical and analytical modelling of BGAs, and mechanical tests, is recommended to harmonise published work, exploit new material data and for more informed analysis of new configurations.

DEDICATION

This work is dedicated to Professor R.L. Reuben, Dr D. Graham, and Chief Petty Officer A.N. Facey Royal Navy retired. All gentlemen and brilliant Engineers. I would not have embarked on this investigation without their support. Also to Mrs L Facey, Roderick Graham and Duncan Graham who's practical support kept it running.

ACKNOWLEDGEMENTS

With grateful thanks to the great many people who made this work possible: EPSRC for support through a PhD studentship, Dr R Ahmed for a first introduction to Abaqus/CAE, Mrs Carol Toole for a rigorous proof reading, the Institute for Mechanics at TU-Berlin for providing access to their test equipment, staff and technicians at Heriot-Watt University and TU-Berlin, particularly Arion Juritza, Christian Liebold and Guido Harneit for ensuring the success of the practical work.

DECLARATION STATEMENT

(Research Thesis Submission Form should be placed here)

TABLE OF CONTENTS

LISTS OF FIGURES

LISTS OF TABLES

Chapter 1 **Introduction**

This chapter provides an introduction to current electronic packaging demands, and the main challenges to accurately modelling the response of electronic packages under thermo-mechanical load. A brief description is given of BGA assemblies including typical materials, standard constitutive models used to quantify mechanical phenomenon, and the unusual issues with respect to measurement of solder material properties. The chapter also presents the problem statement , an overview of the thesis and the original contributions.

1.1 **General background**

Solder is present inside all electronic devices to provide physical and electrical connections between components. Extensive research into solder behaviour has been driven by increasing demands for reliability and compactness of connections. As electronic components become smaller and smaller, there is a need to minimise the amount of metal used in joining the components, resulting in higher stresses, higher temperatures and larger numbers of joints in any given device. These are the major issues concerning manufacturers along with the challenge of replacing lead based solder with lead free solder.

The push from leaded to unleaded solder, as specified in European directive (RoHS) [2002] and UK regulation (WEEE) [2006], has been prompted by environmental concerns around end of life disposal of electronic packages. Today lead-containing solder is still readily available to purchase in the UK, largely due to the reluctance of electronic manufacturers to move away from this familiar material. The 'hands on' understanding of the behaviour of tin-lead solder extends over two millennia. A precise like for like replacement for all applications has not yet been found but there are a number of substitute materials available to suit particular requirements.

The current work considers the behaviour of tin (Sn) based ternary alloys, containing up to 4% silver (Ag) and up to 1% copper (Cu). In particular, unless otherwise stated, in-house modelling and empirical data refers to Sn3.8Ag0.7Cu (387SnAgCu).

Despite extensive research there is a great deal of ambiguity in the literature about the behaviour of unleaded solder connections within typical Ball Grid Array (BGA) structures under load. Complex 3D loading of solder connections under in-service conditions includes; variations in electrical current densities, repeated temperature fluctuations ranging over 100ºC, and possible shock impact loading may also be experienced in mobile devices. The harsh temperature fluctuations induce mechanical loading (low-cycle thermo-mechanical fatigue) within the connected assembly materials, due to their dissimilar coefficients of thermal expansion (CTE). The severity of these effects can be further exacerbated by any reduction in size of solder joints. Ultimately, cyclic thermo-mechanical loading leads to crack initiation and growth within the joint, and a corresponding reduction in the area of intact connection. This in turn leads to either a failure to conduct an electrical current due to increased electrical resistance, or a mechanical failure due to the reduced area of connection being unable to withstand applied loads.

Classical theory of mechanics cannot be used to reliably predict behaviour due to the complex geometries of micro-electronic assemblies. To improve product designs, manufacturers and researchers have traditionally used expensive and time consuming tests to acquire empirical data. Computer simulations, can offer supplementary, cost effective additional data. From a structural point of view the Finite Element (FE) method has become well established and sophisticated commercially available codes have been developed for a variety of applications. Accurate modelling of the problem requires a sound knowledge of test sample geometry, material condition, and mechanical testing arrangement and procedures.

The object of this work is to improve electronic assembly design advice by using FE analysis to achieve a better understanding of the response of a lead free solder joint when it is subjected to complex mixed mode loading. Current work has been validated with reference to published and in-house experimental measurements and analytical

solutions. Ultimately this work will lead into a simple analytical model to predict unleaded solder behaviour, applicable regardless of variations in material, geometry, strain rate, or load parameters. By gaining a more detailed knowledge of material response under specific conditions, solder joint size can continue to be safely reduced (leading to significant savings in cost, weight, size and environmental considerations) whilst maintaining reliability.

Literature shows that even basic constitutive properties such as Young's Modulus and Poisson's Ratio are not well defined, with a wide range of values quoted for ostensibly similar solder materials. Data from standard bulk tensile tests are not always applicable to micro-scale solder joints because a joint can consist of a small number of anisotropic grains. For this reason much of the published work has been done on representative single solder joint or micro-electronic assemblies.

Determining a constitutive behaviour model by applying classical mechanics theories to solve this multi-physics problem is not straight forward due to the complex micro-electronic package geometries, shifting material properties and loading arrangements. Validations of previously published solutions are highly dependent on data obtained from unique sample geometries and these solutions are not generally applicable to determine solder behaviour with respect to different sample geometries. This work describes an attempt to determine a suitable mechanical behaviour solution not only for an in-house sample design but equally a more general (in particular geometry insensitive) solution. This work has highlighted previously unrecognised mechanisms.

1.2 **Electronics, the BGA and associated assemblies**

The BGA is a popular and effective electronic package designed to meet demands for increased number of connections and functions with cost reduction and miniaturisation. Maximising the number of electrical connections (pin-count) within a very small volume, the BGA arrangement can accommodate tens or hundreds of micro solder connections with both solder diameter and interconnection pitch of around one millimetre or less. Briefly, the layered BGA assembly usually consists of: A PCB

(Printed Circuit Board), copper discs or lands arranged in a regular array across the PCB, and connective solder material bonded to the copper lands. There is no set BGA design and a number of dissimilar materials may be included in the assembly (e.g. solder, copper, nickel, gold, composite PCB, ceramic, moulding plastic, and silicon). The left hand side of Figure 1 shows 0.5mm diameter solder balls in a non-uniform solder array design, attached to the underside of a layered ceramic BGA, right hand side image shows a number of similar ceramic BGA packages in position within a larger array.

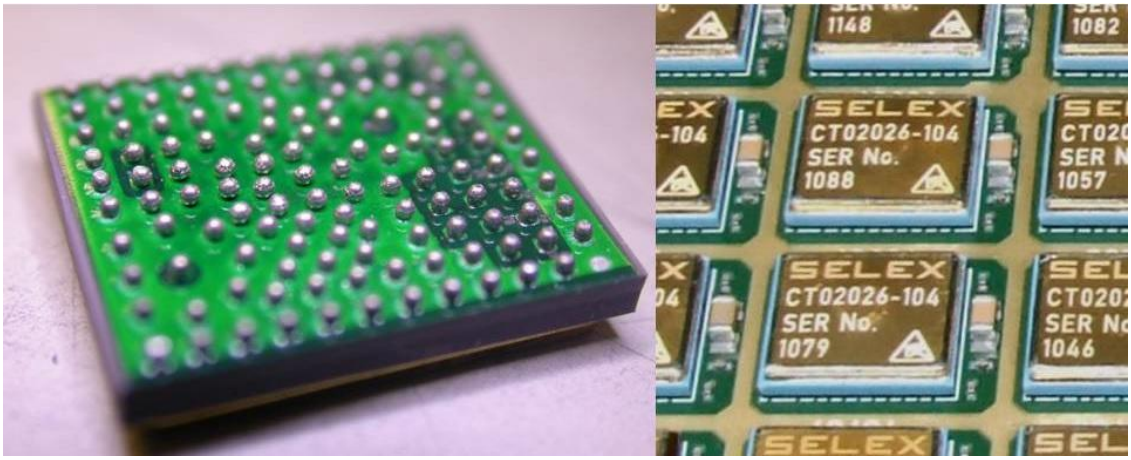

Figure 1: LHS Underside of a ceramic BGA, RHS Hermetically sealed ceramic BGA approximately 12mm^2, images kindly provided by Selex-ES (Edinburgh)

In the solder joint interface, where lead free solder material is bonded to copper, it is usual to apply thin 'flash' finish layers of other metallics to the copper. This is to prevent diffusion of copper land material into the solder. The nickel-gold finish used on in-house BGA samples is a common industry option. The nickel (Ni) layer prevents diffusion of copper but is prone to oxidation. The additional layer of Gold (Au) does not oxidise or degrade, provides a flat surface finish, and has good wettability with tin based solders. Gold quickly dissolves into solder allowing the solder to also bond to the nickel. Au is porous and on its own would not protect copper from dissolution. Inter Metallic Compounds (IMC) of both Nickel and Gold are found in the Inter Metallic Layer (IML), and so 'flash' finish layers of each should be very thin. Under thermal-mechanical load, material migration to the brittle IML continues, leaving behind voids that may act as stress concentrations, potentially contributing to reduced failure stresses.

Electronic components typically fail in the solder joint either through excessive plastic deformation, due to over loading, or thermo-mechanical fatigue. The relatively small solder joints are constrained by larger components such as PCB, resistors, silicon chips, with different coefficients of thermal expansion. Under in-service temperature fluctuations this mismatch induces mechanical strain, and at high homologous temperatures the unleaded solder material will creep. If cyclic loading induces plastic strain, this will result in low cycle fatigue damage.

1.3 **Mechanical phenomena associated with BGA design**

1.3.1 Low cycle fatigue

Low cycle fatigue occurs under high stress loading which causes plastic strains. In solder joints plastic strains are induced by cyclic thermal loads. The simplest empirical Coffin-Manson type equations, see Equation (1), directly relate life-times, N, to the isolated inelastic strain range, ε_p. Isolating plastic strains in solder joints from measurements can be difficult, therefore modelling the entire stress-strain hysteresis loop and identifying discrete constituents, is a pre-requisite of this calculation.

$$\Delta\varepsilon_p = C(N)^{-b} \qquad (1)$$

The Coffin-Manson law does not distinguish between time independent and time dependent plasticity. Coffin [1973], and Kovačević *et al*. [2010] have suggested that during fatigue at high temperatures, taking account of the proportion of strain that is creep can increase the accuracy of life time models by introducing a temperature dependency, half cycle dwell time or frequency modification. Similarly, dependent on load conditions, it may be important to include an elastic strain component and a Basquin type equation may be incorporated, Lee *et al.* [2000].

1.3.2 Time dependent plasticity (creep)

Creep strain is thermally driven and is a particular concern where service temperature with respect to melting temperature of the material, i.e. the homologous temperature is above 0.3. SnAgCu solder at room temperature has a homologous temperature of around 0.6, therefore the creep strain can be a significant proportion of the total strain.

Established laws have been used to relate creep strain rate to stress level and temperature. These laws do not directly account for different microstructural creep mechanisms and a wide range of parameter values have been put forward for SnAgCu solder materials under a variety of test conditions.

Most work has been done on secondary, or steady-state creep and this is reflected in the capabilities of current Finite Element software including Abaqus 6.9 which was used in this study. At the time of writing, Abaqus has announced that the next major release Abaqus 6.14 [2014], will include a significant upgrade to its creep models, including a model which accounts for both primary and secondary creep. Although too late for this work, it illustrates the ongoing interest in this area and the relevance of the current work.

1.4 **Issues with test design and test data for BGAs**

Material modelling is highly dependent on sound measurement of material properties. Laboratory tests may attempt to replicate or accelerate harsh service conditions. It is hoped that analysis of statistically significant empirical data could be used to predict service life of the vulnerable solder connection.

The limitations of material properties obtained from standard bulk tests for micro-structural applications has already been mentioned but there are a number of other concerns surrounding mechanical testing of soft solder material, not least of these being that the literature has given a range of values for a number of key mechanical properties. The origin of some of these inconsistencies has been shown to be in the material condition or test parameter variations. Published sources show many significant parameters and variables which require consideration, further complicating analyses.

For example, thermal history including aging, Zhang *et al*. [2010], microstructure, Keller *et al*. [2011], strain rate, Pang and Xiong [2005], solder geometry, Bhate *et al*. [2008]. There are currently no standard test procedures to address BGA sample preparation and microstructure, sample geometry, test temperature and strain rate.

The current work investigated the effect, under load, of a number of discrete sources of geometric inconsistencies between designs, and has shown sample design has a particular influence on measurements and solder joint displacement. Complex 3D BGA sample geometries result in complex stress distributions and stress concentrations. Stress concentrations may result in low nominal failure stresses. In the literature it is currently assumed that under thermal and/or mechanical fatigue of BGA samples, it is the connecting solder material that undergoes significant inelastic deformation, Che and Pang [2013], Zhang [2013]. Stretching and bending of the PCB component has been previously noted, Lau *et al*. [2014], Darveaux *et al*. [2000], however the current work has shown that the majority of BGA sample deformation is in the low shear stiffness composite. Current FE analysis also showed that less than 5% of the measured BGA shear displacement is strain the solder joint, and that whole sample measurement are unlikely to pick up large changes in solder behaviour. Great care must be taken during analysis of strain data to isolate the solder deformation from adjoining materials.

Shear tests on BGA samples are not suitable for direct measurement of solder mechanical properties. This is as the physical measurement of the whole BGA is not particularly sensitive to solder joint behaviour. In addition to the solder strain, whole BGA measurements include a number of contributing mechanisms as shown in section 3.2.4. The work has also shown that the solder is subjected to complex mixed-mode loading through a non-rigid boundary therefore, even if the solder strain could be extracted from the measurement, it would be difficult to use this data to accurately determine discrete values of solder material elastic moduli.

Published researchers have approximated the thermo-fatigue cycle by applying an equivalent mechanical shear strain at ambient room temperatures to determine joint strength, solder material properties and life-time predictions, Anderson *et al.* [2008]. It should however be noted that at room temperature a true equivalent response may not

be induced, this being due to reduced material recovery at room temperature. The solder material will be subjected to higher stresses and different proportions of constitutive material responses will be generated. Also during the thermo-mechanical stress cycle, strain rate is constantly changing, Ridout *et al.* [2006], this would be complex to simulate under displacement control loading.

1.5 **Problem statement:**

The general requirement is for a more detailed understanding of the response of Sn3.8Ag0.7Cu unleaded solder material under specific thermal and mechanical loading conditions. This knowledge is necessary for the development of a simple analytical solution which describes the various components of deformation, and is applicable to a wide range of sample designs.

1.6 **Overview of thesis**

The thesis is organised as follows;

Chapter 1 Introduction: *This chapter provides an introduction to current electronic packaging demands, and the main challenges to modelling the response of electronic packages under thermo-mechanical load. A brief description is given of BGA assemblies including typical materials, how standard constitutive models may be used to quantify mechanical phenomenon, and the unusual issues with respect to measurement of solder material properties. The chapter also presents the problem statement and overview of the thesis.*

Chapter 2 Literature Review: *This chapter reviews published work that is relevant to state of the art methods of modelling constitutive behaviour in lead free connections. The review examines published data on standard type tests, such as tensile tests, on bulk specimens and summarises the mechanical properties obtained. It then reviews published data on more complex joint type specimens and the mechanical*

properties/constitutive relationships extracted from load - deflection measurements. Finally, the review considers published work on Finite Element analysis of solder joints under mechanical load.

Chapter 3 FEA applied to published force-displacement data: *Using orthotropic material values in the model introduced considerable deformation of the composite, and revealed a previously unreported rotation of the solder joint at the composite/joint interface, shown in Figure 2. Comparison to Park and Lee's published load-displacement data allowed appropriate values of out-of-plane E and G to be derived for the composite FR4 by fitting to the empirical data. Subsequent comparison to other independent data supports using the suggested out-of-plane values in the modelling. Current modelling also showed that the calculated BGA stiffness was not particularly sensitive to the solder modulus value (within bounds of typical published values).*

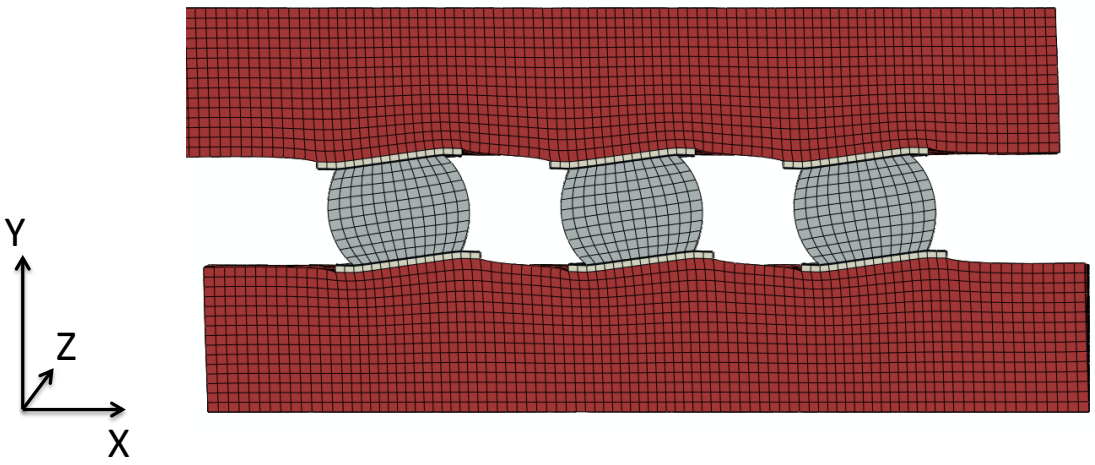

Figure 2: Rotations of Park and Lee [2005]BGA under shear (load applied to top surface), bottom surface fixed, and top surface constrained in Y-direction, material and mesh discretisation shown to clarify deformation, displacement magnification applied

Chapter 4 Parameterisation of the components of sample shear *: Describes an attempt to quantify the composite through thickness shear and the previously unreported solder rotation. The individual components of deflection are isolated using linear FE analyses and basic engineering calculations, with a view to parameterising the FE results in a*

way that they could be applied to more general BGA solder joint samples. Using the suggested method the components of displacement have been calculated for published test-specimens, using design specific correction factors calculated in **Error! Reference source not found.**, *and compared to corresponding published measurements. Comparison of the suggested 'hand' calculations to FEA and published data, Park and Lee [2005], Ghaleeh [2015], confirms that the same components of BGA displacement are present in similar proportions.*

Chapter 5 Discussion and Conclusions*: The current study takes an FE approach towards an improved understanding of the behaviour of BGA samples under thermal and mechanical load, and how empirical data can be used sensibly in the modelling. The conclusions of the work are summarised here, with recommendations for future work and original contributions identified.*

Appendix A Empirical measurement of solder elastic modulus: *Measurements conducted during a collaboration with the Technical University of Berlin.*

Appendix B Comparison with the Pang and Xiong shear lap test: *The proposed analytical solution has been applied here to the Pang and Xiong micro-joint shear lap sample, with comparison to FE calculations and measurements.*

Appendix C Determining correction factors for Park-Lee sample and Ghaleeh sample: *For the wider use of O'Donnell's analytical description of rotation [1960], correction factors have been determined here with respect to the Park and Lee, and Ghaleeh published sample designs.*

Error! Reference source not found. Error! Reference source not found.*: A combined analytical-FEA approach to investigate creep behaviour in unleaded solder bulk material, joints and packages. A comparison of all of the creep modelling menu options available in Abaqus was conducted. Using a range of published creep laws and corresponding parameters, calculations were compared to published measurements. The effect (and potential error) of a parameter set selection was shown.*

1.7 **Contribution to knowledge**

The original contribution was to use numerical modelling to better understand the behaviour of the solder interconnect. It is shown here that experimental whole sample measurements are not sensitive to the proportion that is solder strain, this has not been found in the literature. Using the suggested combined numerical-analytical approach to data analysis, it is likely that legacy experimental data may be unlocked and successful correlation between different data sources will be enabled. The conclusions are;

- Deformation mechanisms in a BGA package under monotonic loading were identified, isolated and quantified. These included the previously unreported solder rotation at the boundary with the FR4 substrate, and the significant shear deformation of the FR4 substrate. Although substrate choice is known to be significant, this work has shown the FR4 to be the largest contributor to sample displacement under shear.

- A new phenomenological, analytical solution, based on classical bending and shear deflection theory, to describe the complex constitutive behaviour of discrete materials within a BGA test sample under monotonic shear load has been proposed. The solution is applicable regardless of geometry but within specified limits. It has been verified against a finite element model of an in-house BGA sample design and a degree of validation has been shown against published measurements.

- The current work has shown that sample response to mechanical load is more complex than previously assumed, with on average of less than 5% of measured sample displacement due to solder strain. This unexpected finding is explained in section 4.4 and with calculated components of displacement shown in Table 16 to Table 19.

- Constituent deformation in BGA samples under mechanical shear is known to be highly dependent on design, and fatigue life correlations based on whole sample deformation will be sensitive to the sample design.

- In Chapter 3, out-of-plane elastic properties for FR4 composite were shown to be essential for accurate prediction of overall deformations.

- Appropriate values of through thickness Young's modulus and shear modulus of FR4 were determined using published data and validated against published test data.

- The elastic modulus of Sn3.8Ag0.7Cu lead free solder was measured over a range of temperatures, including at low homologous temperatures, and reported in **Error! Reference source not found.**. Low homologous temperatures were used in an attempt to induce an isolated elastic response.

- Values for the Abaqus specific creep parameters *m* and *f* were derived from various published creep data, as shown in **Error! Reference source not found.**. No previously published values of these parameters could be found for any lead free solder alloy. Parameters *m* and *f* are specifically required for use with the time hardening creep law and two-layer viscoplasticity creep model in Abaqus/CAE.

Chapter 2 **Literature Review**

This chapter critically reviews the state of the art of mechanical modelling of lead free solder connections. The review examines first the published measurements using standard tests, such as tensile tests on bulk specimens, and summarises the mechanical properties obtained. Published data on more complex joint specimens are then examined and the mechanical properties and constitutive relationships extracted from load - deflection measurements are summarised. Finally, the review considers published work on Finite Element analysis of solder joints. This chapter concludes with the identification of the detailed research questions to be dealt with in the thesis.

2.1 **Published values of lead free solder mechanical properties**

Characterisation tests have reported material elasto-plastic properties including; Young's modulus, elastic limit (yield), Poisson's ratio, plastic hardening parameters, and ultimate tensile strength (UTS). The state of published values for these properties are reviewed below while creep and fatigue parameters are dealt with in section 2.4.

2.1.1 Elastic properties

Young's Modulus, *E*, is a property which, in principle, should be governed by the host metal crystal lattice, in this case, tin. In the practical use of engineering materials, it would normally be expected that *E* should be insensitive to test conditions, material condition, and relatively insensitive to temperature, over service range. Solder service conditions are relatively high in comparison to the melting temperature of the composition. Therefore even at ambient room-temperatures solder response is highly rate dependent, making it is difficult to obtain a universal measurement of true elastic properties.

Table 1 summarises a range of published tests, and values obtained for common SAC (tin, silver, copper) alloys. Given the surprising variety of published values, it was practical for the current study not to be exhaustive in identifying published values but instead to determine the breadth of values, before using FEA with comparison to measurements to determine sensible values.

Where strain rate is noted in the publications, it is assumed that this is set actuator or crosshead speed with respect to initial gauge length. The Müller *et al.* [2010], solder tensile test-piece dimensions were given through personal correspondence. The Zhang *et al.* [2010] values of *E* were taken from a published plot.

As can be seen, values obtained from tensile tests at room temperature (or 25ºC) were mostly from 40 to 60GPa, which might be considered to be a large range for elastic modulus. Values as low as 15 GPa are reported from Fink *et al.*'s tensile test [2008], and 5.4 GPa from Lopez *et al.*'s compressive test, [2010]. Müller *et al.*'s nano indentation tests, [2010], give *E* as high as 69 GPa.

Nguyen's values were the highest found in the literature but were not obtained from direct measurement, having been determined by comparison between FE calculations and measurements of solder displacement under compressive load, using a digital image correlation technique (DIC). Solder mechanical properties were varied in the model, until good agreement was achieved. For his FE calculations Nguyen used isotropic material values for the composite PCB and this is likely to have affected the value of E in a matter which is discussed in detail later. Nguyen *et al.* [2011] used a micro-joint component test to determine values of *E* as high as 97GPa for SAC105, and 86GPa for SAC405.

The main source of the wide range of published *E* values of tin-based solders has been identified as the low melting point, Jalar *et al.* [2007], or rather the high homologous temperature of room temperature tests. This leads to temperature and strain rate sensitivity, and non-linearity from the start of measurements, i.e. even under low stress e.g. Andersson [2008], all of which suggests that something other than *E* is being

measured, possibly creep or plasticity i.e. that solders exhibit very little purely elastic deformation.

Frequently authors publish single material values that are an average of a number of identical tests and some authors report considerable scatter within their own data, e.g. Müller *et al*. [2010], and Andersson *et al*. [2008]. A comprehensive material characterisation study requires an adequate number of identical mechanical tests. Test standards will usually recommend specimen batch sizes, but for full characterisation tens of specimens are required for each test variable/load condition. Lopez tested two samples per condition, Fink tested at least three samples per test condition, and Pang *et al.* [1998] tested three samples per test condition, and other authors do not state their sample numbers. The main measurement concerns are discussed further in the specific section 2.2.5.

Vianco *et al*. [2003] is the only reported measurement of Poisson's ratio that could be found, they used an acoustic technique to obtain their measurement. They do not report any measured values, but suggest a temperature-dependent quadratic function with respective coefficients, determined from his own data. Vianco does not report specific temperature limits for the solution. It is not possible to assess the agreement of Vianco's calculations to measurements, over specific temperature ranges, without published measurements.

Nguyen *et al.* [2011] reported a semi-empirical calculation of Poisson's ratio of 0.42. As in Nguyen *et al.*'s measurement of solder *E*, an optical DIC method was used to measure solder displacement. Material values were then determined by comparison of FE calculations to solder measurements, varying the solder mechanical properties until agreement was achieved. As mentioned above, Nguyen *et al.* used isotropic material values for the composite PCB in his FE model and it is likely this will have influenced his determined value of Poisson's ratio.

Author	Test	Gauge length, width, thickness (mm)	Material composition	Strain rate (s^{-1})	Test temperature (°C)	Sample aging	*E* ,or equivalent (GPa)
Andersson *et al.* 2008	Tensile	30,8,6	Sn4.0Ag0.5Cu	10^{-3}	"room temperature"	100°C, 24hrs	40
Wang *et al.* 2005	Tensile	Not given	SnAgCu; Ag=2 to 4% Cu=0.5 to 1.5%	10^{-3}	25	water quenched, oil quenched, and as cast; 24hrs at 125°C,	31-40
Pang *et al.* 2003	Tensile	15,3∅	Sn3.8Ag0.7Cu	$5.6x10^{-2}$ to $5.6x10^{-4}$	25 to 125	60°C, 24hrs	58-18.8
Zhang *et al.* 2010	Tensile	80,3,0.5	Sn2.0Ag0.5Cu	10^{-3}	25	25°C for 0 days 25°C, 60 Days 125°C, 0 days to 6 months	40 31 25

Table 1: Bulk material test conditions and measured values of E

Table 1 continued

Author	Test	Gauge length, width (mm)	Material composition	Strain rate (s^{-1})	Test temperature (°C)	Sample aging	*E* ,or equivalent (GPa)
Fink *et al*. 2008	Tensile, screw thread	30,5∅	Sn3.0Ag0.5Cu	$5.55x10^{-4}$	room temperature -196 -269	unknown	15.1 32.9 41
Müller *et al*. 2010	Tensile Nano indentation	6.5,1∅ Not applicaple	Sn4.0Ag0.5Cu		room temperature 30 155		60 69 21
Xu *et al.* 2010	Nano indentation	Ball geometry, dimensions not given	Sn3.8Ag0.7Cu	10 1 $1x10^{-1}$ $1x10^{-2}$ $1x10^{-3}$	25		67 62 58 55 51

Table 1 continued

Author	Test	Gauge length, width (mm)	Material composition	Strain rate (s^{-1})	Test temperature (°C)	Sample aging	*E* ,or equivalent (GPa)
Erinç 2007	Nano indentation	1mm thick bulk plate	Sn4.0Ag0.5Cu Sn3.8Ag0.5Cu		room temperature (assumed)		64.1 57.9
Lopez *et al*. 2010	Compression	19,10∅	Sn3.9Ag0.6Cu	4.2 x10^{-5}	-25 to 160	As-cast 150º, 24 hours	5.4 6
Vianco *et al*. 2003	Compression, Dynamic Acoustic						
Nguyen *et al*. 2011	Micro-component compression test	0.53mm interface diameter	Sn4.0Ag0.5Cu Sn1.0Ag0.5Cu		25	100º, 60 minutes	86 97

2.1.2 Plastic properties

Portable devices are likely to be subjected to shock impact or vibration possibly beyond yield (the frequency of which excludes any creep response). Even at relatively rapid loading rates some plastic deformation is expected, and the material should be characterised with due consideration for temperature and applied stress. It has been suggested by Clech, [2005], that under cycled load a kinematic strain hardening component is also required.

Solder materials do not display the distinct linear elastic - plastic behaviour that is typical of other metals. In practice a simple solder tensile test will give non-linear behaviour from low load levels. Andersson *et al.* [2008], reported that plasticity occurs almost immediately, and makes direct measurement of the elastic modulus unreliable, also reporting indistinct yields in several solder alloys under tension. Müller *et al*. [2010] noted the stress-strain behaviour measured under tensile load was unstable, i.e. measured data did not produce a smooth stress-strain curve, as sample displacement measurements fluctuate at each load point. This is not thought to be a real material behaviour but rather a mechanical phenomenon related to the measurement method. A similar effect found in the current measurements, which through comparison of both sets of original data is shown to be more severe, and possible causes have been discussed in **Error! Reference source not found.**.

Some authors report only the yield and/or UTS values of solder, and omit to report other properties such as *E,* Chen *et al.* [2015], Kim et *al*. [2002], Darveaux [2005]. This is probably due to the design requirements of many solder joints, which are more likely to be based on strength than on elastic considerations.

Kanda *et al*. [2012] was the only publication found to report strain hardening parameter values derived from concurrent measurements. Kanda *et al.* provided a temperature sensitive cyclic strain-hardening exponent for a Sn-Ag-Cu micro-joint, useful for cyclic calculations, where it affects the inelastic strain range and calculated lifetimes. The reported temperature and load waveform sensitive values are presumably from Kanda *et al.*'s own displacement controlled shear tests, performed on a single Sn-Ag-Cu micro-

solder joint of height 0.57mm, maximum diameter 0.76mm and with 9mm copper rods attached at each end. Kanda *et al.* showed the influence of hardening on solder constitutive behaviour and the number of thermal cycles to failure. Their suggested values decreased with increasing temperature and coarsening intermetallic compound particles.

Table 2 shows a range of solder yield values from the literature. Again given the disappointing wide range of values, it was practical not to be exhaustive in identifying published values, but instead to determine the breadth of published values and use FEA to determine the effect on calculations. Solder Yield strength is particularly sensitive to temperature and strain rate. Kim et *al.* [2002] reported 0.2% proof stress and the corresponding yield stress values shown in Table 2 were extracted by hand from published plots.

Author	Test	Gauge length, width, thickness (mm)	Material composition	Strain rate (s^{-1})	Test temperature (°C)	Sample aging	σ_{ys} (MPa)
Andersson *et al.* 2008	Tensile	30,8,6	Sn4.0Ag0.5Cu	$1x10^{-3}$	"room temperature"	150°C, 24hrs	33.7
				$1x10^{-4}$			28.8
				$1x10^{-5}$			23
Zhang *et al.* 2010	Tensile	80,3,0.5	Sn2.0Ag0.5Cu	10^{-3}	25	As-cast	29
Kim *et al.* 2002	Tensile	24,4.5,2	Sn3.9Ag0.6Cu	$1x10^{-2}$	Not given	100°C, 30 minutes	28
			Slow cooled $0.012°Cs^{-1}$	$1x10^{-3}$			22
				$1x10^{-4}$			17
			Sn3.9Ag0.6Cu Rapid cooled $8.3°Cs^{-1}$	$1x10^{-2}$			20
				$1x10^{-3}$			30
				$1x10^{-4}$			40

Table 2: Published values of SAC solder yield stress

Table 2 continued

Author	Test	Gauge length, width (mm)	Material composition	Strain rate (s^{-1})	Test temperature (°C)	Sample aging	σ_{ys} (MPa)
Pang *et al.* 2003	Tensile	15,3∅	Sn3.8Ag0.7Cu	$5.6x10^{-2}$ $5.6x10^{-3}$ $5.6x10^{-4}$	25		51.1 40.8 35.1
				$5.6x10^{-2}$ $5.6x10^{-3}$ $5.6x10^{-4}$	75		41.5 33.5 26.0
	FR4 on FR4 micro-joint shear lap sample			$2.6x10^{-2}$ $2.6x10^{-3}$ $2.6x10^{-4}$	75		34.0 24.9 16.9
Bhate *et al.* *2008*	Micro-BGA component shear test		Sn3.8Ag0.7Cu	$2.4x10^{-4}$ $4.02\ x10^{-5}$	25	Not given	41.2 39.0
	Aluminium substrates			$2.4x10^{-5}$ $4.02\ x10^{-6}$			33.1 26.0

Table 2 continued

Author	Test	Gauge length, width (mm)	Material composition	Strain rate (s^{-1})	Test temperature (°C)	Sample aging	σ_{ys} (MPa)
Xu *et al.* 2010	Tensile	15,3∅	Sn3.8Ag0.7Cu	$1x10^{0}$ $1x10^{-1}$ $1x10^{-2}$ $1x10^{-3}$	Not given	60ºC for 24 hours	71.2 60.1 50.2 43.5
	Nono-indentation		Sn3.8Ag0.7Cu	$1x10^{1}$ $1x10^{0}$ $1x10^{-1}$ $1x10^{-2}$ $1x10^{-3}$	Not given		173.3 117.3 83.0 55.5 43.0
			Sn4.0Ag0.5Cu	5.0 $5.0x10^{-1}$ $5.0x10^{-2}$ $5.0x10^{-3}$			129 117.0 88.3 61.7

2.2 **Test configurations used for solder mechanical properties and solder joints**

Given their ubiquity, there is a surprising lack of standard test-piece designs, test configurations or test procedures for solder materials. Rather, the mechanical properties of bulk solder materials have been measured using a range of tests, including tension, compression, torsion, hardness, and dynamic vibration/acoustic methods and in a variety of sizes, test conditions (such as strain rate, temperature and maximum strain) and material conditions (such as composition variation, rate of cooling from molten and subsequent heat treatment). This has resulted in a wide range of values being reported and great difficulty in effectively correlating values from different sources, Dušek *et al.* [2001].

Several current British Standard test methods are available for the characterisation of solder alloys; pull strength test [2007], shear strength [2007], cyclic drop test [2009] cyclic bend test [2009], mechanical shear fatigue [2009], environmental and endurance tests [2014], and temperature cycling [2003]. The pull test and the shear test appear to be quite crude, not representative of common in-service failures, and of limited value to behaviour modelling, but may be used for simple comparisons of one method of assembly to another, Whickham *et al.* [2001]. Interestingly none of the published material properties sourced appeared to have made use of any British Standard test, and therefore the British Standards are of limited use in this study.

There are a number of practical problems to be considered when measuring the properties of a soft tin based alloy material, and these can have an effect on what is perceived to be measured. The major factors, and their effects, are discussed in the following sections, with a view to selecting appropriate values for modelling.

2.2.1 Methods of strain measurement

Accurately measuring the strain in a small specimen can be difficult as strain gauges are not applicable, and it is tempting to measure machine crosshead or grip displacement which may be very inaccurate. Metasch *et al.* [2009] have assessed the effects on tensile tests on bulk samples of 45mm overall sample length (gauge length not published). A linear variable displacement transducer (LVDT) was used to measure

specimen strains directly, and also a second LVDT measured strain taken outside an oven set-up and encompassing the grips. Using the direct sample strain measurement to obtain a corresponding value of E = 41.3GPa, and using the external LVDT measurement to obtain a value of E = 9.7GPa. They showed that considerable extraneous strains can be inadvertently included even in a tensile test where machine stiffness is high and the load path is assumed to be perfectly aligned. This was attributed to effects in the load train, outwith the specimen, and resulted in a reduced value of the apparent Young's modulus. A few other authors have described optical methods used to measure sample strains directly e.g. Pang *et al.* [2003] used a video extensometer, and Müller *et al*. [2010] used a laser extensometer (Young's modulus values are shown in Table 1).

Fink *et al.* [2008], measured the lowest published values of Young's modulus for SnAgCu (SAC) solder (Table 1), and lower than their own measurement for SnPb solder using the same test set-up. Fink *et al.* used a standard extensometer attached directly to one of the largest sample published gauge lengths (30mm). The extensometer was calibrated to ±0.5% of the extensometer gauge length, and Fink *et al*. gave only one example stress-strain plot, which showed non-linear behaviour around 0.5% strain. It is possible that the extracted Young's modulus value is effected by the geometry of the sample, the resolution of the gauge, or even the chemical composition/microstructure as Fink *et al*. reported the condition of their sample material to be 'unknown'.

2.2.2 Specimen clamping arrangements

The method used to grip the soft material can have a significant effect on the test but is often not reported, e.g. Zhang *et al*. [2010]. It is possible that extraneous deformation during manufacture and test set up can occur, particularly for 'dog bone' tensile samples or screw-thread fixing. Shirley and Spelt [2009a] soldered threaded copper rods to the ends of bulk tensile samples to avoid the excessive deformation observed in the threads at elevated temperatures.

Several other methods have been used to circumvent some of these problems. Vianco *et al.* [2003] conducted compression tests on un-aged and aged (at 125°C, for 24 hours) samples at two strain rates ($8.3\times10^{-4}s^{-1}$, $4.2\times10^{-5}s^{-1}$). Compared to other authors, both strain rates could be considered rather slow. They showed that at room temperature, the slower strain rate gave about 25% reduction in yield stress and about 12% reduction in *E*, although their un-aged samples at room temperature were not as significantly affected by strain rate. Vianco *et al.* raised the concern that since typical thermo-mechanical fatigue test strain rates were close to those observed in creep testing, there was a possibility that inelastic deformation was included in the strain measurement. Vianco *et al*.'s compression tests yielded *E* values roughly an order of magnitude lower than other authors. It is unclear how they obtained values of shear modulus, *G*, as using his formula to derive *G* from tensile measurements does not agree with $E/(2(1+\mu))$, a formula used by others to determine a value for elastic modulus from shear tests.

Vianco *et al.* [2003] also used acoustic wave propagation techniques to determine isolated elastic shear and bulk moduli, and Poisson's ratio, at temperature increments within the range of -50 to 200°C.

Alternative tests are not immune to their own particular challenges. Erinç [2007] conducted a number of nanoindentation tests to show the effect of varying test parameters (applied load, strain rate, hold time, repeat loading). For example a hold time of 5 seconds gave some values of *E* above 55GPa, wheras a 50-second hold time reduced *E* to around 40GPa but also reduced scatter of values. Erinç reported the average reduction in *E*, with the increased hold time, to be 22%, and although noting that Poisson's ratio was integral to determining Young's modulus from nanoindentation measurements, he did not state the source of the value he used (0.35). Müller *et al.* [2010] noted that the localised nanoindentation test captures highly localised material properties and measured values are likely to be sensitive to individual grain orientations. They pointed out that this method of measurement showed no significant effect on elastic property values when compared to tensile measurements, but that yield stress values differed by a factor of three. Nanoindentation and acoustic wave propagation

tests do not give a stress-strain curve, therefore much of the non-linear behaviour is not measured.

Zhang *et al*. [2010] used an acoustic method, not to measure mechanical behaviour, but to detect and reject tensile samples containing surface flaws and internal voids larger than 0.4mm. This attention to sample condition has not been found to be reported elsewhere.

2.2.3 Specimen size and scale effects

The stress-strain behaviour of SAC solder has been shown to be highly sensitive to material microstructure and therefore cooling rates, as discussed in section 2.2.8 It can be difficult to replicate solder joint cooling rates, and therefore interconnect microstructures, at a larger scale.

Real BGA solder joints are typically formed of a low number of randomly oriented anisotropic solder grains per interconnect, Gong *et al.* [2007]. Chen *et al.* [2013] observed that no two solder joints showed exactly the same grain orientation pattern, and measured a difference in hardness values of up to 27%, depending on grain orientation. Very small joints (<10μm) may consist nearly entirely of the Intermetallic layer (IML), Bertheau *et al*. [2014]. Bulk sample test data do not account for the effect of diffusion or bonding with material in the IML, Chen et *al.* [2012].

A bulk sample test-piece is normally considered to be a homogeneous material, as it is likely to consist of thousands of discrete grains. When considering larger samples, isotropic behaviour is normally assumed as, due to random grain orientation, the effects of individual grains are assumed to average out. With miniaturisation of test piece, there is a scale limit beyond which material homogeneity of the sample cannot be assumed, nor can its behaviour be assumed to be isotropic.

The sample preparation, stress range and distribution experienced by a bulk sample of uniform design under unidirectional load is very different to that experienced by a solder joint. When compared to interconnects, bulk tests may give quite different material response and so, although it is difficult to determine material mechanical

properties directly from interconnect tests, some micro-solder joint tests are always required.

2.2.4 Testing of soldered component tests and assemblies

Making direct measurement on the solder itself is a challenge because of the very small scales involved. It is common to measure displacements at the package or sub-assembly level and this may involve deformation of substrate materials as well as the solder. There are no standard test procedures for micro-joints and numerous sample designs have been suggested. Samples may be single joint or multiple joint, with solder material bonded to a single phase metallic substrate (e.g. copper) or a complex assembly of several materials, possibly including a composite substrate. Test samples are usually no more than tens of joints (often less) whereas real components can incorporate hundreds of joints. The volume and geometry of the solder material may differ considerably.

The BGA structure under applied load gives rise to non-uniform stress and strain distributions, as has been observed using digital image correlation methods (DIC) of SEM images, Park *et al.* [2007], Chen [2012]. Some have attempted to measure solder deformations directly using sophisticated imaging equipment, Park and Lee [2002], although the utility of such measurements is questionable as the strain distribution within the joint is non-uniform making it difficult to obtain average constitutive information for input into analytical equations. Assuming uniformity in strain distribution during analysis of measurements is at best an approximation.

Joint geometry influences test response, Zhang *et al.* [2014], Qin et al.[2014a], Bhate *et al.* [2006], which can exhibit a complex 3D distribution of forces and bending moments throughout the assembly. The effect of solder joint geometry (concave, convex profiles; volumes, aspect ratios) on test response has been investigated, Kim and Yu [2010].

Park and Lee [2005] tested BGAs in tension, shear and a range of combined loadings. Tension tests have also been conducted on idealised joints, An and Qin [2014], Rosenthal [2010]. The majority of BGA testing appears to be in shear and may consist of an idealised joint, Zhang and Zhang [2011], Keller *et al.* [2011], Kanda *et al.* [2012],

Dusek and Hunt [2006], Déplanque *et al.* [2005], Darveaux [2005] Sundelin *et al*. [2006], Andersson *et al*. [2005] or BGA Shin and Yu [2005], Morris *et al*. [2003].

Park *et al.* [2007] conducted thermal cycling tests on different BGA designs. Using a Digital Image Correlation system (DIC), they observed the anisotropic orientation of the few grains in regular solder joints, and the presence of intermetallic compounds. By comparing strain distribution in a regular joint to that in a joint composed of a single grain, they were able to observe complex strain distribution in the joint with several randomly orientated grains, and how this led (under temperature cycling) to plastic deformation along grain boundaries close to intermetallic precipitates, eventually initiating crack propagation.

Pang *et al.* [2003] reported good agreement between bulk tensile test data and data obtained using a single solder joint/Fr4 assembly shear test, for yield strength and ultimate strength at different strain rates.

Darveaux and Banerji [1991], and Xie and Wang [1998] recognised that substrate material choice and thickness affects the total BGA sample strain and therefore low-cycle fatigue life curves, which are traditionally expressed in terms of strain range. This effect appears to have been largely ignored in the literature with many authors assuming that the global strain measured in BGA samples is mostly due to solder deformation. Although Darveaux *et al*. [2000] did not attempt to assess the contribution of the other assembled materials to whole sample constitutive behaviour, they did experimentally investigate the effect for a number of designs and found that reducing substrate thickness/assembly stiffness increased life by up to 20%.

Darveaux and Banerji [1991] reported that the relative proportion of creep strain to total inelastic strain is dependent on the solder properties and geometry, load cycle range and frequency, coefficient of thermal expansion of all assembled materials, whole component geometry and assembly stiffness. They recognised that assembly geometry, substrate material and substrate thickness have an effect on assembly stiffness, solder strain, and therefore fatigue lifetimes. They made this deduction from their own calculations, made using isotropic composite substrate material properties. As

discussed in Chapter 3, the use of isotropic properties in the calculation will restrict the perceived contribution of substrate material to whole sample displacements. For creep of solder joints within assemblies, Darveaux recognised that the assembly stiffness, as well as load, would determine onset of creep.

Kim, [2007] calculated that FR4 visco-elastic behaviour contributed to component stress relaxation.

Xie and Wang [1998] noted that sample displacement increased by about 10% when increasing composite substrate thickness from 0.45 to 1.6mm, under a 165°C temperature increase, and a 20% increase when changing the substrate material from FR4 to a BT composite. Bismaleimide Triazine is an alternative resin used in composite PCB manufacture for high temperatures and composite PCB containing Bismaleimide Triazine resin is commonly referred to as BT. A higher isotropic modulus was given by Xie and Wang for BT substrate, but no through thickness properties were given for either. Xie and Wang conducted temperature change tests and BT composite has a higher coefficient of thermal expansion than FR4, hence the increased strain observed, despite a higher elastic modulus.

Kariya *et al*. [2004] conducted shear-fatigue tests on BGA samples with a FR4 substrate. They noted that direct measurement of the total sample displacement included deformation in all assembled materials solder (elastic and plastic strain), silicon chip (elastic) and FR4 substrate. They also loaded only the FR4 substrate material in shear to a load about 3.5 times higher than used for the BGA sample, and observed no non-linear behaviour.

Kariya *et al*. [2004] also observed that failure commonly started in the corner solder balls, global location depended on whole sample geometry and solder ball geometry influenced strain within the joint. It is that often found that an interconnect on the outermost row of a BGA will see most accumulated strain and is the site of failure initiation, Darveaux et al. [2000], and Herkommer *et al.* [2010], and Lee *et al.* [2014]. BGA design and material choice will determine the position of maximum thermal or mechanical stresses and strains. The position of greatest mismatch of thermal

expansion or location of a sudden change in assembly stiffness is often under the edge of a chip assembly, Zhang *et al*. [2014], Chandran *et al*. [2000].

In some solder joint tests, authors have used relatively stiff copper or Aluminium substrates, Zhu *et al.* 2014, Huang *et al.* 2011, Maio *et al.* 2010 [REF]. Presumably this is intended to isolate solder deformation through the mitigation of substrate deformation, but of even the relatively stiff metallic substrates are likely to experience some deformation and have some influence over global deformation.

Other non-BGA assembly tests have been conducted, for example Zhang *et al*. [2009] attempted a solder elastic modulus test on an assembly of a thin layer of solder, inserted across the entire width of the mid-line a copper tensile sample. Although the determined elastic modulus values were within the expected range, such a test cannot be compared to other tensile tests without extreme care in consideration of the complex stress state, particularly as the material contraction, due to the Poisson's ratio and transverse to the load direction, is restricted.

Using over simplified isotropic composite substrate material properties, material strains cannot be believed but this work does illustrate a significant influence over package response and importance of suitable consideration of the substrate geometry and material in any analysis.

Presumably in an attempt to isolate solder behaviour from substrate deformation, several authors have conducted mechanical tests on solder joints with novel test-piece designs that incorporate aluminium, Bhate [2008], or copper only substrates; Zhang *et al.* [2009] and An and Qin [2014] tensile tests, Huang *et al*. [2012] fracture toughness, Kanda and Kariya [2012] tensile fatigue, Dušek and Hunt [2006] shear test.

Shrotriya and Sottos [1998] measured FR4 creep behaviour in both the warp and the fill directions (a different material response was shown with direction). A three point bend test was carried out under a combined load of 1MPa for 20 minutes and temperature range of 30 to 155°C and spanning the glass transition temperature of 139°C.

2.2.5 Effect of experimental parameters on measured properties

In addition to test-piece geometry and configuration of test, there are a number of experiential parameters that also influence the measurements. The most important of these are temperature, strain rate, and material history, and these are discussed below.

2.2.6 Temperature effects

Solder joints are required to work at high homologous temperatures. Even at room temperature, lead free solders are typically at a homologous temperature of about 0.6, Jalar *et al.* [2007]. This can increase the induced effect of temperature sensitivity, strain rate sensitivity, plasticity and creep, which makes characterisation of solder elastic properties using traditional test methods difficult.

Several authors, e.g. Pang and Xiong [2005], Vianco *et al.* [2003], Gao *et al.* [2009] and Fink *et al*. [2008], have demonstrated the effect of temperature on measured bulk material properties. Figure 3 shows a range of published Young's modulus values with respect to temperature, although the values shown also cover a range of strain rates and materials. The majority of the data has been obtained at room or elevated temperature, but there are some data for very low temperatures. Although the measured values show considerable scatter, within data sets there is a definite trend for the modulus to reduce with increasing temperature. It may be worth noting that during elevated temperature tests, Lopez *et al.* [2010] were unique in using thermocouples to check for any sample temperature gradients.

Empirical relationships correlating moduli with temperature for unleaded solders, have been put forward by a number of authors e.g. Pang and Xiong [2005], Cheng and Siewert [2003], Qi *et al*. [2006], Kanda and Kariya [2012], and Vianco *et al.* [2003].

Vianco *et al.* [2003] presented data fit formula for elastic moduli, with respect to temperature. This was determined from mechanical tests carried out between -25°C to 160°C. The formula does not exactly agree with source measurements and so a degree of error would likely be introduced with application of this type of data fit formula.

These type of temperature dependent formulae are popular in the literature and have been used by several authors, e.g. Bhatti *et al.* [2006].

It would normally be expected that testing at homologous temperatures below 0.3Tm (about 150°K for SAC solders) would eliminate or reduce creep strain from measurements revealing a true Young's modulus. Tensile measurements by Fink *et al.*, [2008], at temperatures as low as 0.008Tm (about 4°K), continued to show an increase in Young's modulus with a decrease in temperature. They obtained values considerably lower than all other authors and admit the unknown as-received state of their material. Unfortunately Fink omitted to publish the low temperature stress-strain plots.

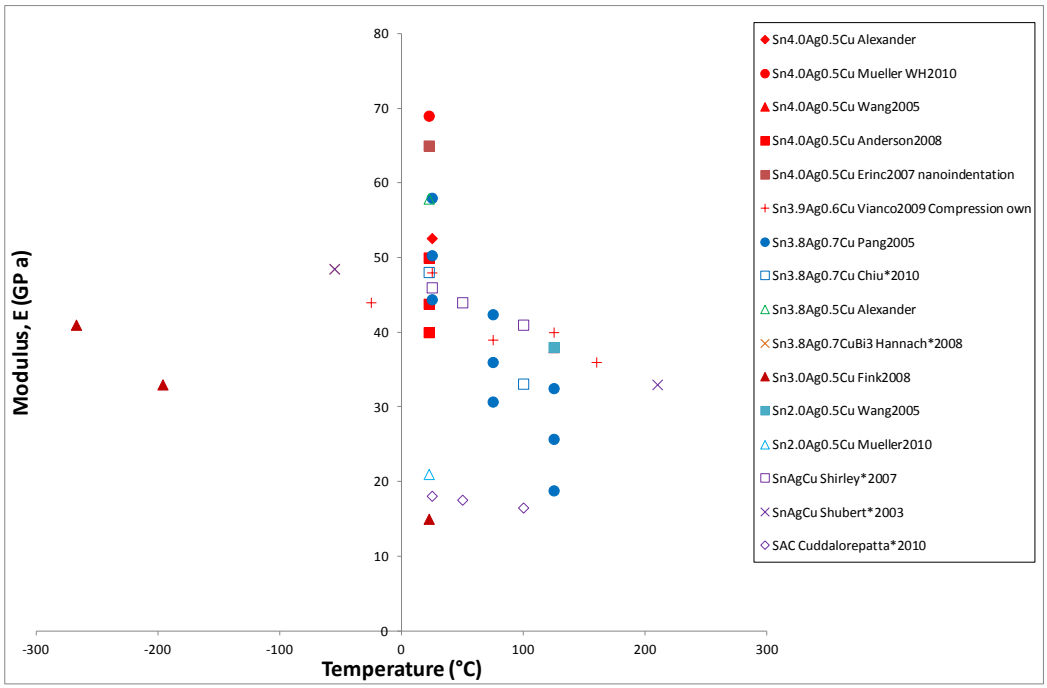

Figure 3: Young's modulus of SnAgCu with respect to temperature.

2.2.7 Strain-rate effects

Data from a number of sources' are summarised in Figure 4.

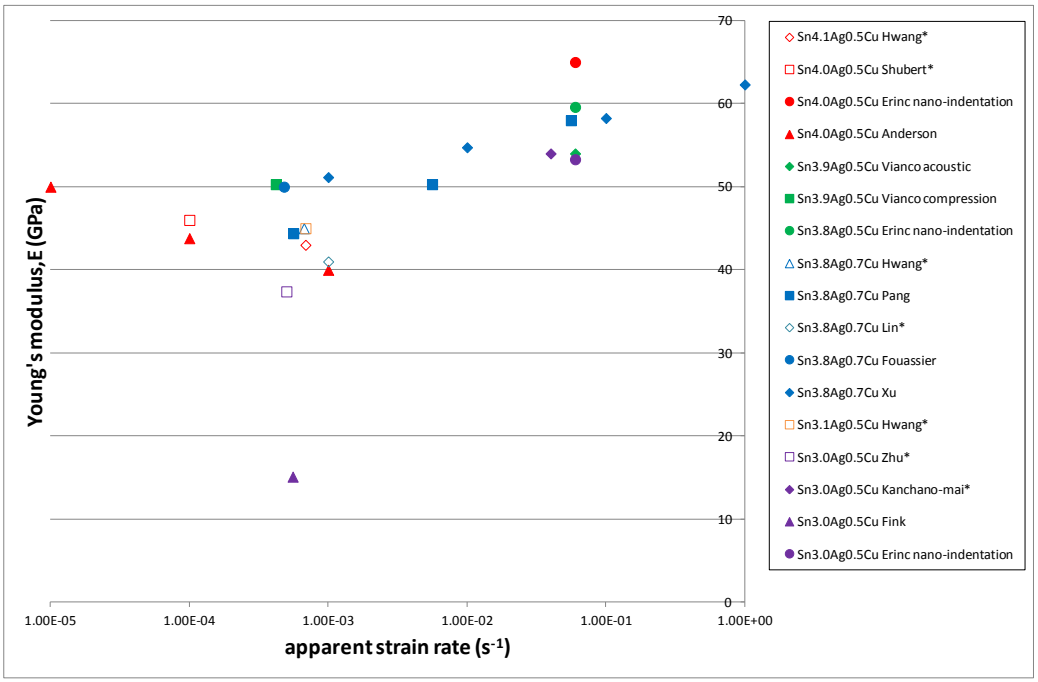

Figure 4: Young's modulus of SnAgCu with respect to apparent strain rate.

Most authors at least report the strain rate at which tests were carried out and many have investigated the sensitivity to strain rate. Despite significant scatter, the data in Figure 4 shows a trend for *E* to increase with increasing apparent strain rate, Zhang *et al.* [2009], and Andersson *et al*. [2008] have suggested that viscoplastic effects predominate at low strain rates and reduce with increasing strain rates, which would mean that higher strain rates would approach more closely the true elastic modulus. However, saturation of the effect is not observed in the data in Figure 4.

Xu *et al.* [2010] compared their his own tensile and nanoindentation measurements of yield stress and showed good agreement for low strain rates. They proposed a strain-rate sensitive empirical relationship for yield stress, for a number of SnAgCu alloys, based on their own empirical data, assuming the yield stress (MPa) to be one third of the value of the measured hardness.

Darveaux [2005] noted in BGA Shear lap tests on SAC solder joints using alloys of similar composition, that at room temperature and fast strain rate, all showed similar maximum shear strength. Only tests at lower strain rates showed a maximum shear strength sensitivity to strain rate. This possibly indicates a material strength dependence on the contribution of creep strain to total strain, also size and distribution density IMC.

This appears to be in line with the findings of others, in that it would normally be expected that testing at very high strain rates (5.6×10^{-2} Pang *et al.* [2003], and $2^{-2}s^{-1}$ for SnPb, Nose *et al*. [2003]) would eliminate or reduce creep strain from measurements revealing a true Young's modulus.

2.2.8 Effect of material composition and condition

There is some debate within the literature as to the significance of small variations in SAC solder chemical composition on material stress-strain behaviour. Wang *et al*., [2005], Kim *et al*., [2002] and Schubert *et al*., [2003], found that small variations led only to little or no difference in Young's modulus. These observations are not surprising, as manufacturer stated tolerances are relatively large, Henkel [2014], i.e. commercial solders marketed with small variations in composition may in fact be the same material.

Yet there is a surprisingly wide scatter in the measured data for what may be considered the same material. This is possibly due to the effect of tolerances in composition on the solidus temperature and ensuing microstructure, the reflow temperature profile, effect of tolerances in composition on the solidus temperature and ensuing microstructure, subsequent aging conditions and test conditions.

The literature shows the popularity of SAC solders of around the generally agreed eutectic composition of Sn3.58±0.05Ag0.96±0.04Cu, Moon and Boettinger [2004], and wider bounds of up to 4% silver and 1% copper. Park *et al*., [2003], used SEM images to show that the microstructure of rapidly cooled Sn3.8Ag0.7Cu is essentially the same as the generally agreed eutectic constution, however the alloy microstructure was found to be unstable under annealing at 210°C.

Mechanical properties of the ternary solder are dependent on the microstructure. The effect of temperature profile during manufacture (reflow temperature and time), cooling profile and aging conditions has been shown to be more significant than small variations in chemical composition, Wang *et al.* [2005]. To establish realistic microstructures in his own bulk tensile samples, Wang *et al*. studied the effect of fabrication technique, including cooling options, carefully assessing chemical composition and microstructure of samples using spectroscopy and inspection of micrographs. They found that was the oil cooled samples had a microstructure that was most like a chip scale package solder joint, and water quenched samples showed the finest grain structure, but all alloys with all cooling rates, showed microstructure coarsening and a decrease in mechanical property values after just 24 hours aging at 125°C, discussed further in section 2.2.9.

2.2.9 Effect of aging and thermal history

High homologous temperatures lead over time, stress, and temperature, to significant reductions in solder mechanical properties and creep resistance occurs. This is due to changes effected within the microstructure and metallurgy (hardening, softening, aging, grain coarsening, recrystallization, growth of intermetallic and voids, Park *et al*. [2003], He *et al.* [2005], Sabri *et al*. [2014], Nguyen and Kim [2015]). Microstructure evolution of solder joints under ambient temperature conditions has been studied separately, Zhang *et al.* [2010], and others have studied the microstructure coarsening effect is further escalated under temperature fluctuations with and without mechanical cycling as experienced in-service, Puttlitz and Stalter [2004], Wang *et al*. [2005], Chen *et al*. [2012]. Böhme and Müller [2007] have suggested a theoretical diffusion-precipitation method to predict coarsening of binary alloys (particularly AgCu) under specified thermal or mechanical load.

Zhang *et al.* [2010] used a bulk test sample (80×3×0.5mm) to study the effect of aging, at a range of temperatures, on mechanical behaviour changes. These changes were found in as little as 24 hours with the degradation continuing for 6 months. The most significant reduction occurred in first 5 days with increased creep strain rates after 10-30 days of aging.

Wang *et al*. [2005] conducted tests on SAC samples with small variations in alloy composition, and subjected to different cooling techniques. They found that thermal history, cooling rate and aging had more effect on mechanical properties than small compositional changes. Mechanical properties were dramatically reduced after aging at 125°C for 24 hours and, after 100hrs, subsequent reduction was minimal.

Again, it is difficult to correlate published empirical material properties, for use in general analysis, because a diverse range of sample designs and test conditions have been used in the reported studies.

2.3 **Solder and joint degradation with time**

The main purpose of modelling of BGA assemblies is to design joints against failure over time. Whereas the modelling requires mechanical properties of constituent components, these are only useful if applied to an appropriate deformation model. The main mechanism of deformation in solder joints is thermo-mechanical fatigue, which is a type of cycle-dependent failure. It is assumed that thermo-mechanical fatigue in solders is usually in the low-cycle range, this means that there is significant plastic deformation within each cycle. Added to high homologous temperatures means that it is also necessary to consider creep strains as well as time-independent plastic strain. This section discusses the literature on creep and fatigue of solders.

2.3.1 Creep properties

Time-dependent plastic-strain in metals can be manifest as additional strain under constant stress (creep), or stress relaxation under constant strain. It can make a significant contribution to inelastic solder strain at high homologous temperatures under applied thermal and/or mechanical load, and can appear under loads too small to cause yield.

Darveaux [1991] recognised the importance of this time dependent material behaviour in solder strain range/fatigue life relationships, particularly at relatively slow strain rates where creep strain that dominates behaviour. Creep and stress relaxation may be described by choosing an appropriate creep model with empirically derived parameters.

Creep strain can be due to a number of microstructural atomic diffusion mechanisms; dislocation creep, boundary diffusion creep, or bulk diffusion creep. Which creep mechanism(s) proliferate depends on the microstructure, load condition, temperature and load level, Pang *et al*. [2004]. There are several standard models which predict steady state creep, e.g. power law, or hyperbolic sine Law, Dieter [1988], as discussed in **Error! Reference source not found.**. These models relate the creep strain rate to temperature and stress level. A number of authors, e.g. Schubert *et al*. [2003], Xiao and Armstrong [2005], Wiese and Wolter [2007], Sidhu *et al.* [2008] have published parameters for these models but these can vary considerably.

To calculate approximate creep strain or strain rate, standard creep models do not directly address underlying creep mechanisms, but rather use material-specific empirical relationships, requiring the determination of unique parameters. Because of the strong stress-strain and temperature-dependence of creep, empirically derived parameters are usually limited to the of stress and temperature over which evaluations are made.

When compared to a power law, a hyperbolic sine model has been shown to give an improved data fit for a larger range of temperatures, stresses and resultant strain rates, Clech [2005]. Application specific refinements of these standard models is common place, for example the use of Anand type temperature compensated creep laws. It has been suggested by Cottrell, [1980], that even when using a temperature compensated creep law, a single set of parameters is not sufficient to describe creep over a wide range of loading conditions because of the different dominant creep mechanisms and resultant strain rates.

The literature contains a range of steady state creep rate laws and wider range of associated parameters for SAC solders. The creep laws of particular interest to the work are those available in the Abaqus FE software, these include all of the types commonly

found in the literature: Garafolo's, and both strain hardening and time hardening power laws. These laws and their effects on the modelling have been discussed in detail in **Error! Reference source not found.**.

There appears to be no standard test-piece design for characterising solder mechanical properties. Flat and round dog-bone, and cylinder designs with a considerable range of sample volumes have been used to measure creep strain rates, following fairly standard creep test procedures e.g. hold at constant load whilst measuring extension over time. The problem of applying bulk solder material properties to analysis of micro-joints has already been noted, however there have been additional concerns that standard steady-state creep models (based on traditional constant high tensile stress) may not adequately represent typical cyclic load in BGA assemblies. Shirley [2009b] was concerned that traditional creep tests are often carried out at high stresses and therefore, together with associated creep models and parameters, were not representative of low fluctuating in-service stresses as experienced in BGAs.

Mechanical testing at the small scale brings associated challenges as discussed in section 2.2.4. Wiese *et al*. [2008] showed that testing the same solder material at bulk and micro-BGA scale gave different empirical creep parameters. To accommodate small solder joints, test sample designs need to include adjoined substrate material(s), in this case Alumina. Darveaux and Banerji [1991] recognised that the assembly stiffness, as well as load, would determine onset of creep and creep rate. Isolation and direct measurement of solder strain from test data is also a concern.

The significance of primary creep of solder, particularly under cycled or stepped load, has been investigated experimentally and theoretically in the literature; Kumar *et al.* [2012], Darveuax and Banerji [1992], Shirley [2009a], [2009b] Darveaux [2005], Déplanque *et al.* [2005].

In typical BGA cyclic load tests, a single cycle may be in the order of a few minutes and many load direction reversals are expected. Shirley's calculations showed for his own monotonic tensile test at 800 seconds, transient creep is nearly three times steady state creep. This disagreement was shown to decrease with time but does not fall to zero.

Any improvement in a steady state creep model accuracy would likely be overshadowed by the error of ignoring transient creep, particularly at load cycles of less than 1000 seconds. A low estimate of creep strain could have a significant effect on predicted fatigue life times, which are based on inelastic strain range.

Déplanque *et al*. [2005] measured creep strain under cyclic load in a novel sample design, consisting of two solder joints in a shaped copper substrate. They found that a steady-state model underestimated the creep strain under cyclic load by up to 24% for SnAgCu material. They also found that previously published primary creep models and parameters did not describe their measurements. They determined that the saturated transient creep strain was related to the steady state creep rate, and reflected this in their creep model, which was adapted from Grivas *et al*. [1979].

Others have published creep models that include a primary creep term with corresponding empirical parameters determined from their own creep strain measurements, Darveuax and Banerji [1992] used SnAg BGA samples with ceramic substrates and Vianco and Rejent [2002], as cited by Lau *et al*. [2003], and are assumed to have used a bulk sample.

Kumar *et al*. [2012] measured the creep strain of a BGA sample with aluminium substrates. He proposed a sophisticated creep model incorporating primary and secondary creep, with an inter-particle spacing term to account for grain microstructure coarsening during thermal aging and thermo-mechanical cycling. He showed the effect of thermal and strain aging, separately, on measurements.

Clech, [2005], suggested that tertiary creep needs to be considered for a full understanding, although it is unlikely to be important in fatigue reliability modelling. Clech showed that applying parameters determined from one data source to predict creep strain for another source can give variable results, highlighting the importance of selecting the correct parameters for a specific application. He showed that, for good agreement to a number of similar measurement sets published by others, a unique set of parameters was required for each measurement source.

Déplanque *et al*., [2005], and Shirley *et al*.,[2008], reported, from analysis of their own experimental data over a range of temperatures, that the total strain of SnPb was less sensitive to transient creep than the SnAgCu. Shubert *et al*. [2003], Déplanque *et al*. [2005] both also found difficulty in applying published creep models and parameters to data from different sources. This suggests that parameter sets are design and load range specific and raises concerns over their broader use in modelling.

2.3.2 Thermo-mechanical fatigue

Since thermo-mechanical fatigue is the main failure mode of solder-joints in BGAs, it could be said that the sole reason for modelling BGA behaviour is to design against fatigue. Although, as well as an empirical cumulative damage law, it is important to have static deformation of the solder joint in order that the cycle dependent behaviour can be established.

Under thermal load which emulates power cycling in service life of electronic devices, assembled materials with dissimilar coefficients of thermal expansion (CTE) exhibit different strains. This will effect a complex strain distribution within the solder, and a very different response than any bulk test. As temperature fluctuates the creep strain (rate) contribution will vary.

Appropriate accelerated thermo-mechanical low cycle fatigue tests can be used to indicate BGA sample reliability under in service power cycling. In order to do this, it is necessary to develop predictive life time relationships, based on empirical parameters determined from the measured number of cycles to failure under specified loading conditions. Mechanical data may not reflect hermetic integrity or conductivity. Accelerated BGA tests have consistently shown either the solder material or the IML (inter metallic layer) to be the failure site, and therefore solder has been the focus of interest, intensified by the continued reduction of solder interconnect size, also reducing solder volume proportionately increases the size of the IML, which responds very differently under fatigue loading.

Original low cycle fatigue life tests were designed to quantify fatigue resistance of the material, not a specific component or design. The test procedures and samples were

designed to minimise influences such as sample geometry and volume. Simple axial tension and/or compression, rotational (torsion) or flexural (bending) loads were applied, rather than any mixed mode loading, to allow straight forward inclusion of data to life-time calculations. The sample designs were mainly straight (or hour-glass) and typically over 100mm in length. These conditions allow deflections to be measured directly, allowing strain control (assuming little change in sample cross section) and allowing stress to be directly related to measured load. Other influences, such as temperature gradients within the sample and corrosive environments, were also kept to a minimum or excluded from tests.

Much work has been published in developing early thermo-mechanical fatigue models, to address some of their limitations in predicting the BGA package fatigue life. Particular factors include frequency, variable load range, temperature range, temperature differences between substrate and component, solder joint geometry and size, Pang *et al*. [1998], Agarwala, [1985], Norris and Landzberg [1969], Vaynman [1989], Kovačević *et al*. [2010], Chai *et al.* [2014]. Many of these model modifications were developed for solid solution, binary leaded solders and should be applied with caution to the ternary, precipitate hardened, lead free solders.

Many variations of empirical fatigue-life models have been proposed, originally developed for high strength engineering materials, and later developed for SnPb solder material, Lee [2000] has categorised these into five types; strain-based (Chai *et al.* [2014]), energy based (Che and Pang [2013]), creep-based (Darveaux and Banerji [1991]), damage based and other, and identified some of their limitations.

No matter how sophisticated the investigator's model of choice, one basic task that cannot be ignored is the requirement to isolate solder strain from micro-joint assembly measurements and to identify adequately elastic, time-dependent and time independent-plastic constituents. Because of the irregular and variable shape of individual solder balls, there is also a difficulty in verifying relevant solder stress from a force measurement.

Published BGA fatigue tests assume that the global or complete package deflections equate to solder deflection, and it is these global measurements that form the basis of life-time relationships, Qin *et al.* [2014a]. The appropriateness of directly equating calculated solder strain to whole sample strain-fatigue relationships is a cause for concern, Darveaux and Banerji [1991].

Darveaux and Banerji [1991] applied a cyclic thermal load to micro-component assemblies with a range of temperature differences and frequencies. He recognised that with increasing average temperature over load cycle, slower ramp rates and longer dwell times, a larger proportion of the strain is due to creep. They state that in order to determine the true solder response a knowledge of both solder material properties and assembly stiffness is required, and furthermore that any suggested empirical behaviour relationship is limited to specific test set-up and load conditions.

The simplest Coffin-Manson criterion does not consider temperature, it is unclear if high temperature modifications are generally acceptable. Similarly it is unclear how creep affects the creep-fatigue relationship, particularly whether it can simply be assumed that creep is part of the total inelastic strain and if the relationship is unchanged by the additional consideration of reversed or cycled load.

In temperature cycling tests, some authors have suggested replacing the plastic strain term in lifetime relationships with the applied temperature, Norris and Landzberg [1969], and Goldman [1969], as cited by Dauksher [2008]. This approach is not applicable in analysis of mechanical fatigue tests.

Unleaded material joints visually look quite different from leaded joints, and have a rough irregular appearance. It is common for fatigue cracks to form at the material surface co-incident with intrusions as small as 1μm, which could be formed during movement of slip bands.

2.4 **Numerical analysis applied to mechanics of solder joints**

Finite Element Analysis (FEA) has been widely used to analyse the behaviour and reliability of solder joint assemblies. This is an appropriate use of powerful computing facilities and sophisticated numerical modelling software, given the complex BGA sample geometries, number of material interfaces and complex strain distribution. It has been used to determine effective solder deflections, or maximum equivalent inelastic strain, which can then be input into a Coffin-Manson type strain-fatigue life relationship, e.g. Kariya *et al*. [2004], Darveaux and Banerji [1991]. It is, however, crucial for validation purposes that FE models suitability represent reality, incorporating appropriate constitutive models and relevant material properties. Likewise, this can require FE to also provide supporting data through the simulation of physical tests and interpretation of empirical data.

Unfortunately published FE analyses of solder joint assemblies often lack full details regarding material properties, and it is not uncommon for authors to omit details of some or all material property sources and/or original test parameters, Modi *et al.* [2005], Tee *et al.* [2003]. This lack of reported sources raises concerns for the suitability of material properties used, particularly when given the unusually large range of reported solder material properties, and direct relationship between this and specific solder material condition/thermal history.

Furthermore the results of FE are often presented without evidence of adequate mesh refinement and quality checks. This is illustrated by a lack of uniformity of mesh and/or mesh refinement in areas of high stress. The absence of a modelling methodology, including descriptions of element type, load and boundary conditions, makes it difficult to reproduce these models or conduct independent verification.

Generally during FEA, the polycrystalline solder material is assumed to be isotropic. There are a few researchers who have used FE modelling to show the effect of grain orientation and overall anisotropy on creep and reliability under thermal mechanical fatigue loading conditions, Gong *et al.* [2007], Liu *et al.* [2009], Ubachs *et al*. [2007], Park *et al*. [2007].

For BGAs and other micro-joint assemblies, FEA has been used to study the effect of joint geometry, Bhate *et al*. [2006], [2008], Kim and Yu [2010], Zhang *et al*. [2014], Qin *et al*. [2014a], Lau [2014] and to show the effect of solder joint array pattern on stress distribution, possibly leading to a failure site prediction, Lau *et al*. [2012], Chaillot *et al*. [2007], Che *et al.* [2005], Modi *et al*. [2005].

FE modelling has also proven to be useful in the stress analysis of the whole BGA or larger assembly, for example Ma and Lee [2013] have shown the influence of board design on BGA joint failure location. Kim and Hwang [2015] showed the solder joint stresses were sensitive to array location, board design and in particular the component size. They showed the effectiveness of under fill to eliminate joint failure in lab tests. Often, an interconnect at the extreme corners or on the outermost row of a BGA will see most accumulated strain and is a common site of failure, Darveaux *et al*. [2000], and Herkommer *et al*. [2010]. Where the substrate and components, joined by solder, are of different size, stiffness, and/or thermal coefficient of expansion, this sets up a strain mismatch particularly under the edge of the smaller substrate.

Lau *et al.* [2012] suggested that inadvertent, design induced, board level temperature gradients can cause residual stresses to be setup during uneven cooling of the solder joint. They used experiments and FEA to show that joint array pattern, rather than joint number, affected the thermal gradients at board level during cooling. Their FEA showed that the thermal gradients lead to location dependent residual stress patterns in the joints, suggesting that joints with the highest residual stress would be the most likely to fail. Lau *et al*. also used FEA to show that, by altering the array pattern, critical joint locations could be altered and stress levels could be reduced by up to 25%. Bhatti *et al.* [2006] used FEA and experimental data to show that a thermal preload could change the position of the critical joint location. Qin *et al*. [2015] showed good agreement between empirical data and FE simulation in the prediction of position of solder joint failures in BGAs.

Lau *et al.* [2014] used FE to investigate the effect of the solder profile on the reliability of BGA samples. They considered a variety of solder shapes including cylinders, convex 'barrel' shapes and concave profiles with different aspect ratios, and two

isotropic substrates, a thin, low modulus polyimide and a thicker, stiffer FR4. They showed that the solder joint shape affected reliability predictions, and that BGA response was also affected by substrate choice. For example, the predicted failure joint location varied with solder profile, but not by changing the substrate from a polyimide to the stiffer FR4 substrate.

Relatively little has been published on BGA failures where components other than the solder balls experience cracking. Ma *et al.* [2011] investigated failures due to crack growth in the epoxy matrix of the laminate composite, under critical solder joints. Localised failure occurring in the epoxy matrix is known as pad cratering. Published studies of ceramic or plastic component BGAs have highlighted concerns for the integrity of the PCB epoxy matrix under the critical joints.

Of the above studies of board design influence on solder joint reliability most did not state the mechanical properties used in the FEA. Only Lau *et al*. [2012] reported the use orthotropic FR4 properties, although Qin *et al*. [2015] used a (very low) isotropic value of 6.2GPa.

The importance of whole assembly design, and resulting overall stiffness, to both fatigue life and stress relaxation was stressed some time ago, Darveaux and Banerji [1991]. Despite this, many authors using FEA to model micro-interconnect assemblies have assumed isotropic elastic or thermo-elastic properties for the FR4 composite, e.g. Lau *et al*. [2014], Chaillot *et al.* [2007], Ridout *et al.* [2006]. Others have used a wide range of orthotropic values, Lau *et al*. [2012], Williams *et al*. [2010], Liu *et al*. [2009]. Chaillot *et al*. used isotropic elastic properties, but in-plane and out-of-plane coefficients of thermal expansion (CTE). Dudek *et al.* [2009] included orthotropic properties for the FR4 composite and calculated the effect of temperature gradients on warpage of the substrate.

The use of constitutive models determined by others is common place in published FE studies of solder joint behaviour, despite numerous reports citing difficulties in modelling using empirical parameters determined from measurements by others (particularly when considering creep or fatigue of BGA assemblies); Lau [2003] used

Vianco and Rejent 's [2002] steady state creep parameters to model a FR4-on-FR4 BGA sample, and Shirley *et al.* [2008] used Vianco and Rejent [2002] and Déplanque *et al*. [2005]. Both Lau and Shirley *et al*., used isotropic FR4 material values in their FE analyses.

Darveaux and Banerji, [1991], [1992], used FEA to determine the assembly stiffness of a BGA sample under thermal load. This was then used to determine solder creep strain and time-independent strain, prior to reliability analysis. Two substrate materials were considered, an aluminium oxide substrate and a polyimide, and assembly stiffness increased with increased substrate modulus. Isotropic material properties where used for both composites. Déplanque *et al*. [2005], was concerned that creep models readily available in FE codes assume a constant load. In FEA, most authors have used standard secondary creep models. As discussed in section 2.3.1, where authors have used models which identify primary and secondary creep, the proportion of primary creep has been shown to be significant. Shirley *et al.* [2008] used an FE model to study the effect of omitting plastic and primary creep strain from the constitutive model. The model described a micro-joint sandwich of Silicate, solder and FR4. Shirley used isotropic FR4 material values.

The use of an epoxy-fibre reinforced composite may also require a temperature dependent visco-elastic term to be considered. Stresses are probably too low to require a composite damage model. For detailed modelling of cyclic load, the effect of load reversal on should be considered and measured values of the effect of load reversal on Sn3.8Ag0.7Cu (hardening), and FR4 epoxy-FR composite used. The influence of the metallic pads and their metallic finishes were shown to be insignificant within the bounds of the current work.

Shirley *et al.* [2008] used an FE model to study the effect of omitting plastic strain and primary creep strain, without physical tests. The model described a micro-joint sandwich of Silicate, solder and FR4. Shirley used isotropic FR4 material values. He concluded, in this load case, that plastic strain was insignificant but omitting primary creep led to large errors, up to 8% in the Sn3.8Ag0.7Cu sample. He also showed that the difference varied dependent on applied temperature and ramp rate.

FE has been used in a variety of applications but often in a supporting role and so full details of were often not reported. Finite Element Modelling approaches or methodologies have been quite diverse and the quality of calculations difficult to assess. Despite the large number of studies involving FEA of solder joints, this has not led to agreement on a suitable design approach. This is probably because most authors are concerned with solving a specific problem rather than trying to build an overall framework for BGA design.

2.5 **Summary and identification of thesis topic**

The current work is concerned with developing suitable numerical modelling methods for micro-electronic component assemblies, containing SnAgCu lead free solder, under thermal and mechanical load. The appropriate use of the extensive range of material values available is fundamental to the success of interconnect modelling, whether these values are measured or theoretical.

In this section, published material properties and other constitutive parameters have been collated and their effects have been considered. Published work on Finite Element analysis of solder joints has also been reviewed. The intention was to isolate useful published material properties and constitutive models for use in the current numerical modelling.

The literature review has revealed a choice of material behaviour models and a wide range of published mechanical properties. A number of authors have demonstrated that these variations in empirical data are due to test conditions and to a lesser extent small changes in chemical composition. Interpreting this empirical data in a form that can be used requires an understanding of its limits and range of applicability to; complex geometries, complex loading conditions (e.g. thermo-mechanical), and non linear behaviour.

Published FEA has previously been used to determine assembly stiffness of micro-joint samples, and isolate solder deformations particularly equivalent creep strain under

fatigue load. Nevertheless, there may be many, possibly as yet unidentified, contributors to non-linearity, particularly when considering such a diverse range of tests and test conditions.

Yet no study could be found to clearly quantify constituent deformation mechanisms in all assembled materials.

This is particularly of concern in BGA samples, where published measurements and FEA has shown the significance of whole sample stiffness. In spite of that measured displacements have often been directly attributed to the solder material, possibly as the majority of the measured inelastic strain is assumed to be in the solder material. Hence the enduring limitation in Coffin-Manson type relationships is their reliance on bench-mark empirical fatigue data from a specific package geometry.

The requirement is for a simple analytical solution accounting for all mechanical phenomenon within the BGA assembly, applicable regardless of geometry. The intention is to use Finite Element Analysis as a research tool towards improved understanding of BGA behaviour and, in conjunction with published measurements, to provide a comparison for current analytical calculations. For the initial development of modelling methodology, typical material values used in previously published analysis were adopted, it was hoped that comparison to measurements with consideration for the measured test parameters, would indicate the correctness of this approach.

Most of the calculations in the current work have been linear-elastic and the models used reflect this. Chapter 4 and **Error! Reference source not found.** describe in detail the published constitutive models that have been considered, and ultimately how the selected models have been used during the current work.

Chapter 3 **FEA applied to published force-displacement data**

This chapter develops the modelling approach and applies it to published experimental data. Because of the difficulty in finding well-characterised data, only two sources have been used, Park and Lee [2005] and Ghaleeh [2015]: First FEA is used to show the critical effect of the composite FR4 out-of-plane properties, Section 3.2.3. Next appropriate out-of-plane values of E and G are determined through comparison with Park and Lee [2005] shear and tensile data, Section 3.3.1. These values are then shown to be appropriate through application to independent experimental data from similar tests, including Ghaleeh [2015], Section 3.4. Finally, having substantiated the FE modelling and the material properties used, it was confirmed that the components of displacements of a BGA under shear are real effects, shown in Figure 2 and described in Section 3.2.4.

3.1 **Description of the data sets used**

Park and Lee describe numerous tests on a 9 ball BGA sample. Specimens were loaded monotonically to destruction in pure shear (90°) and uniaxial tension (0°), and in fatigue under pure and combined loading (0°, 27°, 45°, 63°, and 90°). Ghaleeh [2015] also carried out numerous tests, some of which are referred to later in this thesis. In this chapter, however, only some of his pure shear data is used. Data from the Park and Lee shear and tensile tests were used to develop an FE model of the specimen, establish the modelling approach and determine suitable material properties, whereas their combined loading and Ghaleeh's shear loading were used as a kind of validation of the approach and properties.

The initial analysis highlighted the sensitivity of the whole sample behaviour to the substrate through thickness properties. These are properties commonly ignored in published work or, where presented, show considerable inter-investigator disagreement.

Although similar to the Park-Lee test, Ghaleeh's sample differed in the following ways;

- Park-Lee used Sn3.5Ag0.75Cu, but Ghaleeh used Sn3.8Ag0.7Cu, although, within the limits of the manufacturer's stated tolerances, both may be considered to be the same material.
- The Park-Lee test piece geometry, as detailed in Figure 6 uses 9 solder balls, whereas Ghaleeh's uses 4.
- The loading method, as detailed in Section 3.2.1, differed, in that the Park-Lee shear loaded test-piece introduced a shear force in the FR4 substrate.
- The Park-Lee test piece used a thinner FR4 substrate, as detailed in Table 3. Ghaleeh used a 1.6mm thick FR4 substrate.
- The top and bottom substrates of the Park-Lee sample were of different dimensions, as detailed in Table 3.
- The materials coated over the copper pads, as detailed in Table 3, differ from those employed in the Ghaleeh sample.
- The displacement rate for the Park and Lee test was 0.002 mm/s and Ghaleeh tests used an average 0.0247mm/s.

The displacement rate for the Park and Lee test was 0.002 mm/s and Ghaleeh tests used an average 0.0247mm/s.

Additional support for the modelling assumptions was sought by comparing FEA of a shear lap test to published data of Pang and Xiong [2003]. The calculations showed sensitivity to FR4 through thickness properties, but the not insignificant substrate bending coupled with the incomplete description of the test set-up (grip and load) limited the usefulness of this data to the current work, see **Error! Reference source not found.**.

3.2 **Modelling of the Park-Lee shear and tension experiments**

The Park-Lee experiments were chosen for this part of the study because of the good description of the BGA packaged test-piece and the wide range of monotonically loaded force-displacement measurements. In this part of the study only the tensile and shear data will be used, corresponding to test conditions (a) and (e) shown in Figure 5.

Later other loading condition data will be used as part of the independent validation of the FE modelling. The BGA samples were adhered to steel grips using cyanoacrylate using a rigid alignment method. During the test one grip was attached to the actuator and one grip was fixed.

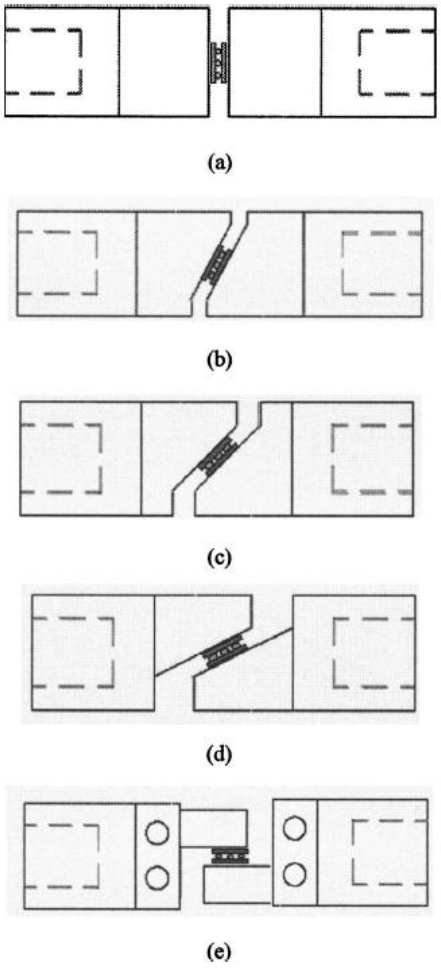

Fig. 5 Test grip configurations. Loading angle of each specimen is (*a*) 0 deg (pure tension), (*b*) 27 deg, (*c*) 45 deg, (*d*) 63 deg, (*e*) 90 deg (pure shear)

Figure 5: Sketch of Park and Lee test arrangements, taken from Park and Lee [2005]

3.2.1 FE model parameters; geometry, materials and boundary conditions

All FEA was carried out using the Abaqus package. An in-depth 2D study of modelling techniques including element types, mesh refinement, and geometric idealisation was conducted, before progressing to the 3D study reported here. The 2D study was used to identify and assess; stress values and distributions, geometry approximations, smoothing singularities where required, meshing techniques, and suitability of element type based on observed behaviour. The original mesh quality checks study is summarised in Section 3.2.2.

The element C3D8, a fully integrated, first order or linear continuum element, was chosen so as to give continuity with a previous in-house 3D study, Graham [2013]. The C3D8 element was shown to capture bending and shear deformations adequately and with computational economy, provided that an appropriate mesh density was chosen to accommodate the wide range of material thicknesses.

To reduce unnecessary computational effort, a plane of symmetry, in the x-y plane, was used to model one half of the Park-Lee 9-ball test-piece, as shown in Figure 6. Figure 6 also shows the discrete materials used as assembled in the model, differentiated by colour. The model consisted of a single part that was partitioned into the individual material components allowing a continuous mesh to be applied. The dimensions used in the FEA model are shown in Table 3. The copper pads were modelled as plated with nickel with a gold flash on the exposed surface. The solder mask has been omitted from the FE model as it is assumed not to contribute to the system response, other than to define the solder material interface diameter.

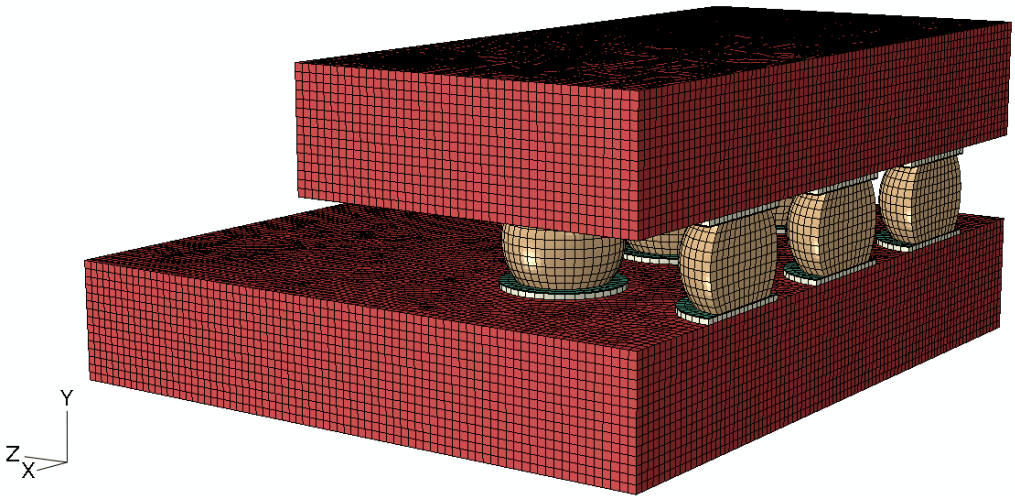

Figure 6: Model of one half of Park-Lee test specimen; discretisation of materials and mesh

Material	**Dimensions (mm)**		
	X	Y	Z
FR4 Substrate: Top Bottom	4.8 4.8	0.8 0.8	4.8 8.54
Gold	0.787Ø	$1x10^{-3}$	
Nickel	0.787Ø	$5x10^{-3}$	
Copper	0.787Ø, Pitch 1.27	$35x10^{-3}$	
Sn3.5Ag0.75Cu Solder	0.76 Ø mid height	0.52	Solder mask opening 0.584 Ø

Table 3: Park-Lee Model Dimensions

All of the material properties used in the Abaqus model are shown in Table 4. The copper, nickel, gold and solder were considered to be elastic - perfectly plastic with a single yield stress given for each. Initially the FR4 substrate material was modelled to be linear elastic and isotropic as in previous studies (e.g. Lau [2014], Li [2007], Chen [2006], Lau [2001], Dušek *et al*. [2001]) and no yield was considered. No material temperature dependencies were considered.

The following loads and boundary conditions were applied to the FE model to replicate the test set up described by Park and Lee;

- The lower FR4 substrate was fixed on the bottom surface only.
- A Multi Point Constraint (MPC) was used at the top surface to spread the load, which was applied at a single node, in accordance with the Park-Lee tension and shear tests, respectively.
- A monotonically increasing load was applied and the elastic-perfectly plastic model was run until the maximum load was reached.

	Material Properties				
	FR4 Glass-reinforced epoxy laminate [Lau, 2001]	Copper [Kayelaby. NPL, 2014]	Nickel [Lau, 2001]	Gold [Kayelaby .NPL, 2014]	Sn38Ag0.7Cu Solder [Puttlitz and Stalter, 2004]
Young's Modulus (MPa)	22,000	129,800	205,000	78,000	45,950
Poisson's ratio	0.28	0.343	0.31	0.44	0.4
Yield Stress (MPa)	---	70	103	207	47.1

Table 4: Material properties used in preliminary FE model of BGA

In the original Park-Lee tests, load was applied through the extreme surfaces of the substrate in several directions discretely, and measurements to failure in shear and tension published.

In the model of the Park-Lee tension test, the top surface of the upper substrate was constrained using a MPC to move as one in the Y direction. This is to approximate the Park-Lee method of holding the test sample. A monotonic tension load was applied to a single node on the upper substrate top surface. The applied load was the equivalent of applying 300N to a complete 9 ball test-piece and the model was run to its limit load.

In the Park-Lee shear test, the top surface of the upper substrate was constrained using an MPC to move as one in the X direction and a Y constraint to model the rigid test machine. A monotonic shear load was applied to a single node on the top surface of the upper substrate. The applied load was the equivalent of applying a 100N load to a complete 9 ball test-piece. This model was also run to its limit load.

3.2.2 Mesh quality checks

The accuracy of FE analysis is dependent on a number of things including the quality of the mesh and element type used. The mesh quality checks conducted during the work are discussed here. Other sensitivities of the method are discussed in **Error! Reference source not found.** along with the reasons for choosing FEA for this type of work.

Abaqus CAE conducts a number of automated mesh quality checks. If a model fails these automated checks then the calculation will not run. It should be noted that it is very possible to generate a model that passes these automated checks and does run, but that is not optimum or even suitable for the problem in hand. There are a number of other mesh considerations, or metrics, not addressed by the automated Abaqus quality checks. The operator must apply his or her own checks to ensure the mesh is entirely appropriate.

The Abaqus automated checks refer to element shape (angle of element sides also called skew, and to what extent are element sides parallel also called jacobian). If a model is less than ideal on these considerations, automated advice warnings are issued but the

model will still run. It is then for the operator to decide in the pre-processing stage what is acceptable for mesh density, mesh pattern, element aspect ratio, element type, and how to deal with any stress concentration. This should be done with particular attention to the specific problem in hand including geometry, load, and key areas of interest etc.

To study the perceived benefits of mesh refinement compared to computing effort, a 2D plain strain model was used. A total of seven models were run using the following continuum element considerations: first order (linear shape function) reduced integration elements both coarse and finer mesh, first order full integration both coarse and finer mesh, incompatible modes (with internal bending degrees of freedom, an economic element) both coarse and finer mesh, and a coarse mesh of second order (quadratic shape function) elements with reduced integration. Comparison of the constitutive results showed that the coarse mesh was sufficiently converged. Provided a mesh has adequately converged, a mesh should not be overly dense for efficient computing effort. All of the models ran successfully and showed good agreement for limit load (to about 6%), apart from the incompatible modes element model which terminated in the linear region and below the non-linear region peak load extracted from the other models. Standard 1st and 2nd order elements with coarse or fine mesh predict a load limit to within about 6%. Incompatible mode elements coped poorly with extensive plasticity and did not predict the expected limit load. This correlates to published recommendations in the Abaqus Getting Started manual to use fully integrated, first order solid elements in elastic-plastic simulations. The study was then repeated using both 2D plane stress and 3D element types. There was very good agreement between the data extracted from the models using the 2D element types. Although as might be expected, both of the 2D models (plane strain and plane stress) appeared to predict a stiffer response than the 3D element model.

Next a 2D study was made of the meshing technique. When meshing every effort should be made to achieve square elements as irregular element shapes are likely to behave inconsistently. This is of particular concern in locations of interest or high stress. To optimise the FE results, following the comparison of meshing techniques, it was decided to use second order elements, with free, advancing front, using mapped

mesh where selected in the 2D study. The equivalent mesh pattern in 3D required Hex (also known as brick shaped elements) structured or swept with advancing front mapped mesh.

3.2.3 Effect of substrate properties

The overall specimen displacement responses, to both the tensile and the shear loads, for the Park-Lee physical experiment were extracted manually from their published plots and these are shown in Figure (7). Values extracted from Park-Lee published plots are shown in solid markers and a solid line shows progression of the constitutive values. Values extracted from FEA are shown by unfilled markers and a broken line. The good agreement between calculated and experimental limit loads in (7) suggests that the solder fails in plastic shear with little or no contribution from the composite substrate. However, there is obviously a severe discrepancy between the test and model elastic displacements which would, for example, give serious problems in using an energy method for describing fatigue properties. A possible reason for the discrepancy between measured and calculated displacements, given that these originate in the elastic region, is that one or more model elastic modulus is incorrect.

As pointed out above, the shear load was applied not only to the solder joint but also to the substrate in the Park-Lee tests. The substrate was made of FR4, a Glass (Fibre) Reinforced Plastic (GRP-Epoxy). Isotropic material properties were used initially in the FE calculation because, as in other published FEA studies, Lau [2014], Li [2007], Chen [2006], Lau [2001], the substrate was not considered an area of interest and it was assumed that its method of loading was quite straightforward and its anticipated response quite unremarkable.

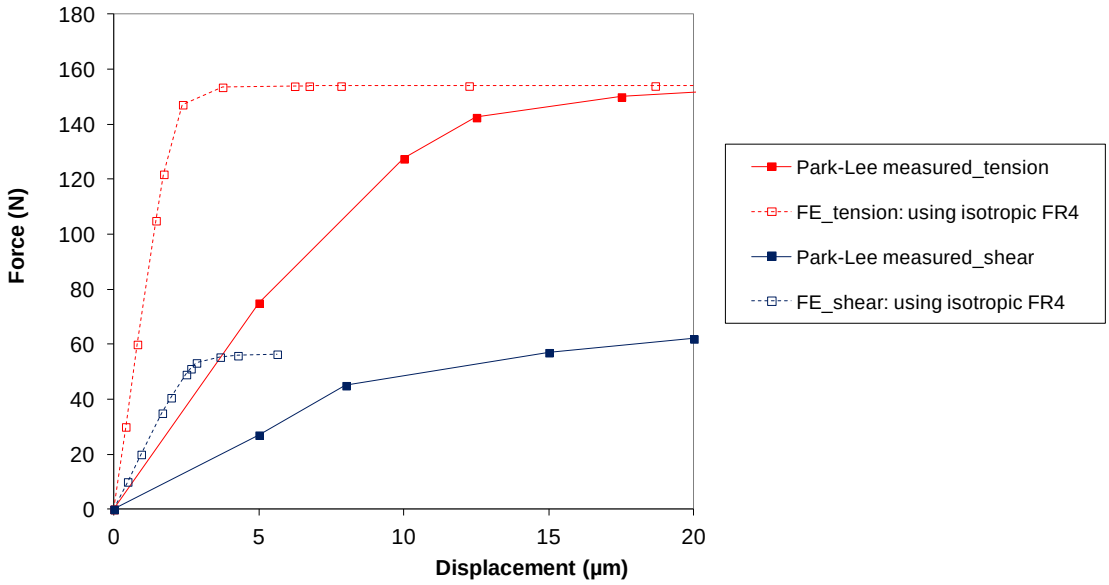

Figure 7: Monotonic loading in shear and tension for Park-Lee specimen, measured data points extracted manually from an enlarged copy of a published plot

By their nature, composites are strong and stiff in-plane but can have low Young's modulus (*E*) and shear modulus (*G*) in the through-thickness direction. Figure 8 shows a schematic diagram of a 0°/90° fibre-reinforced laminate, in which the usual mechanical loading direction is to put some of the fibres in tension (σ_{xx} or σ_{zz}), reflecting the main mechanical function in circuit boards, which is to provide bending stiffness. In the Park-Lee test (and many other solder tests) the load was not applied so as to put the fibres in direct tension, but was either through-thickness shear (σ_{yx} or σ_{yz}) or direct stress (σ_{yy}). The deformations under these loadings will be sensitive to the through-thickness properties, which are difficult to measure and often unavailable.

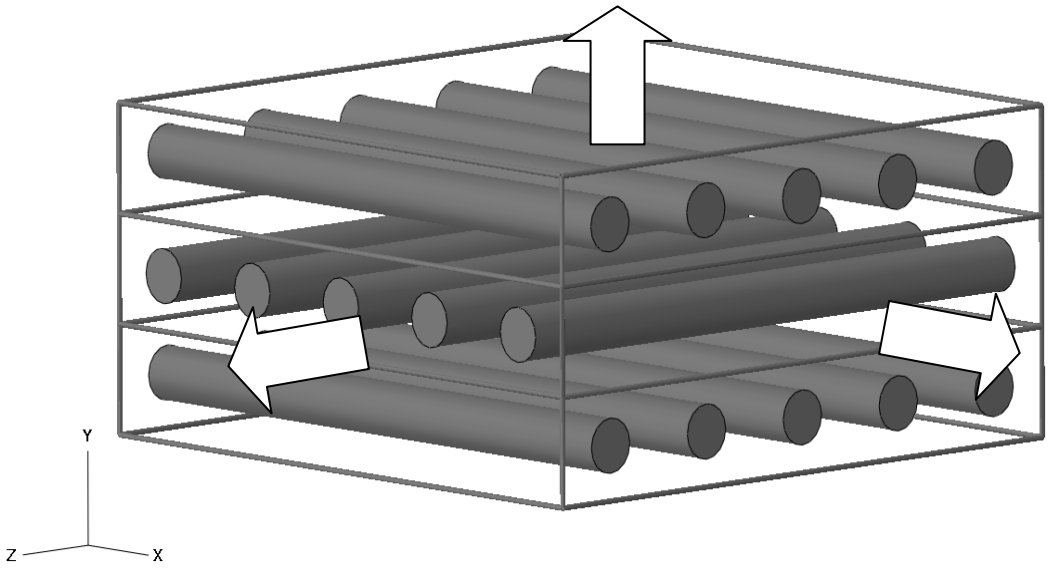

Figure 8: Schematic 0º/90º laminate showing in-plane and out-of-plane direct stresses

Park and Lee did not give any details of their FR4 laminate, nor mention its elastic properties. The published values found in the wider literature are quite different from each other, and the effects of fibre volume fraction and fibre direction not always acknowledged. Little has been published on the out-of-plane properties, also called through thickness properties, of FR4 (this is assumed to be because it difficult to measure, and is not normally of interest, particularly for thin material which is usually assumed to be in plane stress or bending). Rare exceptions are the papers by Ferguson *et al.* [1998] and Broughton *et al*. [2001]. Furthermore, the provenance of published properties can be vague.

The values of the elastic properties of FR4 laminate from six different sources are listed in Table 5, re-indexed to correspond to the *x*-, *y*- and *z*-directions used in the model, Figure 6. The reported properties have some common elements, all, as expected, having the orthogonal in-plane Young's moduli equal $E_x = E_z$ and the out-of-plane E_y, lower than the in-plane ones. The through-thickness shear moduli, $G_{yx} = G_{yz}$, and the in-plane shear modulus, G_{xz}, is higher than the through-thickness.

A simple orthotropic composite requires three Young's moduli to describe its directional stiffness. Moduli in both fibre directions may be equal if the fibre weave design is essentially the same in both directions, see E_X and E_Z in table. The same composite requires three independent Poisson's ratios to describe the amount of lateral strain induced with respect to a perpendicular load. The directional values of Poisson's ratio will obviously be affected by the corresponding directional stiffness. It should be noted that different FE software may require a different set of directional Poisson's ratio to characterise an orthotropic model. Material values are entered into Abaqus/CAE interms of directions 1,2, and 3. It is for the operator to define the orientation of orthogonal directions.

A description of each required Poisson's ratio required for an Abaqus FE orthotropic model is given in Table 6. Where $\nu_{xy} \neq \nu_{xz} \neq \nu_{yz}$ in a woven laminate and are independent. The values of ν_{xy} and ν_{yx} are assumed to be inversely related to the directional moduli ($\nu_{xy}/E_x = \nu_{yx}/E_y$). Similarly, $\nu_{xz}/E_x = \nu_{zx}/E_z$, but this approach could not have been used to subsequently refine Kim's values of Poisson's ratio with respect to the new E_y value suggested as the three Poissons ratio required in Abaqus/CAE are independent of each other. Further experiments would be required to measure Poisson's ratio, this is difficult to do sucessfully. Given the critical influence of the through thickness E2 and G12, it is assumed that any further refinement of the Poisson's ratio values would have very little effect on agreemnet with measurements.

Source	E_x (MPa)	E_y (MPa)	E_z (MPa)	ν_{xy}	ν_{xz}	ν_{yz}	G_{xy} (MPa)	G_{xz} (MPa)	G_{yz} (MPa)
Murai *et al*. [2000]	22400	1500	22400	0.1425	0.2	0.094	199	630	199
Rodgers *et al*. [2004]	21000	7720	21000	0.39	0.18	0.1434	3114	8898	3114
Kim [2007]	12000	7600	12000	0.22	0.27	0.139	3000	3100	3000
Lau [2001]	22000	Not given	22000	Not given	0.28	Not given	Not given	3500	Not given
Li *et. al.* [2008]	1600	Not given	1600	Not given	0.28	Not given	Not given	Not given	Not given
Chen and Chen [2006]	18200	Not given	18200	Not given	0.25	Not given	Not given	Not given	Not given

Table 5: Published FR4 material orthotropic elastic properties

The Poisson's ratio value of most materials is between about 0.1 and 0.5. In composites this is not an inherent material property but rather a structural property, Herakovich [1984], and it is possible to create laminates with Poisson's ratio that is negative or greater than one, Sun and Li [1987]. Measurement of Poisson's ratio is difficult particularly in the out-of-plane direction, and hence validation is limited. In reality the Poisson's ratio is sensitive to local variations in fibre orientation, resin volume and fabrication process. This may account for the variations in published FR4 values. Values can be calculated using a rule of mixtures approach but when comparing to measurements the error is variable.

Poisson's ratio	Description
ν_{xy}	strain in Y-resin direction caused by pulling in X-fibre direction
ν_{xz}	strain in Z-fibre direction caused by pulling in X-fibre direction
ν_{yz}	strain in Z-fibre direction caused by pulling in Y-resin direction

Table 6: Description of corresponding Poisson's ratio with strain for a woven laminate

Kim [2007] measured the in-plane moduli and found them not to be significantly different to the data provided by the manufacturer, although the magnitude of their values of in-plane *E* are only about half of those of other authors. The Rodgers *et al*. [2004] in-plane properties were also measured, and both Rodgers *et al*. and Kim calculated the through-thickness properties using established composite micromechanics equations. Despite their similar approaches and different in-plane properties, both Kim and Rodgers *et al*. have arrived at similar values for the through-thickness moduli. Rodgers *et al*. in plane shear modulus is much higher than Kim's, which is consistent with the higher in plane Young's modulus. The origin of the Murai *et al*. [2000] and Lau [2001], values is less clear. The through thickness Young's modulus and the shear moduli of Murai *et al*. are much lower than the others, and the reason for this is not clear either. The in-plane Murai *et al.* and Rogers *et al.* Young's moduli properties are close to the isotropic values used by Lau, and Chen and Chen [2006], The isotropic value used by Li *et al*. [2008] is between the in-plane values of Kim and the others. The selected range are considered sufficiently representative of current knowledge for use in the current analysis. The original source of Lau, Chen and Chen, and Li are unclear.

Three analyses were carried out using the Murai *et al*, Rodgers *et a*l and Kim orthotropic properties, in the interest of assessing the sensitivity of BGA behaviour to these discrepancies.

The Abaqus CAE composite capability can define general anisotropy or orthotropic material *via* the "Engineering Constants" definition (3 *E*s, 3 ν s and 3 *G*s). To check that this did not inadvertently introduce any changes in the model, initially the isotropic

material data was re-input using the "Engineering Constants" command (i.e. identical values for each of the *E*s, ν s and *G*s). Figure (9) shows that the model responses were, as expected, identical.

Next, the orthotropic FR4 data were input and Figure **Error! Reference source not found.** shows the calculated values for each of the 3 sets of properties against the measured Park-Lee data in shear and tension.

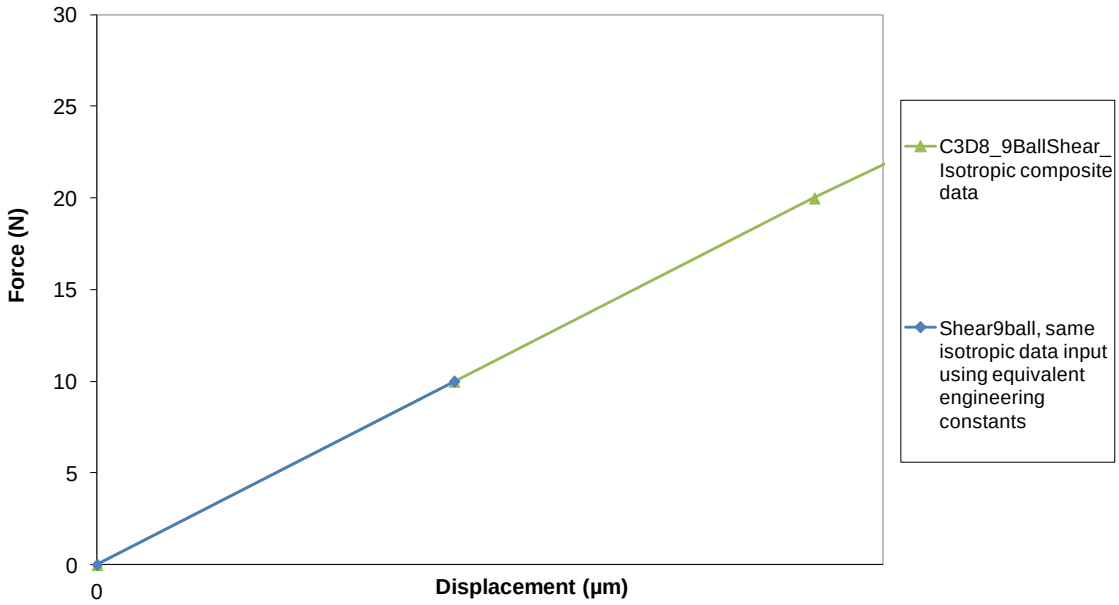

Figure 9: Monotonic shear test using FR4 isotropic data and FR4 isotropic data entered using Engineering Constants (EC) option, excellent agreement is shown

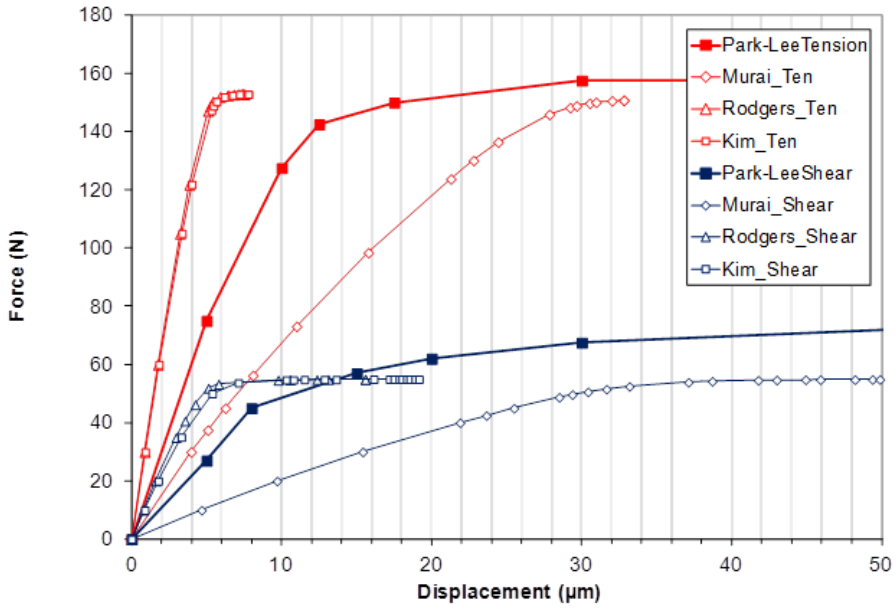

Figure 10: Calculated and measured force displacement curves for tension and shear, taking account of orthotropic FR4 properties

As can be seen, the Rodgers *et al*. and Kim moduli give very similar results for both shear and tension, despite having very different in-plane properties. Both underestimate the displacement, although not as much as using an isotropic assumption with the modulus set in the fibre direction. In contrast, the Murai *et al*. moduli overestimate the displacements in both shear and tension. Murai *et al.* and Rogers *et al.* have very similar in-plane values of Young's modulus.

This shows that composite through-thickness properties have a substantial effect on predicted overall displacement of the specimen, for both sets of loading. Furthermore, none of the sets of orthotropic properties describe the measured displacements well, although all give a reasonably acceptable value for the limit load, as might be expected since this is determined by the model for the solder.

3.2.4 Identification of sample constituent displacements

From the geometry of loading, it might be expected that the value of E_y would dominate the tension response, whereas G_{yx} would dominate the shear response, which explains the relative compliance of the Murai *et al*. response compared to the other two, and

suggesting that the most appropriate values of the two moduli lie between 1500MPa and 7600MPa and 199MPa and 3000MPa, respectively, rather a wide range. However, the deformation is not as simple as this. For example, in shear, the orthotropic FE model exhibits not only increased overall model displacement but also increased localised rotation of the solder ball resulting in localised compression and tension of the FR4 material, as seen in Figure 11. The rotation of the solder into the substrate and the development of a parameterised approach to obtain some simple analytical equations is investigated in Chapter 4.

Figure 12 shows that, in tension, orthotropic FE models indicate local out-of-plane stretching of the substrate, although there is also shear in the *y*-direction. Most of the deformation under tension appears to be in the FR4 substrate. It should be noted that, in the FEA model deformation plots shown in Figure 11 and Figure 12, the deflections have been grossly magnified using a 'deformation scale factor', a display-only option which does not affect calculations.

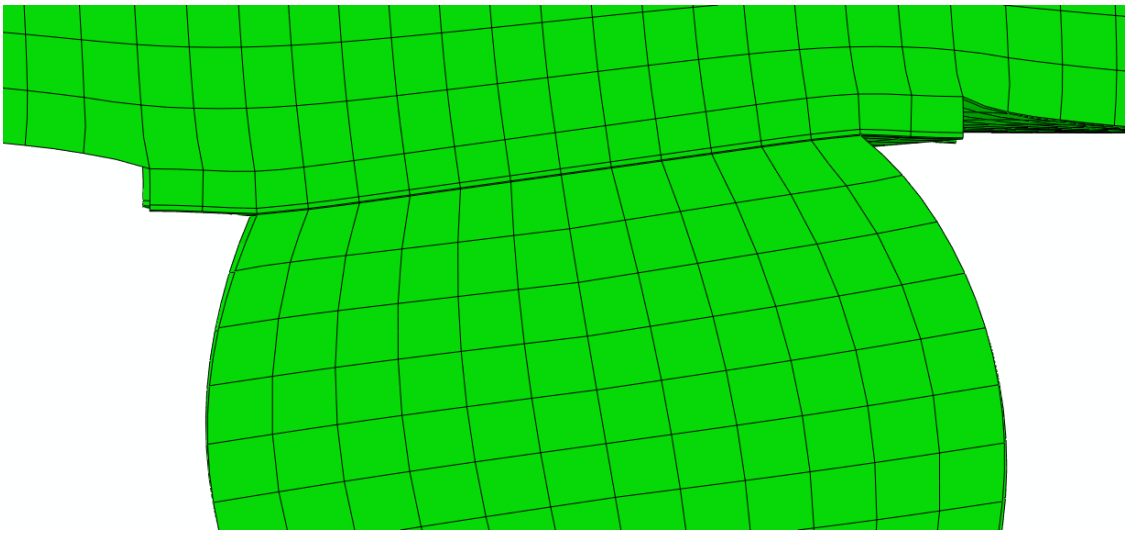

Figure 11: Deformed shape of model of Park-Lee shear test, showing localised rotation of solder joint, Abaqus deformation scale factor X10

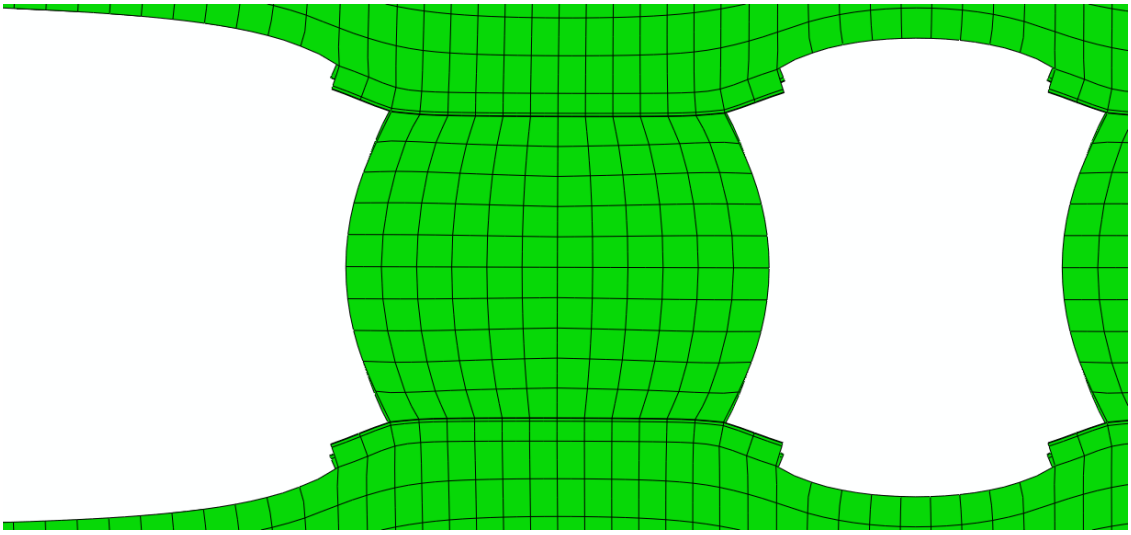

Figure 12: Deformed shape of model of Park-Lee tension test, Abaqus deformation scale factor X10

This substrate deformation was further investigated by creating a simple model of the solder ball as a cylindrical column with an encastré condition at both ends (no substrate material). The shear displacements of the top relative to the bottom due to bending and shear of the metallic column were calculated separately using basic mechanics and using a simple FE model (shown in the right hand side of Figure 13). The agreement between the FE and analytical calculations was within 1% for a 'long' column (length = 20 × depth) and 5% for a 'short' column (length = ½depth).

Using these classical shear and bending theory equations, later detailed in Section 4.1, the displacements calculated for an (isolated) geometry representative of the solder balls in the test specimens were much smaller than those measured in the tests and calculated by FEA of the BGA sample. The explanation for this discrepancy can be seen in Figure 13, which compares representative FE models with and without an FR4 substrate, and clearly shows that the solder material not only deforms through shear and bending, but also rotates as a whole within the substrate material. On top of this, there is also a shear deformation of the FR4. Again the deflections have been grossly exaggerated using the display-only option, 'deformation scale factor', which does not affect calculations.

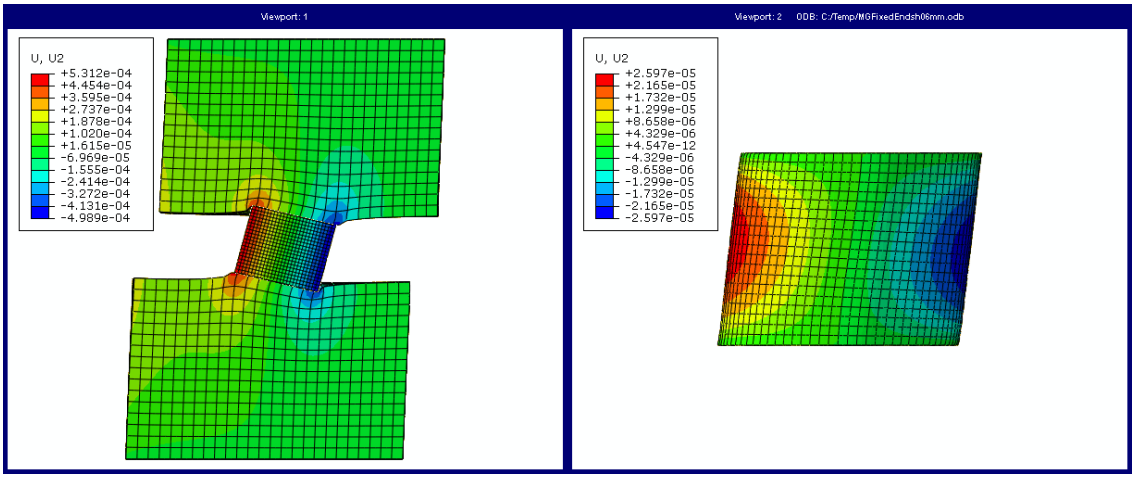

Figure 13: Idealised FE model of solder column - LHS: with substrate, RHS: without substrate, a deformation scale factor has been used to emphasise effects

3.3 **Determining suitable material properties**

3.3.1 Determining substrate out-of-plane properties

It has been seen that the in-plane FR4 properties have little effect on the overall response (both in shear and tension) but that accurate through-thickness properties (out-of-plane) are required for satisfactory modelling. The difficulty with published through-thickness FR4 properties has already been highlighted, so an attempt was made to refine the material properties to match the Park-Lee results. It was hoped this would produce, within published bounds, verified realistic through thickness material properties which could be used to enhance the accuracy of the FE models. The Kim properties were chosen as a starting point as their in-plane elastic properties were measured and validated against those given by the manufacturer.

- Leaving E_x, E_z, G_{xz} and the Poisson's ratios unmodified, the values of G_{yx} and G_{yz} were adjusted (keeping them equal) until the best agreement with the measured shear load-displacement curve was obtained.
- These values were then used in the tensile load-displacement curve and the value of E_y was adjusted until agreement in tension was achieved.
- It was noted that the Young's modulus, E, has a small (but not zero) effect on the shear test displacement and the Shear modulus, G, has a small (but not zero)

effect on the tension test displacement, so the process was repeated until values of *E* and *G* converged and gave good agreement in both tension and shear.

- The resulting FE calculations are shown in Figure 14, with the Park-Lee measurements for tensile and shear load. The agreement between the FE data using the suggested FR4 properties and the Park-Lee measurements is within 10% (or 0.5µm at a displacement of 5µm) during the initial loading of interest.
- The measured Park and Lee data used to derive the proposed values, was extracted manually from a plot of force against displacement [Park and Lee 2005]. Without the original raw measured data and detailed knowledge of the test set-up, it would be difficult to further refine the material properties. It does however demonstrate that appropriate properties can be derived using this method.
- The final proposed properties are given in Table 7. Where direction X,Y and Z, as noted in Figure 6, have been respectively re-labelled directions 1,2 and 3 for suitable entry into Abaqus/CAE. The modified properties are within the bounds of the published data and represent realistic through thickness material properties.

Chandran *et al*. [2000] have published orthotropic values for FR4, which they used in the FE analysis of thermal cycling of a BGA. They say that the values, shown in Table 7, have been 'validated numerous times during previous studies' although they have not given a reference for this. The values for *E* are very close to those derived in this work. The shear values do not agree quite as well, but are still closer to the proposed values than those published by others. This may be explained by Chandran *et al*. not having conducted shear tests.

The FE analyses using the newly derived orthotropic properties, shown in Figure 14, were run under load control and terminated at the maximum load which means they have not captured much of the post-yielding behaviour exhibited by the specimens. This could be improved by running under displacement control. Also, including post yield hardening in the material property definitions could improve post-yield stability of the analysis. Although mesh refinement studies showed that the results converged for the initial linear response, further refinement in the areas of yielding in the solder balls might improve the predicted non-linear response. At this stage, however, the focus was on obtaining consistent elastic constants as a basis for further developments.

Data Source	E_1 (MPa)	E_2 (MPa)	E_3 (MPa)	ν_{12}	ν_{13}	ν_{23}	G_{12} (MPa)	G_{13} (MPa)	G_{23} (MPa)
This work: final result of optimised data	12000	3000	12000	0.22	0.27	0.139	1500	3100	1500
Chandran *et al.* [2000]	10470	3080	10470	NA	NA	NA	2390	6870	2390

Table 7: Comparison of Orthotropic FR4 properties used by Chandran et al. with the current work

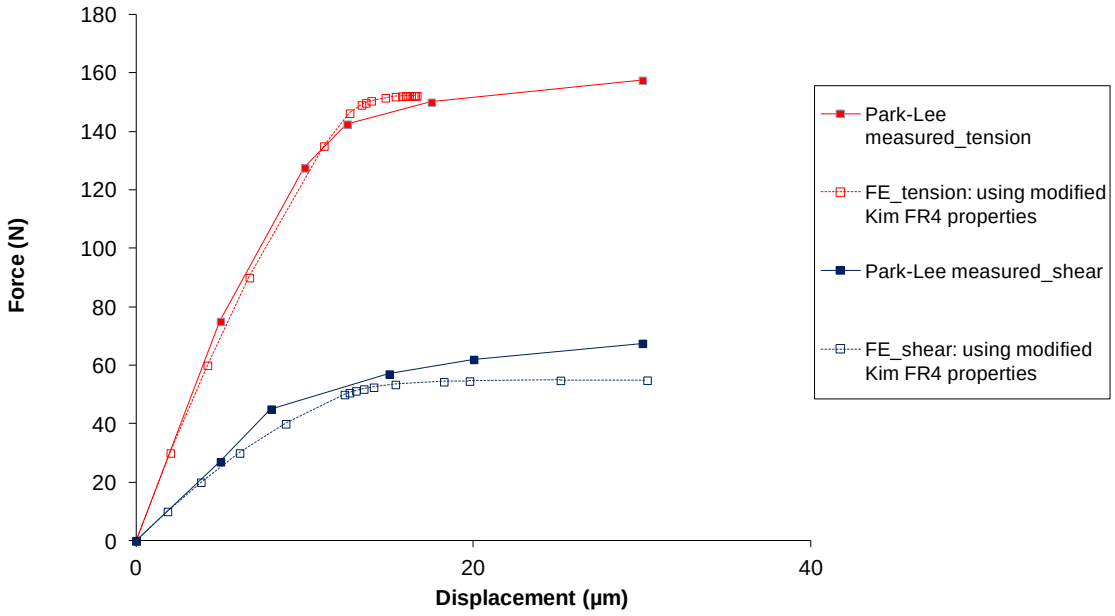

Figure 14: Park-Lee experimental data compared with FE calculations using optimised FR4 properties

Only the initial response, up to 30μm, is shown as this is more than adequate to model the positive displacements used in the Park and Lee fatigue tests, see Figure 18 to Figure 20. Only the FE model under tension did not achieve this displacement, as it was run under applied force and once this force was reach the FE calculation stopped. The model could be run again under a higher load or under an applied displacement to capture larger displacements however, the current model was considered sufficient to capture the initial linear response and limit of proportionality.

Initially, in the interest of computational efficiency, a tied contact was used to facilitate a mismatched mesh, coarsened in the substrate. However, it has been shown that popular assumptions regarding the mechanical behaviour of the FR4 substrate material are incorrect. It was therefore considered prudent to refine the substrate mesh and study the effect on results. Also for simplicity, a single part with partitions for material discretisation was then employed.

Refining the substrate twice produced little effect on the overall response, as shown in Figure 15 and Figure 16. However, refining the substrate did bring about changes in the localised stress patterns. Stress/strain data, extracted from the area at the solder/FR4 interface, was sensitive to refinement of a mismatched mesh. Given that the calculations also showed that the overall response of the structure is little affected, and considering that an orthotropic model does not take into account the laminar structure of the FR4 anyway, it was decided not to pursue this effect further during the current work and the model was deemed to be adequate.

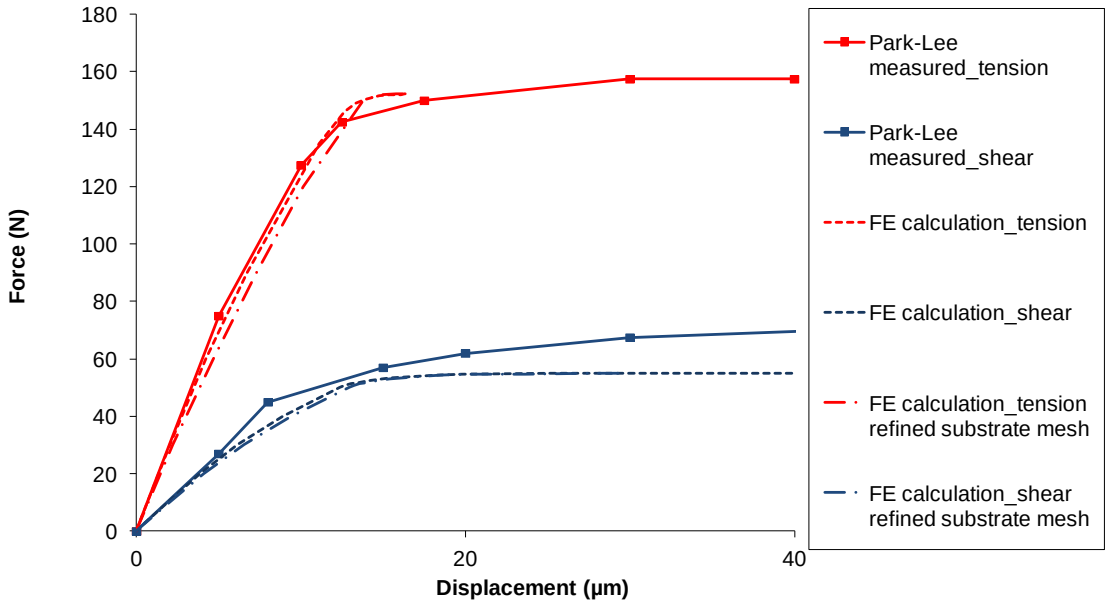

Figure 15: Effect of refining substrate mesh on overall shear and tensile response

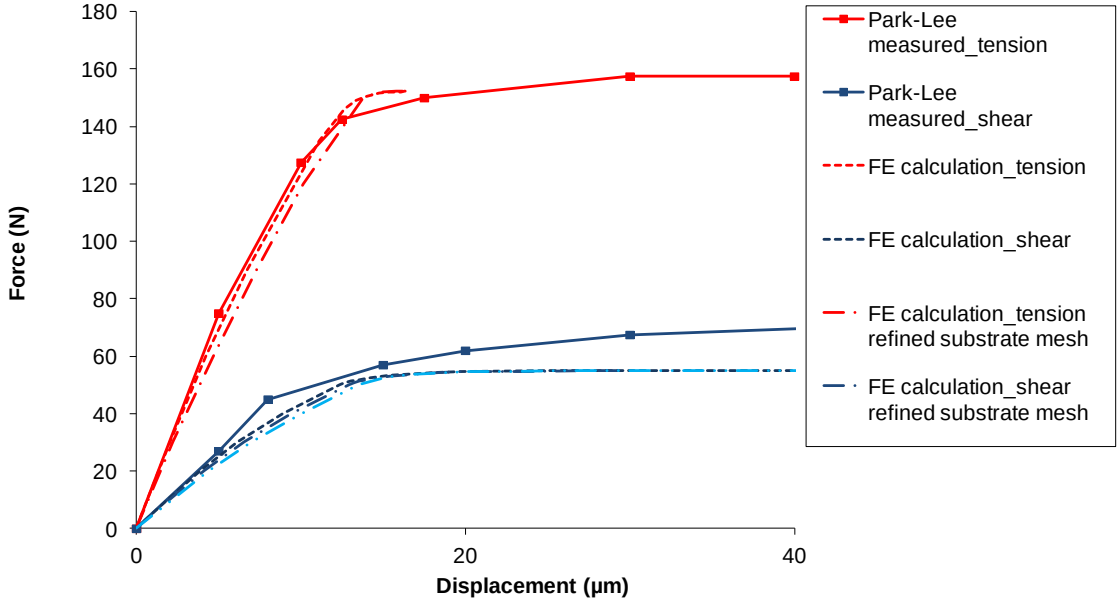

Figure 16: Effect of further refining substrate mesh on overall shear response for small displacements

3.3.2 Solder elastic modulus

Due to the surprisingly large range of published values for Young's modulus of SnAgCu (SAC) lead free solder, and its reported sensitivity to strain rate, it was decided to look into the effect of solder modulus value on calculated BGA behaviour. Most measured, room temperature values of Sn3.8Ag0.7Cu Young's modulus are between 40 to 69 GPa. In the current FEA study a value of 46GPa has been used consistently, unless otherwise stated. The implicit models shown here were quasi-static and did not account for strain rate, or material creep properties.

As part of the current work and in collaboration with staff at the Technical University of Berlin, an acoustic method was used to measure an elastic modulus for SAC material at a range of temperatures. This work is described in **Error! Reference source not found.**. The acoustic method (used to avoid suspected parasitic creep strain in mechanical tensile tests) gave an average measurement at room temperature of 56.9GPa.

3.3.3 Solder strain hardening

The model was further enhanced by introducing linear strain hardening. No published hardening property values could be found for Sn3.8Ag0.7Cu. Kanda *et al.* [2012] published strain hardening exponent values for Sn3.0Ag0.5Cu, but Kanda *et al*. used a different specimen and loading arrangement, so it is likely that the published stain hardening values would not characterise the Park and Lee data. So in the FE model values of the strain-hardening exponent were selectively modified to change the bi-linear slope. Unfortunately as agreement was improved for the shear test it deteriorated for the tensile test, as shown in Figure 17. In this case the linear strain hardening assumption is probably too simple. , In the absence of a more detailed stress-strain curve this was not pursued.

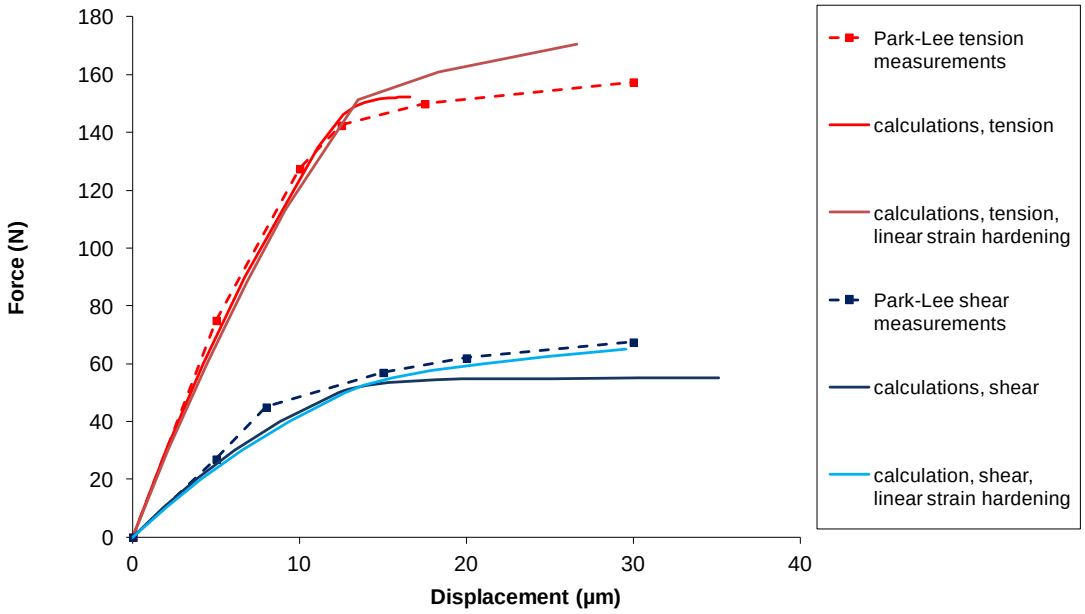

Figure 17: Park-Lee data and calculated force-displacement with and without hardening

3.4 **Independent validation against other data**

The FE approach is validated in this section against some of the Park-Lee data and some of the data from Ghaleeh. These are covered, respectively, in the two following sections. Unfortunately it proved difficult to obtain other examples of independent data with sufficient detail of sample design and loading.

A third sample design, Pang and Xiong's single joint shear lap [2003, 2005], was investigated. Using the proposed through thickness FR4 properties in a hand calculation, developed for BGA tests in Chapter 4, showed good agreement to FE calculated displacement. Although the measurements were not particularly useful in validation, this was an interesting exercise in applying the developed methodology to a wider range of published test design and so the exercise has been included in Appendix B.

3.4.1 Park and Lee 45° data

As well as the tension (0°) and shear (90°) measurements used in the previous section, Park and Lee [2005] published a single force/displacement cycle for a load angle of 45° using the same 9-ball sample, see Figure 5. This published 45° load angle cycle is used here to partially validate the FR4 orthotropic properties and modelling approach.

The proposed orthotropic properties shown in Table 7 were input (without further manipulation) to the model described in Section 3.2.1. The FE calculations made using the proposed FR4 mechanical properties are shown in Figure 18, along with the 45° load angle data. Measurements were again extracted by hand from a published plot [Park and Lee 2005]. Park and Lee did not publish the first uptake of load against displacement at 45°, nor did they indicate the cycle number associated with Figure 18.

The measurements provide a reasonable general validation of the proposed FR4 values, in that this gives a slope approximately diagonal to the hysteresis loop, whereas using other published FR4 properties shown in Table 5 correspond to the extremes of the slope of the hysteresis loop. However, the hysteresis loop is very wide indeed, indicating that there is a considerable contribution either from viscoelasticity or plasticity associated with the cyclic deformation.

To improve the usefulness of the comparison shown in Figure 18, Park and Lee's published empirical data under monotonic load was compared to the corresponding load cycle data, separately for both the 0° and 90° measurements, in Figure 19 and Figure 20. In the comparisons of Park and Lee's monotonic and cycled loading measurements, sample and loading arrangement are assumed to be the same and load is similar. It is not known if other test parameters were varied, but these comparisons confirm the qualitative validation shown in Figure 18.

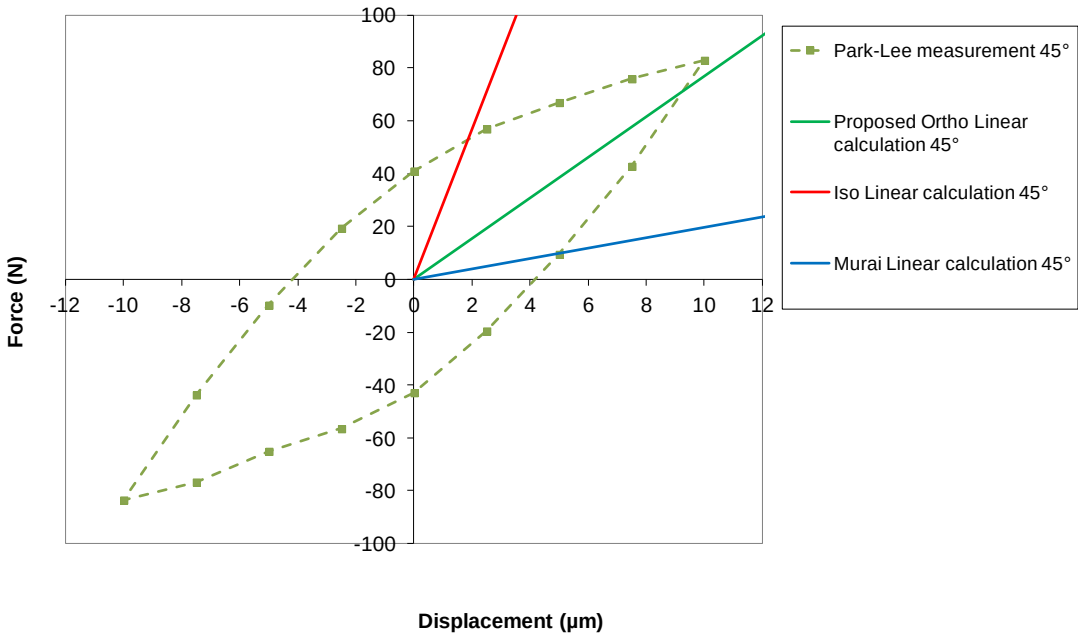

Figure 18: Calculated behaviour under monotonic load shown with measured Park-Lee 45° cyclic data

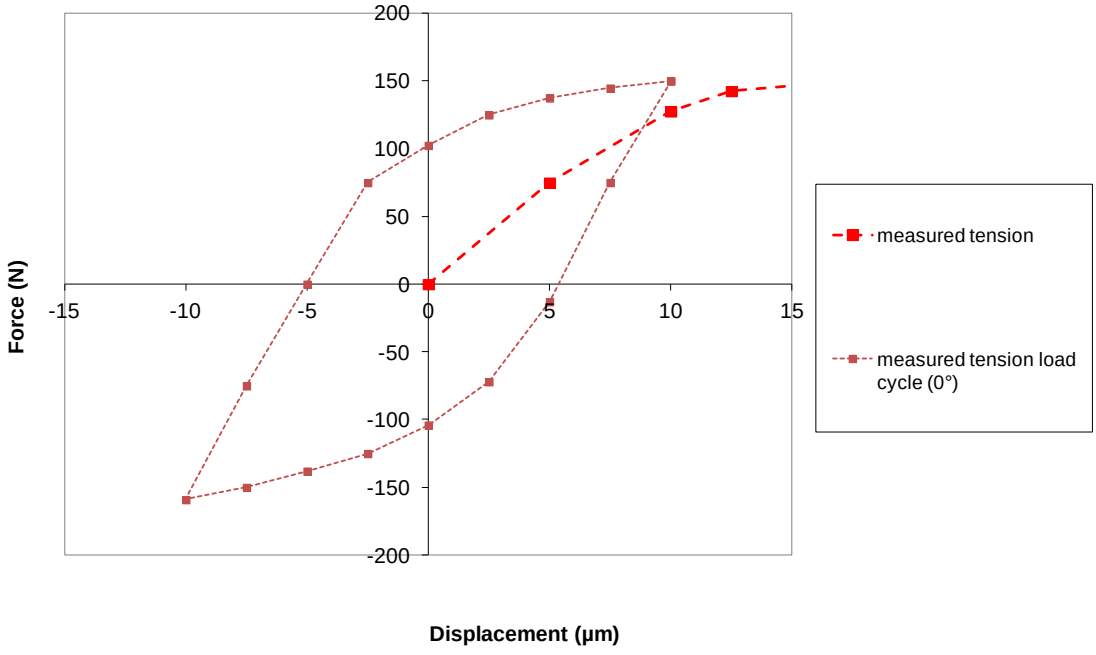

Figure 19: Park and Lee [2005] measured monotonic and cyclic shear data

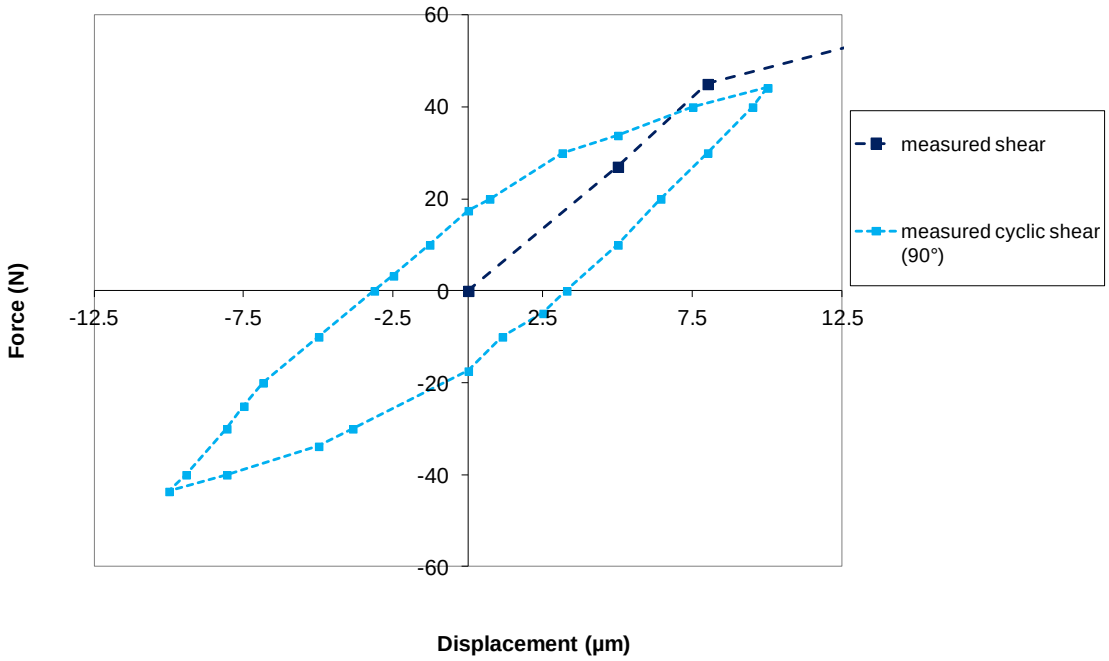

Figure 20: Park and Lee [2005] measured monotonic and cyclic tensile data

3.4.2 Further independent validation using Ghaleeh data

The 4 ball FR4 on FR4, BGA sample shown in Figure 21 was devised as part of an experimental programme to study the thermo-mechanical fatigue behaviour of SnAgCu lead free solders, Ghaleeh [2015]. All of the dimensions used in the 4 ball Abaqus model are shown in Table 8. During the physical experiment the test piece was subjected to a shear load at room temperature. A schematic diagram of the test set up is shown in Figure 22, Ghaleeh [2015], which essentially involves the use of an actuator to effect shear displacement control, an LVDT to measure the shear displacement and a load cell to measure the reaction force.

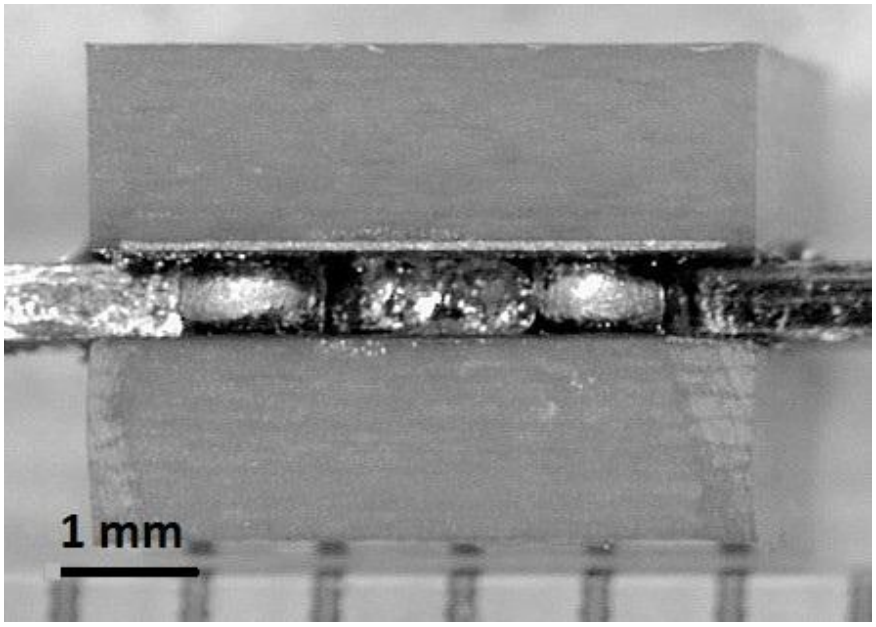

Figure 21: Example of 4-ball BGA test-piece, from Ghaleeh [2015]

Material	**Dimensions (mm)**		
	X	Y	Z
FR4 Substrate	5.0	1.6	1.25
Tin	0.73Ø	0.008	
Copper	0.73Ø	0.035	
Solder	0.8 Ø mid height, 0.7 Ø interface, pitch 2.5	0.6	

Table 8: Ghaleeh sample dimensions

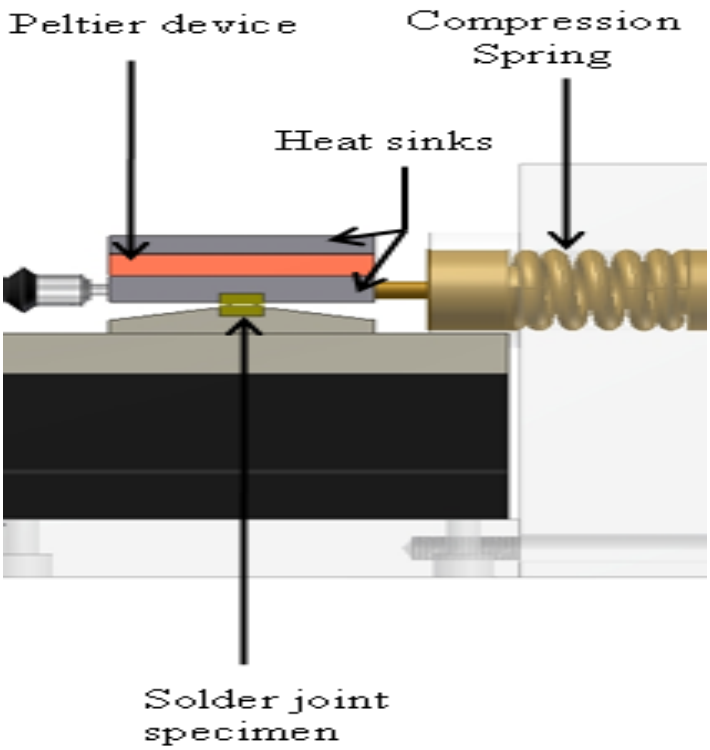

Figure 22: Shear test set up for 4-ball BGA, Ghaleeh [2015], adapted from larger image

The shear force is applied through a metallic heat sink which has a square well machined into it, into which the sample fits. The sample is therefore loaded along the edge of the square piece of PCB, which in turn transfers the load to the solder balls. Sample measurements were taken through the heat sink, some distance from the sample, but considered by the designer to be in line with a point at half the height of the upper substrate.

An Abaqus General-Static model of the Ghaleeh 4 ball shear test specimen was generated (to capture large non-linear geometric deformations); with a geometry one quarter of the true sample geometry as shown in Figure 23. The orthotropic properties obtained from fitting the Park-Lee measurements, as detailed in Table 7, were input (without further manipulation) into the model. All other material properties, as detailed in Table 4, also remained constant.

To simulate the original Ghaleeh measurement: The displacement is extracted at a point half way up the extreme surface of the upper substrate, exactly in the centre of the upper substrate extreme surface. The extreme YZ surfaces of the lower substrate and the bottom surface of the FE model are fixed.

Two methods were used, in turn, to apply the load. Exactly the same sample response was achieved using both methods.

Given the wide range of discrete material volumes, appropriate mesh densities were selected as shown in Figure 23, including a considerably coarser mesh in the substrate compared to the metallic material. Further refinement of the substrate mesh showed no significant change in calculated global displacements. The clamping/loading arrangement, as described above, was quite different from that used in the Park-Lee set up. This is reflected in the Abaqus model commands. A 12.5N load was applied to the quarter model, equivalent to 50N to the whole sample.

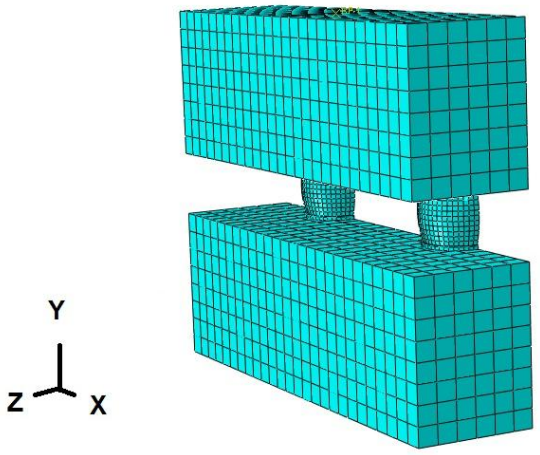

Figure 23: Model of 1/4 of the Ghaleeh 4 ball BGA test piece, showing discrete mesh densities

The results are shown in Figure 24 for an initial model using isotropic FR4 properties, a second model using the suggested orthotropic properties shown in Table 7 and original raw measurements from Ghaleeh [2015]. Markers have not been shown on the plotted measurement values, as due to the great number of measurements in the raw data this would not be practical. FE extracted forces, from the quarter model, have been

multiplied by a factor of 4, for a direct comparison to whole sample measurements. Excellent agreement with the measured response and orthotropic model can be seen, including a degree of non-linearity. This non-linearity is thought to be geometric as further loading of the FE models (beyond 24N applied in the real test) showed the sample still to be in the elastic region. The comparisons support the conclusion that the modified properties are sensible.

Ghaleeh [2015] discovered, within his physical test set-up, a significant proportion of the measured displacement came from outwith the sample, e.g. deformation in grips/adhesive. He reported this extraneous strain to be a problem largely undocumented by other authors with respect to BGA micro-samples. Ghaleeh, like other authors reported significant scatter in data from nominally identical tests.

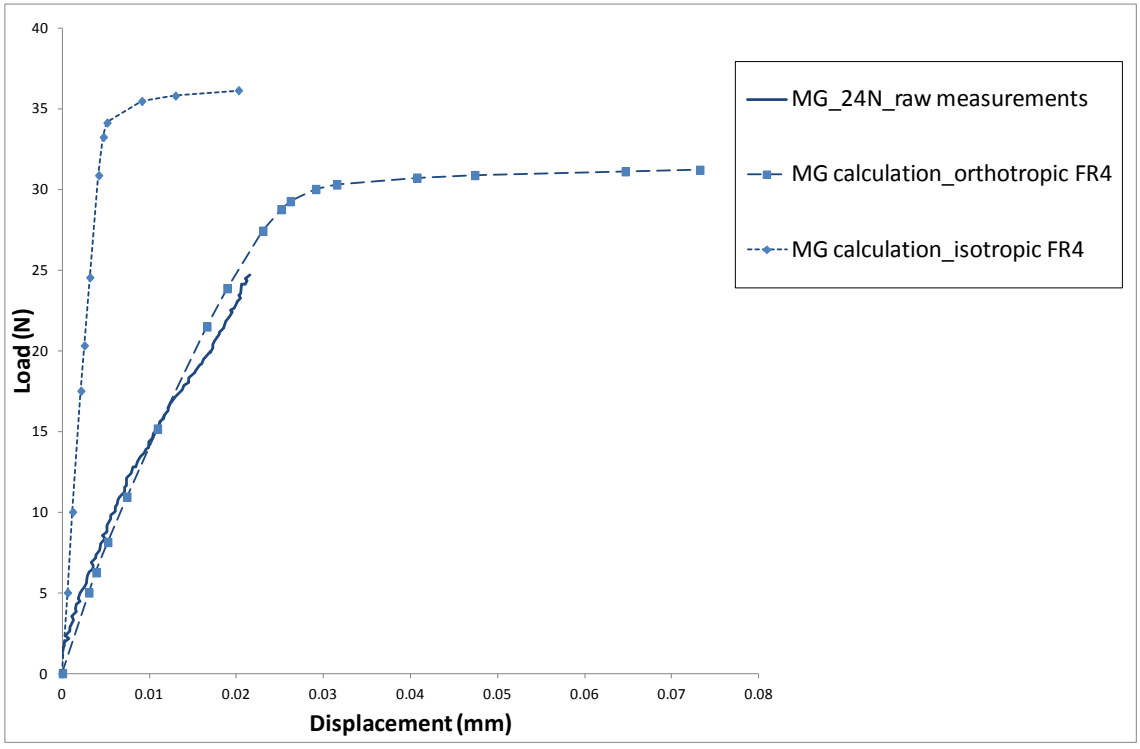

Figure 24: Measured 4 ball test sample force-displacement curve and calculations, with published isotropic and with suggested orthotropic FR4 properties

In the FE model, force was applied directly to the sample and the overall FE model displacement was extracted directly from the sample, unlike the physical test set-up. As per the above description of the physical measurement, displacement was extracted at

half height of the upper substrate, on the centre line. It was noted, as expected, that there was variation in FE calculated displacement (U1) through the sample height and, had a different point been selected for extraction of FE data, this would have been reflected in the comparison. This suggests that, although the proposed FR4 properties again give greatly improved agreement than when using other published properties, see Figure 24, the excellent agreement shown may be misleading. This matter is dealt with later in Chapter 4.

The solder material used in Ghaleeh's tests was measured, as part of the current study, at the Technical University of Berlin to have an E value of 56.9GPa. This value was input into the 4 ball orthotropic model and showed no change in calculated overall sample behaviour.

3.5 **Discussion of effect of chosen material properties and sample configuration**

Section 3.2 has highlighted the importance of using accurate orthotropic properties when modelling FR4 composite material in BGA assemblies. For the current modelling using the same in-plane properties has shown good agreement to the measurements, it may be that future modelling may consider the influence of composite warp and fill direction mechanical properties. Only one publication was found to measure FR4 warp and fill direction properties, Shrotriya and Sottos [1998], and this was to obtain creep data. More sophisticated anisotropic material models are available in the Abaqus software.

The simplified FR4/solder assembly shown in Figure 13, left hand side, clearly shows that the solder material not only deforms through shear and bending, but also rotates as a whole within the substrate material, this is addressed. On top of this, there is also a shear deformation of the FR4.FE calculations also showed that the overall BGA sample behaviour was not sensitive to the solder modulus value (within bounds of typical published room temperature values), for all of the sample designs considered. This reinforces the common understanding that empirical laws, used to directly relate whole

sample strain to the fatigue life of micro-solder joints in this type of composite sample, cannot be applied universally.

The current comparison to published data showed that the FR4 dominates the elastic response of the sample and the through thickness moduli, *E* and *G*, are crucial to this. This was shown through FEA of several BGA sample designs under shear and tensile loads; Park and Lee, Ghaleeh, and Pang and Xiong (see **Error! Reference source not found.**).

No previous publication could be found that highlights the extreme influence of FR4 through-thickness properties shown in the current work. This is particularly important in studies of cyclic loading of solder joints as it is routinely assumed that hysteresis effects are due to plasticity and/or creep in the solder although, in practice, some of this may well be associated with the substrate.

Using an orthotropic material model introduced considerable composite deformation, and revealed a previously unreported rotation of the solder joint at the composite/joint interface. Poor agreement with measured data was shown when using a range of published composite elastic values and, suitably validated, through thickness values of *E* and *G* have been proposed, shown in Table 7.

Validation of the proposed FR4 mechanical properties with the current analysis, was only possible with a limited set of published sample designs and data. Considering the vast quantity of related publications, it appears surprising that few publish measured solder joint behaviour under mechanical load in sufficient detail that a coherent modelling approach can be developed in order to harmonise published findings and properties.

It is usual, in any engineering research, reliability or manufacturing situation, that a full characterisation of all materials is obtained at the outset. It is therefore surprising that there appears to be, as yet, no standard test or sample designs for micro-solder joint mechanical testing. Given the range of tests used, the range of material properties (reported and used in published analyses) is not surprising.

The known sensitivity of solder material mechanical properties to sample volume and processing, requires test data to be obtained from realistic solder joints. To facilitate mechanical testing of the small solder joints requires the soft solder to be attached to other material(s). In using glass fibre composite for this function, the soft solder material has been attached to a material of softer through thickness strength. Some authors, e.g. Zhang *et al*. [2014], Kanda and Kariya [2012], Maio *et al.* [2011], Suhling *et al*. [1994], have circumvented this problem by attaching to stiffer metallic substrates, although these materials, generally copper or aluminium, also exhibit a degree of elasticity and do not reflect common in-service configurations for solder joints. The solder joint volume presents a challenge to directly and accurately isolate solder strain and, for this type of measurement, specialist equipment not normally deployable throughout an array is required.

Complex assembly geometry, mixed materials and ensuing stress and strain distributions, limits the usefulness of classical analytical approaches to interpreting test results.

The current work highlights the need for a simple analytical solution to adequately describe the mechanical behaviour of all of the assembled BGA materials. The solution is required to quantify FR4 deformation and solder rotation, accounting for the influence of all the material properties (particularly the anisotropic composite) and sample geometry. This is a prerequisite to isolating the proportion of solder deformation, for any given interconnect package design under a (possibly complex) range of loads.

Chapter 4 **Parameterisation of the components of sample shear displacement**

In this chapter the relative magnitudes of the individual components of deflection are isolated using linear FE analyses and basic engineering calculations, with a view to parameterising the results in a way that they could be applied to more general BGAs. The theoretical analysis developed here has been applied to both the published Park-Lee [2005] 9-ball sample design and the 4-ball sample design, Ghaleeh [2015]. In Chapter 3 it was established that the FE model reflected very well the global load-deflection behaviours of these real samples and the function of this Chapter is to establish the extent to which this global agreement can be encapsulated in simple analytical expressions which help to explain the effects of aspects of the design of BGAs.

In Chapter 3 it was shown using FEA that the calculated deformation in a solder ball accounted for only a small proportion of published measurements of total sample displacements. The major components of overall displacement being shear deformation in the substrate and the shear displacement associated with rotations at the solder / FR4 interface. Having identified the component deformations, this chapter is devoted to finding a systematic way to quantify each using the following approach.

In sections 4.1 to 4.3 strength of materials analysis, backed up with FEA, is used to describe the components of deformation:

- Shear and bending of solder material; including the effect of solder aspect ratio (height/average diameter) on accuracy of solder shear and bending calculations.
- Shear of substrate material; including the effect of solder joint diameter on substrate shear
- Boundary rotation, backed up by published analysis [O'Donnell 1960];

The O'Donnell rotation solution, and simple shear and beam theory are intended for use with specified geometries. In the following sections each of the components of BGA displacement are examined in turn, and where the BGA geometry inhibits use of simple strength of materials solutions, FEA is used to either quantify the error or to generate legitimate modifications so that the analytical formulae may be applied with confidence to a range of designs.

The shear and bending calculations were straightforward. Although FEA showed that solder deformation is reduced when substituting a rigid boundary for an elastic boundary. Also, to account for the variation in stress through the height of the composite and therefore total composite shear displacement, the basic shear calculation was modified. This modification appears to work very well without further manipulation for differnt designs under shear load.

Background analysis of the original O'Donnell boundary rotation solution, using FEA, confirmed the accuracy of the published solution for application to O'Donnell's original test specimen design. To enable the O'Donnell solution to be used with other designs, including BGA designs, each of the key effects of geometry is isolated and quantified (parameterised). This is based on the artificial assumption that the effects are not interdependent. FEA and curve fitting is used to quantify the effects of geometry with respect to boundary rotation, for a range of geometries:

- Effect of solder aspect ratio
- Length of beam (height of solder ball)
- Substrate, height, depth, width
- Cross sectional area and shape of solder
- Effect of mixed materials in assembly

These curve fits have been used here to generate correction factors for each parameter for a given geometry. In section 4.4, the usefulness of the hand calculations with these correction factors is demonstrated against published data, Park and Lee [2005], Ghaleeh [2015]. Additional effects on BGA deformation, not addressed by the solution, are considered in section 4.5, solder joint array, substrate overhang.

First, a solder ball was modelled simply as a cylindrical column with an encastré condition at both ends (no substrate material), Section 4.1. The displacements of the top relative to the bottom due to bending and shear were calculated separately using basic mechanics and using a simple FE model, shown in Figure 13 right hand side. This confirmed that displacements calculated, assuming a fixed foundation, were much smaller than those measured in the tests and calculated by FE models with a substrate material defined with realistic orthotropic values, as in Chapter 3.

Next the complex stress distribution in the composite substrate was considered, Section 4.2. This was dealt with by artificially 'smearing' the strain, in order to develop a parametric equation which provides an analytical solution to predict overall substrate shear displacement.

Finally, a method suggested in Young and Budynas [2002] was used calculate (previously unreported) boundary rotations using an analytical solution for a stepped-depth cantilever of uniform thickness. Examination of the original source, O'Donnell [1960], revealed that the solution had been validated by the author's own experimental data obtained from a specially-designed test-piece. To ensure appropriate application of the solution, a sensitivity study was conducted to identify the key geometric and material parameters. Each of these steps is described in detail in the following sections.

4.1 **Deformation of the solder ball, approximated as a column**

Equations (2) and (3) were used to determine the lateral displacement of an isolated solder column, Munday and Farrar [1979], Hearn [1997]. Where δ, F, h, E, I, A, G are deflection, applied force, solder height, Young's modulus, second moment of area, cross sectional area and shear modulus. Where the column diameter is here taken as the average diameter of the real solder joint (that is the 4 ball sample described in Chapter 3). The calculation was performed for columns of different lengths.

$$\delta_{bending,\ solder} = \frac{F_{shear} h^3}{12EI} \qquad (2)$$

$$\delta_{shear} = \frac{F_{shear} h}{AG} \qquad (3)$$

For comparison, an FE model was generated of the isolated solder column with an encastré condition at one end, and encastré apart from lateral movement at the other end, see Figure 13, right hand side. Figure 13, left hand side, also shows a solder column of identical geometry, built in at both ends between FR4 substrates.

Both the analytical and FE encastré command assume a fixed boundary. The agreement between FE without substrate and analytical calculations was within 1% for a 'long' column (length = 20 × depth) and 5% for a 'short' column (length = ½depth). This is in line with published recommended limits for the use of Equation (2) and Equation (3), Dieter [1988], Gere and Timoshenko [1997].

The solder displacements measured in the tests and calculated by FEA of whole BGA samples shown in Chapter 3 are much larger than those calculated for isolated solder material of geometry representative of the solder balls in the test specimens using Equation (2) and Equation (3) and the FE model of isolated solder material shown in Figure 13, right hand side. The explanation for this discrepancy can be seen in Figure 13, which compares representative FE models with and without an FR4 substrate.

4.1.1 FE verification of approximating the solder joint as a column

Using linear analytical calculations cannot capture potential non-linearity in the real geometry, material and test conditions. This section shows that, using the simplified solder geometry, linear FE and the simple analytical calculations of material behaviour can quickly give a reasonable approximation of BGA behaviour.

The assembly shown in Figure 13 left hand side, is an Idealised representation of the 4 ball sample described in Chapter 3. A more realistic, detailed, non-linear 'full' FE model, which includes a spherical solder ball geometry and copper lands with metallic finishes, is described in Chapter 3. Table 9 shows agreement to within 1% between FE calculated whole sample global deflections of the model shown in Figure 13 left hand side, compared with the more detailed 'full' model of the 4 ball described in Chapter 3. Both FE assembly models used the proposed FR4 orthotropic material values determined in Chapter 3. The load shown, 11.55 N applied to the whole sample, was selected for the comparison as it is believed to be close to the elastic limit but within the region of whole sample elastic response. The excellent agreement between measurement and 'full' FE is possibly misleading given the number of initial assumptions, approximations and unknowns. It does however provide some validation for the modelling.

	Load per solder connection (N)	Global displacement (µm)
Idealised FE	2.88	6.77
'Full' FE	2.88	6.83
Measurement	2.89	6.82

Table 9: Comparison of FE calculated global sample deflections with measurements

The use of beam theory to quantify shear displacement and bending deflection in a short solder connection does raise concerns, as highlighted in Young and Budynas [2002] and Gere and Timoshenko [1997]. However, by using beam theory in conjunction with FE, it was possible to determine the proportion of shear and bending components in the short solder 'beam'. Both methods agreed that solder deformation only accounts for around 5% of measured global sample deflection in the BGA designs examined.

4.2 **Shear deformation of the substrate**

Figure 25 and Figure 26 show the upper substrate of the FE model shown in Figure 13, left hand side. In both plots the Z plane shown represents the plane of symmetry above the solder joint, and the location of the solder joint interface is shown. The solder joint and lower substrate are not shown. Figure 26 also shows a second cut view taken in the XZ plane, 0.3mm above the solder interface. Both views show how complex the shear strain distribution through the substrate is, particularly around the interface with the solder ball. Orthotropic composite material properties have been used in the model.

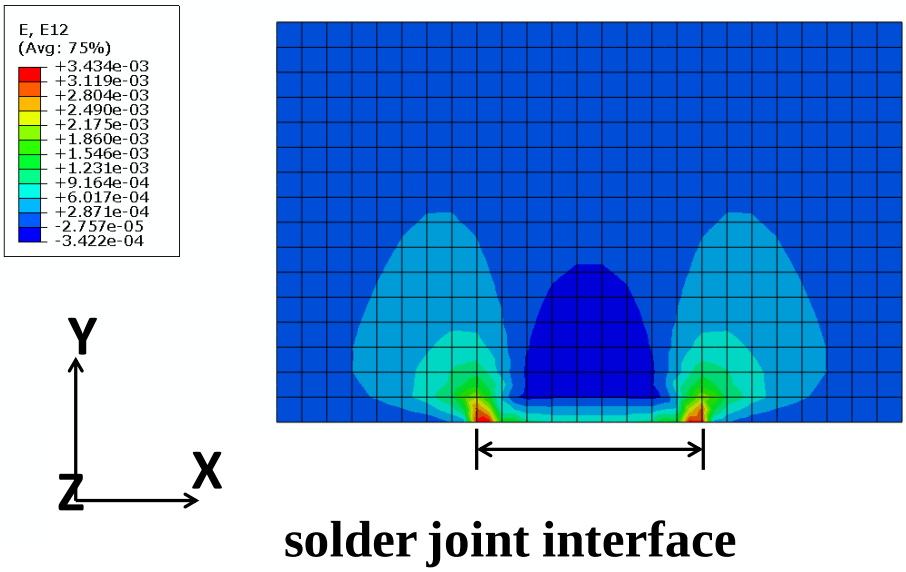

Figure 25: Through thickness view of shear strain distribution within FR4 substrate

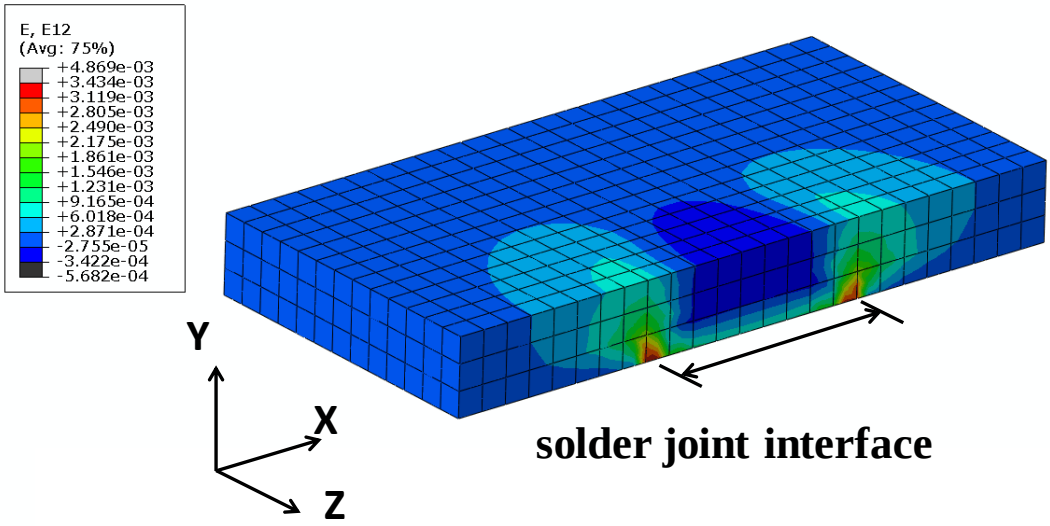

Figure 26: Plan view of shear strain distribution within FR4 substrate, 0.3mm above mid-line of connection interface

At substrate through-thickness heights, h_y, of 0, 0.4, 1 and 1.6mm, several paths were created in Abaqus along the view shown in Figure 25. The XY shear strains were extracted along these paths and are shown in Figure 27. To obtain a simple analytical description, it was assumed that the substrate shear strain could be smeared around the solder ball interface into an effective uniform shear strain over a cylinder of height equal to the substrate thickness and with an effective diameter to be determined. To estimate this effective diameter a goal-seek command was used in Excel, with Equation (3), to find the value which would give the lateral displacement corresponding to the FEA. The through thickness shear modulus of 1500MPa, determined in Chapter 3, was used.

The effective diameter thus found was 1.44 × the average solder diameter. Using the determined effective substrate diameter, overall effective shear strain was calculated and shown in Figure 27. As can be seen, although the local FE results deviate considerably, the overall effective shear strain does appear to bound these sensibly. When calculating the whole sample deformation component due to shear deformation of the substrate material, it is, of course, necessary to sum the shear deformations of both substrates.

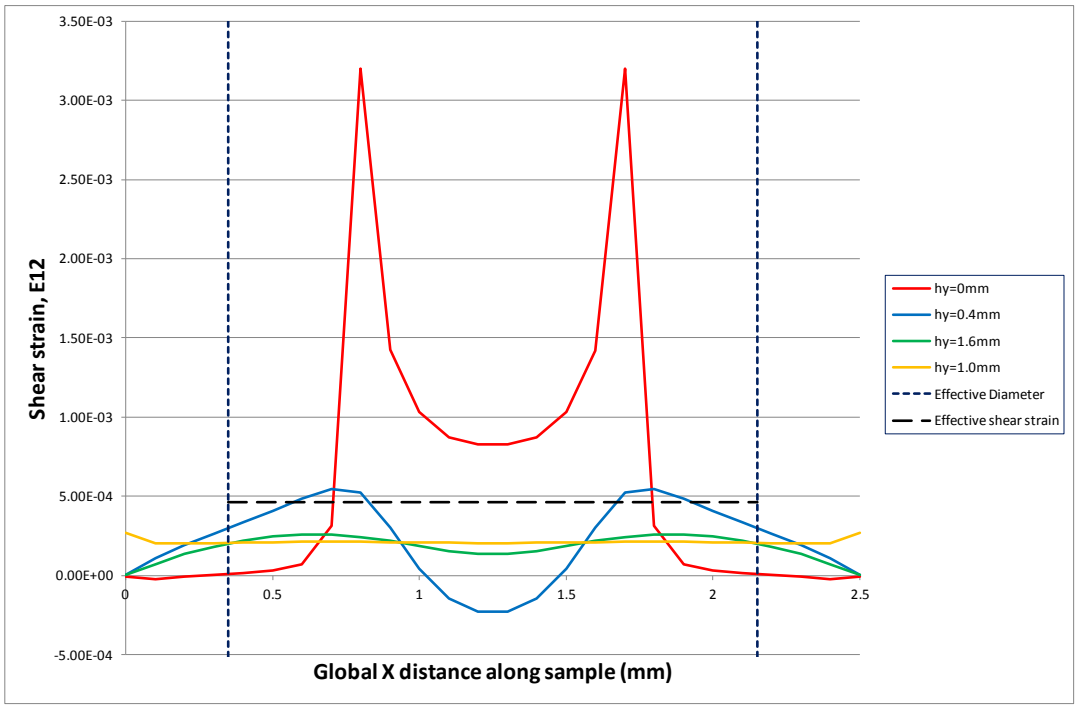

Figure 27: FR4 substrate shear strains extracted at various through-thickness heights along with effective strain and diameter

The relative geometry of the 4 ball sample was used to fit the effective diameter formula (1.44 × the average solder diameter). As a test of the parameterisation described above, the same effective diameter correction factor was applied to the 9-ball Park-Lee sample which has a thinner substrate. Table 10 shows the calculated FR4 shear displacement per unit lateral force, top and bottom substrate displacement combined, with and without the effective diameter correction factor. For comparison, Table 10 also shows the predicted FR4 displacement from an 'idealised' linear FE model of a single connection from the Park-Lee sample. The FE model approximates the solder material as a cylinder of diameter 0.672mm (average solder ball diameter), between two orthotropic FR4 substrates of section 1.27 × 1.27mm (pitch size), with copper/tin pads intentionally omitted. The comparison shows that applying the correction factor, gave shear deformations with a good degree of agreement to corresponding FE data.

	Calculated shear displacement in both FR4 substrates (μm)
Analytical calculation using true interface diameter	3.0075
Analytical calculation using effective interface diameter	1.4504
FE	1.4542

Table 10: Comparison of idealised linear FE with analytical equations for a single Park-Lee connection under 1N load per connection

4.3 **Boundary rotation**

To parameterise the rotation due to an elastic foundation, the following equation, Young and Budynas [2002], was used as a basis: Where $\Delta\theta$ is the rotation of the support boundary, in Radians. M, h_1, and V, are the bending moment per unit width (w), depth of beam and shear force per unit width.

$$\Delta\theta = \frac{16.67 \times M}{\pi \times E \times h_1^2} + \frac{(1-\nu) \times V}{E \times h_1} \qquad (4)$$

However, in citing this equation, it is not made clear that the original author, O'Donnell [1960], derived the expression for a very specific test geometry. A study was therefore carried out to investigate the possibility of generalising this equation for application to the current problem and, indeed, for wider use.

O'Donnell proposed Equation (4) to quantify the rotation of a cantilever beam due to flexibility in the support, and with validation by his own experimental data (given in the

paper) obtained from a unique test-piece design. Figure 28, Top, shows the design with dimensions in inches and Figure 28, bottom, shows the test set-up. Where A, B, C, D, E, F and G are the test cantilever, the reference cantilever, the roller of loading bolster, the cylindrical seat of the loading bolster, the roller of support bolster, the extensometer and the clip gauges.

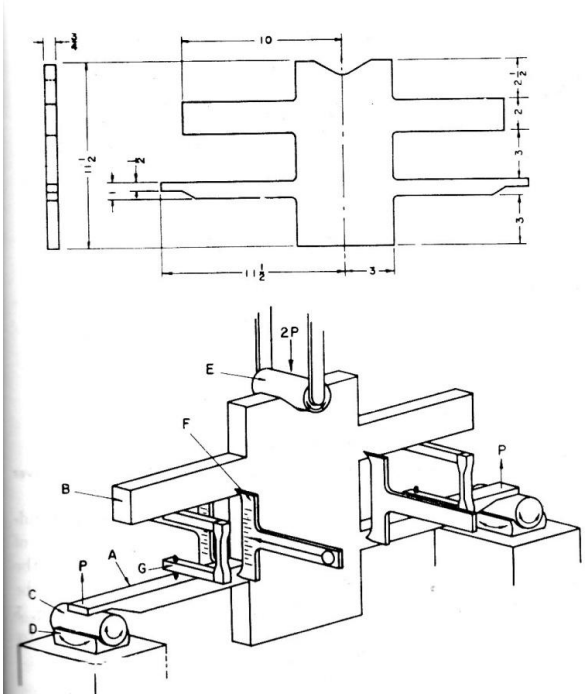

Figure 28: Top: sketch of O'Donnell sample, Bottom: experimental set-up, O'Donnell [1960]

4.3.1 FE analysis of the O'Donnell specimen

To verify the O'Donnell equation, a Finite Element model of the O'Donnell steel test-piece was used to obtain rotations over the range of O'Donnell's original data. Comparison of the hand calculated data with FE calculations showed excellent agreement to within 0.36%. The left hand side of Figure 29 shows the FE model of one half of the O'Donnell test-piece (an appropriate symmetry command was used to model the whole sample). O'Donnell applied a vertical load to the lower built-in beam and measured the rotation at the beam/substrate boundary.

The right hand side of Figure 29 shows a simplified geometry also used during in the investigation and described in section 4.3.2. The original O'Donnell (OD) sample was cut from a single sheet of steel of uniform thickness, the beam being of rectangular cross-section, built into a support made from the same isotropic material, and was subject to a shear force and a bending moment. As a first stage in likening the FE model to BGA fixing methods, approximating the true X-plane symmetry boundary condition to a Y=0 edge and an encastré command in the same X-plane was found to make no difference to calculations.

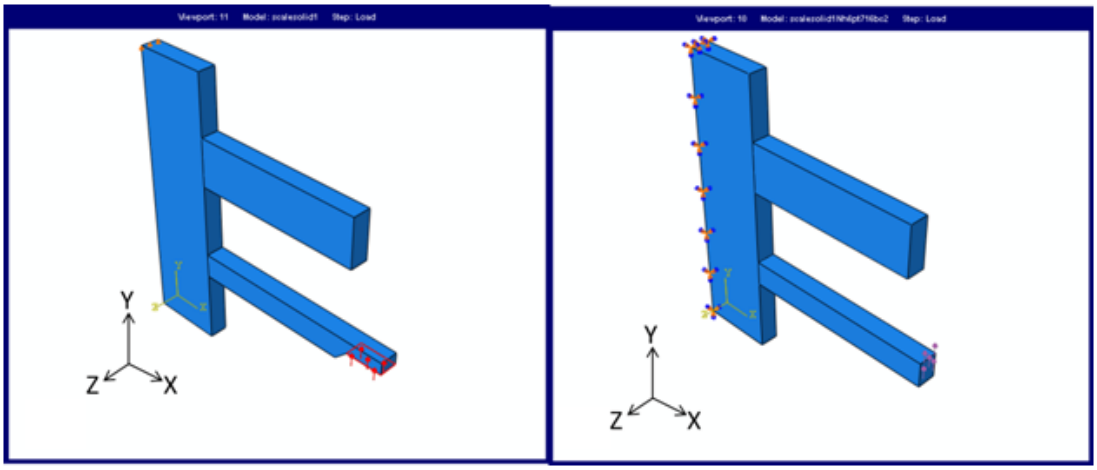

Figure 29: Left hand side: FE model of one half of the O'Donnell test piece, Right hand side: FE model of a simplified geometry

As noted by O'Donnell in his original paper, the rotations vary across the depth of the beam boundary and he took care to extrapolate his measured rotations to the beam centreline. To simulate this, the FE rotations were calculated, by extracting the longitudinal displacement of the beam from nodes closest to either side of the neutral axis of the beam. The combined displacement of both nodes (U1) was divided by the distance between the specified nodes to obtain rotation. The exact value extracted for rotation is therefore dependent on distance between selected nodes, and it is very important in the FE analysis to use a consistent mesh refinement.

To illustrate the method used to obtain FE rotation data, Figure 30 shows FE-calculated longitudinal boundary displacements (U1) for different beams under 1N load, where U1 is the displacement in the X direction, orientation as shown in Figure 29. The data shown has been extracted from models used later in the current study, see sections 4.3.3 and 4.3.5. Deflections calculated from the FE model have been extracted through the beam depth, Y, on the vertical centreline and at the boundary with the substrate.

The data shown in Figure 30 includes displacements from two long beams of length equivalent to the original OD sample beam length, and two short beams of length approximately proportionate to the 4 ball Ghaleeh BGA sample solder height (with respect to beam cross sectional area).

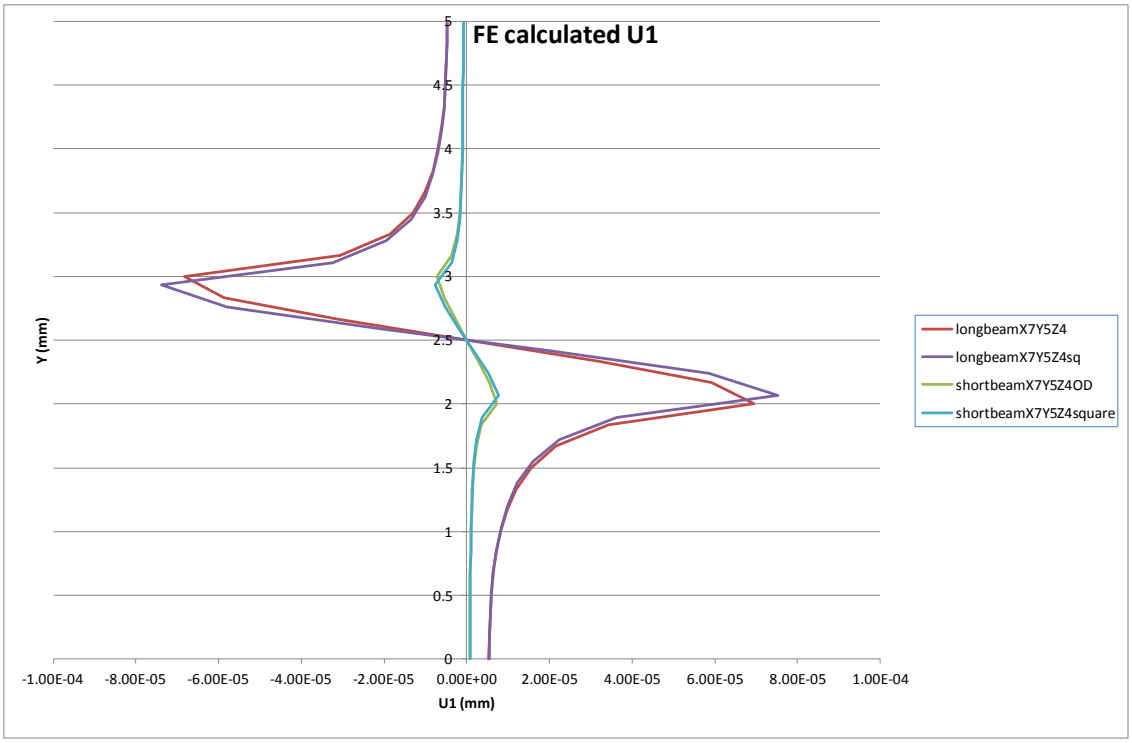

Figure 30: Boundary deflections through the beam depth, Y, for long beams and short beams of square and rectangular cross sections, under 1N load

Geometry of the FE models used to generate the data shown in Figure 30 is described in Table 11. Boundary rotation is clearly visible in the short beam model. In comparison, the long beam models show considerably more U1 lateral boundary displacement, as expected due to a higher value of applied moment. All models shown have the original

OD beam cross sectional area (CSA 0.75mm^2), one of each of length having the original OD beam shape and one having a square cross section shape. Beam shape (with constant CSA and subsequent small change in *I*) is shown to have a small effect, for this model design and value of *I*.

FE model label	Description of FE model geometry
longbeamX7Y5Z4	Beam length/beam depth ratio is 7, beam cross-section shape is as per original O'Donnell specimen, beam depth is scaled to unity, substrate geometry is modified from original O'Donnell specimen to saturation of substrate volume effect as described in Chapter 4.
longbeamX7Y5Z4sq	Beam length/beam depth ratio is 7, beam cross-section shape is square, beam depth is scaled to unity, substrate geometry is modified from original O'Donnell specimen to saturation of substrate volume effect as described in Chapter 4.
shortbeamX7Y5Z4OD	Beam length/beam depth ratio is 0.8, beam cross-section shape is as per original O'Donnell specimen, beam depth is scaled to unity, substrate geometry is modified from original O'Donnell specimen to saturation of substrate volume effect as described in Chapter 4.
shortbeamX7Y5Z4square	Beam length/beam depth ratio is 0.8, beam cross-section shape is square, beam depth is scaled to unity, substrate geometry is modified from original O'Donnell specimen to saturation of substrate volume effect as described in Chapter 4.

Table 11: Explanation of FE model labels used in Figure 30 legend

4.3.2 Applying the O'Donnell equation to BGA designs

Having determined excellent agreement between O'Donnell's Equation (4) and FEA calculated displacements for the original O'Donnell geometry, next Equation (4) was used to calculate rotations for a simplified representation of the 4-ball sample, Ghaleeh [2015]. The simplified model, shown in Figure 13 approximates the solder ball as a cylinder, with the joint consisting of only solder and composite substrate material, i.e. no copper pad, metallic finish, or intermetallic layer. Previous calculations of whole sample displacements made using this simplified FE model have shown good agreement to whole sample displacement data from a more detailed FE model of the full 4 ball BGA sample and measurements, see Figure 24.

Rotations were calculated using both the simplified FE model shown in Figure 13 left hand side and Equation (4), with solder and FR4 materials defined using a single modulus value of 3000 MPa, i.e. the substrate through thickness modulus. For inputs w and h_1, the solder average diameter was used. For beam length, solder height was used. For Young's modulus and Poisson's ratio, the through-thickness properties of the orthotropic FR4 support were used. The calculated rotations for this geometry differed by 22%, which is perhaps unsurprising given the obvious differences between the OD test piece and the BGA specimens, shown in Figure 31 and discussed in detail below.

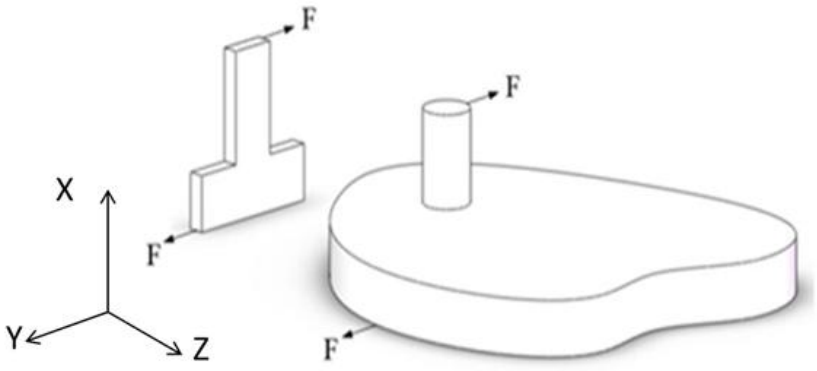

Figure 31: Comparing O'Donnell sample substrate shape with typical BGA solder joint (approximated as a cylinder)

It was assumed that FE analysis could be used to modify Equation (4) to confidently extend the range of applicability of the O'Donnell equation, in particular to predict rotations in BGAs. Therefore before using equation (4) to predict boundary rotations in a BGA sample, the following differences need to be considered and taken account of;

When applying the analytical parametric solution to BGAs, it is assumed that the solder column is the beam and the FR4 composite is the support.

1) Length of beam/depth of beam or aspect ratio

2) Substrate shape and volume, proportionate to beam dimensions

3) Shape of beam cross sectional area (CSA)

4) Substrate and beam elastic moduli

5) Solder joint boundary conditions

The following sections investigate each design effect, in turn. Before commencing the parametric study, the beam length of the O'Donnell sample was reduced slightly in order to apply an equivalent surface traction boundary condition on one vertical plane (as opposed to O'Donnell's original pressure on a horizontal plane), see Figure 29 right hand side. This modification simplified the modelling process whilst having no effect on the FE results.

The O'Donnell FE model was then scaled to have a beam Cross Sectional Area (CSA) close to the 4-ball sample joint interface CSA. As expected, the excellent agreement with Equation (4) was preserved (within 0.3%). This CSA-scaled model (still with a relatively long cantilever) is referred to as “OD Scale” and will be used extensively as a reference in the following parametric FE study. The OD Scale model material remains unchanged (uniform steel) and the beam is a cantilever.

4.3.3 Effect of beam length on rotation

The solder joint aspect ratio, length divided by diameter, is significantly different to that of the original O'Donnell sample, making the proportion of shear stress to bending stress considerably different for a given applied force, see Figure 6 and Figure 28. The isolated effect of aspect ratio on accuracy of calculations made using Equation (4) is investigated here.

Starting with the OD Scale model geometry of original uniform steel, the beam length was progressively reduced and the response to a surface traction load of 1N was calculated for each length using both FE and Equation (4). The resulting rotation, as a ratio of FE to Equation (4) calculated values, is plotted in Figure 32 as a function of beam length/depth ratio.

As can be seen in Figure 32, Equation (4) reproduces the FE calculated rotations only for relatively slender columns. Agreeing to within 2% for length/ depth ratios above 3. As the beam length gets shorter, significant errors can result. For example, considering the ratio for the 4-ball sample geometry, Ghaleeh [2015] with a beam length to beam depth ratio of 0.89 shown dotted in Figure 32, Equation (4) overestimates the rotation by about 18%. As the aspect ratio approaches zero, corresponding to pure shear, the overestimate goes through a maximum (minimum on the curve) of about 80%, returning to around 25% in the pure shear limit.

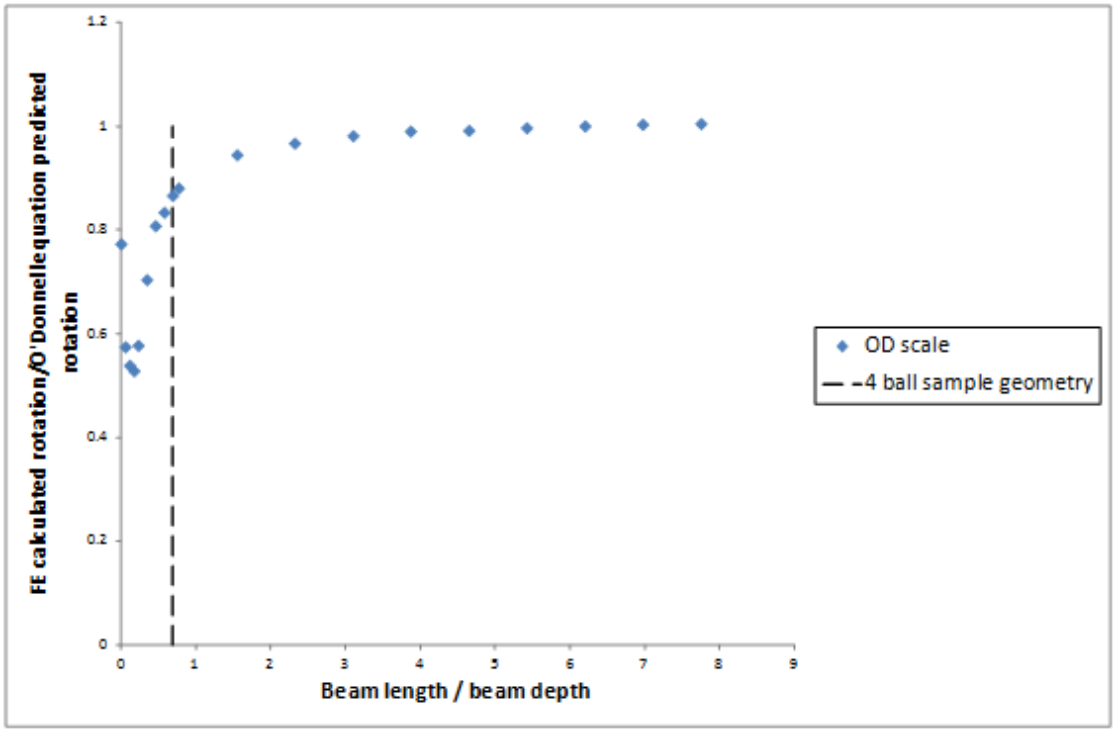

Figure 32: Effect of beam length/beam depth on accuracy of Equation (4) compared with FE model. Dotted line corresponds to 4-ball geometry

A third order polynomial was fitted to the data in Figure 32, proposed for use within the limits of beam length/beam depth ratios of 0.69 to 6.97, which covers all practical cases considered and also fits with the OD Scale model. The resulting correction factor, C_2, is represented by Equation (5) where x is the beam length/beam depth ratio. For example, the calculated correction for the simplified 4-ball sample is 0.89. The quality of the fit is shown in Figure 33, on average less than 1% different to the value determined by FEA:

$$C_2 = 0.0017x^3 - 0.0253x^2 + 0.1219x + 0.7999. \qquad (5)$$

It is intended that these reported equations and corresponding parameters could be used for independent verification of the work, and to this end an unusual number of significant figures have been shown in all rotation correction factor equation multipliers as the calculated correction factor value is highly sensitive to the equation multiplier values.

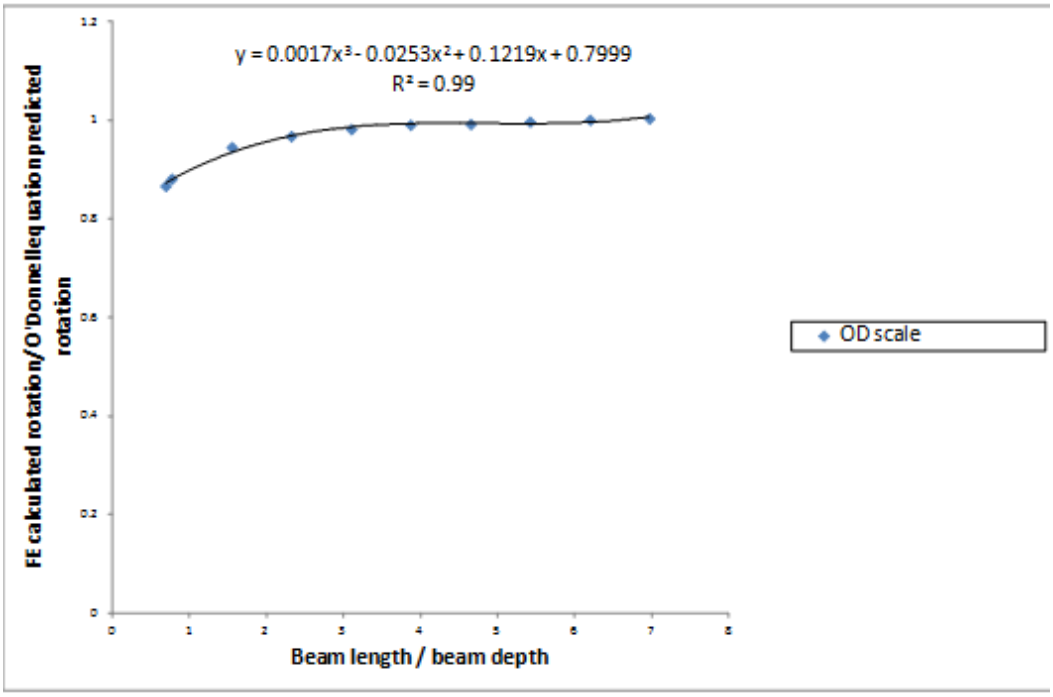

Figure 33: Best-fit polynomial for boundary rotation beam length correction factor, C_2

4.3.4 Effect of substrate volume on rotation

One key difference between the OD Scale model and a solder BGA ball is the volume of substrate surrounding the contact area. As can be seen in the schematic representation in Figure 31 the volume effect has three dimensions, X, Y and Z and these are considered in turn in each of the following sub-sections. In reality commercial substrate through thickness height can be a factor of 5 larger than the BGA solder height, but this detail has been ignored here in order that both scaled sample designs could be shown together.

To investigate the effect of substrate size and volume on boundary rotation, the OD Scale model was progressively altered towards the 4 ball sample substrate geometry. The discrete effects of each of the three substrate dimensions (Y, X, Z, as shown in Figure 31) were examined by sequentially reducing or increasing the relevant dimension, keeping all other model dimensions constant. For comparison the sketch uses the same coordinate system shown in Figure 29. Again the resultant FE rotations, under 1N load, were compared to Equation (4) calculations and plotted.

4.3.4.1 Substrate Y dimension effect on rotation

The substrate Y dimension was sequentially reduced, starting from the OD Scale model down to the minimum value of unity, all other original OD dimensions being kept constant, orientation shown in Figure 34. As before, the results are presented, see Figure 35, as the ratio of the FE calculations to the Equation (4) hand calculations against substrate Y dimension/beam Y dimension (substrate Y ratio). The original OD and 4-ball sample substrate Y ratios are also shown in Figure 35, where pitch has been used as the BGA substrate Y dimension. It was not felt necessary to show calculations for Y ratios above 10 as the effect has reached saturation at Y ratio's well below 10.

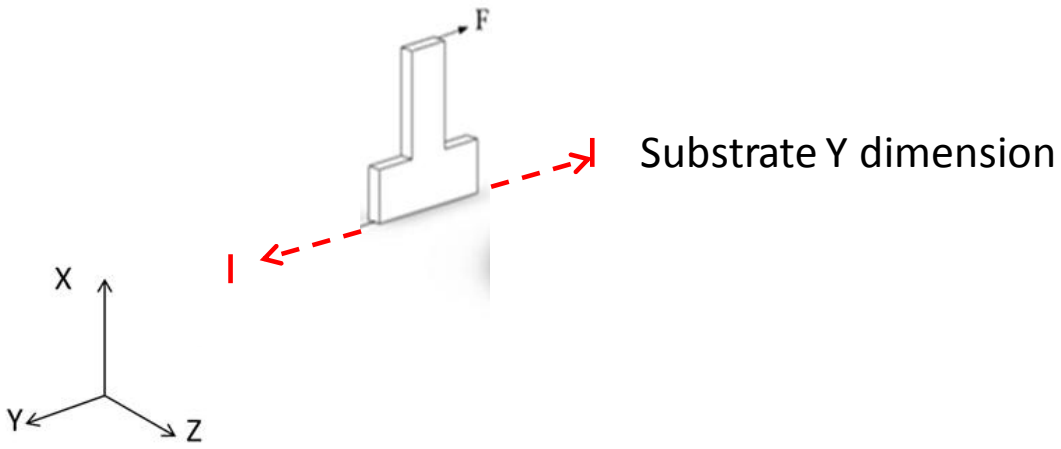

Figure 34: Visualisation of substrate Y dimension, sequentially reduced in FE models from original O'Donnell design towards BGA designs and unity

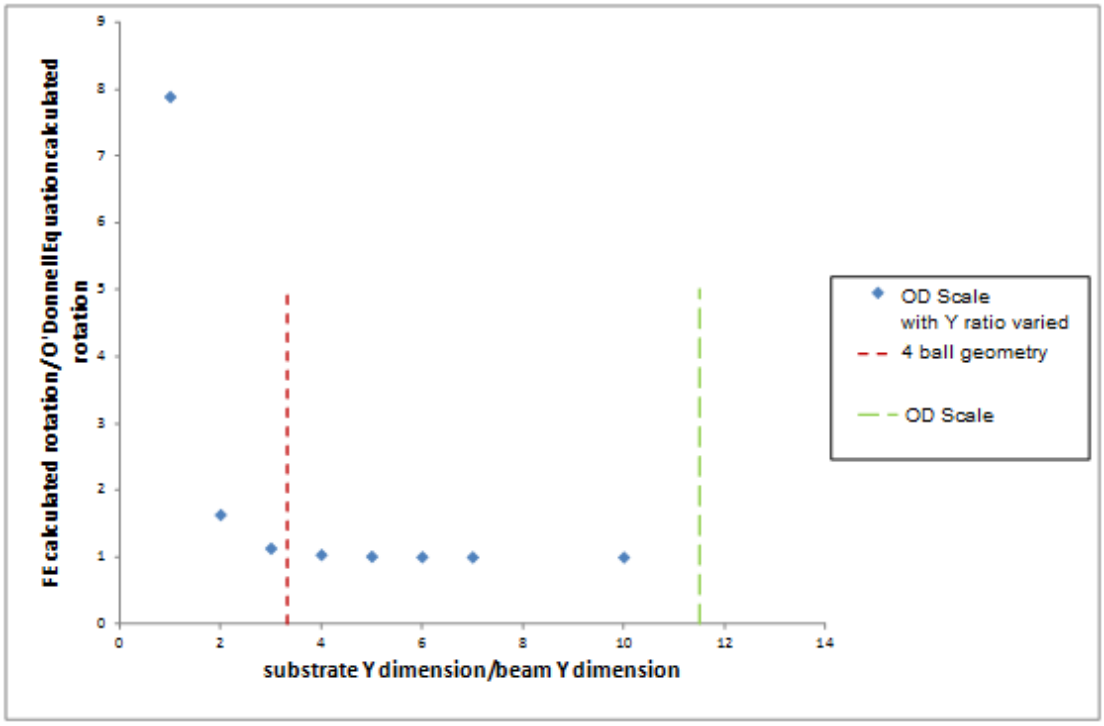

Figure 35: Effect of substrate Y dimension reduction on accuracy of Equation (4)

Figure 35 shows that for substrates of Y ratio above 5, substrate Y dimension/beam Y dimension, the Y dimension effect has saturated and FE calculated rotations give agreement to O'Donnell's Equation (4) to within 1%.

It was noted, as substrate Y value is reduced, the substrate itself is able to act as a beam and contributes additional rotation/deflection and, in the limit where the Y-ratio is unity, the substrate depth essentially adds to the length of the beam and the rotation is entirely due to the local slope of the beam at the "interface". At a Y- ratio equivalent to the 4-ball sample (3.33), Equation (4) underestimates the FE-calculated rotation by about 6%. For ratios below 3 this effect rapidly increases to a maximum factor of about 8 (typical commercial BGA geometries have Y ratios of around 1.6 to 1.7, Selex ES [2015], Altera [2014], Intel [2010]).

To account for the effect of variations in Y substrate dimension on rotation a fourth order polynomial was fitted to the data in Figure 35, for Y ratios between 2 and 10, and is correction factor C_4:

$$C_4 = 0.003x^4 - 0.070x^3 + 0.649x^2 - 2.562x + 4.676. \qquad (6)$$

As indicated by the R^2 number, using a 4th order polynomial ensured a good fit when comparing the calculation to FE data over the range of beam lengths selected. As shown in Figure 36. Where x is substrate Y-ratio. Again the number of parameter multiplier significant figures shown reflects the detail required for any future independent verification.

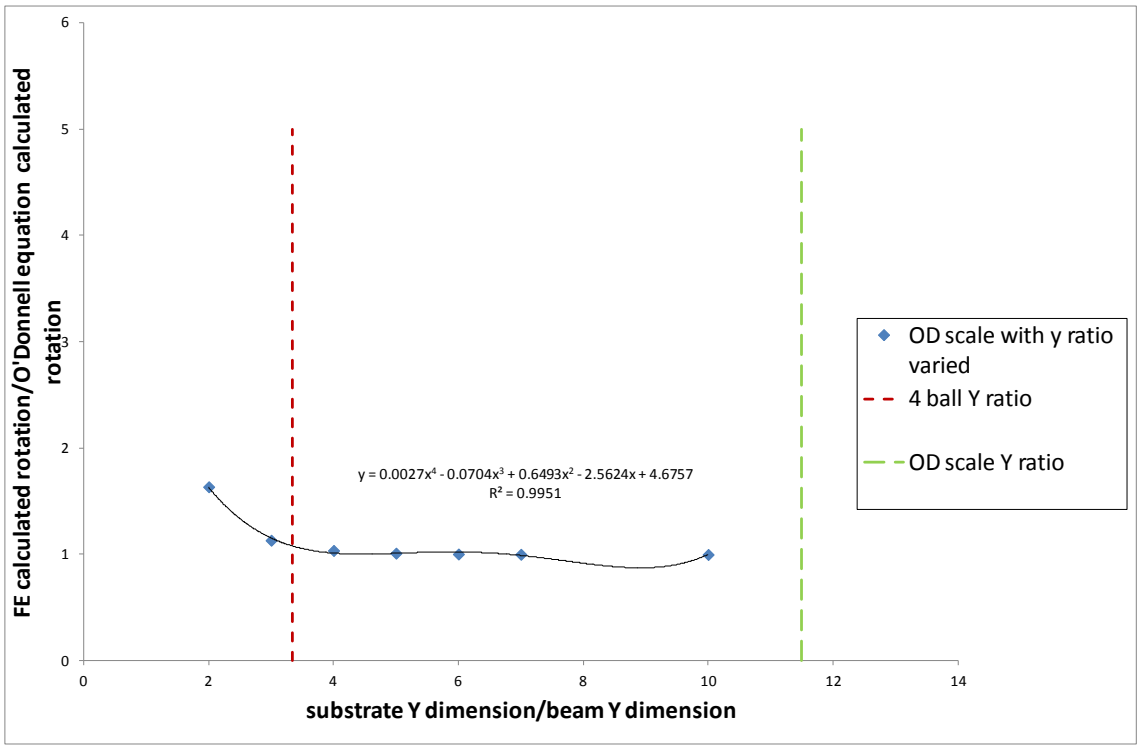

Figure 36: Best-fit polynomial for boundary rotation substrate Y ratio correction factor, C4

4.3.4.2 Substrate X dimension effect on rotation

To observe and quantify the substrate X dimension effect (through thickness), the OD Scale model substrate X dimension was progressively reduced, then increased, following the global coordinate system shown in Figure 31. The Y-ratio was kept constant at 5, to be within the saturation of the Y-ratio effect, but not excessively so. A unity beam depth (beam Y-dimension) was used and the X ratio was defined as the X-dimension (i.e. substrate thickness/beam depth where beam depth is 1). All other OD Scale model dimensions were kept constant.

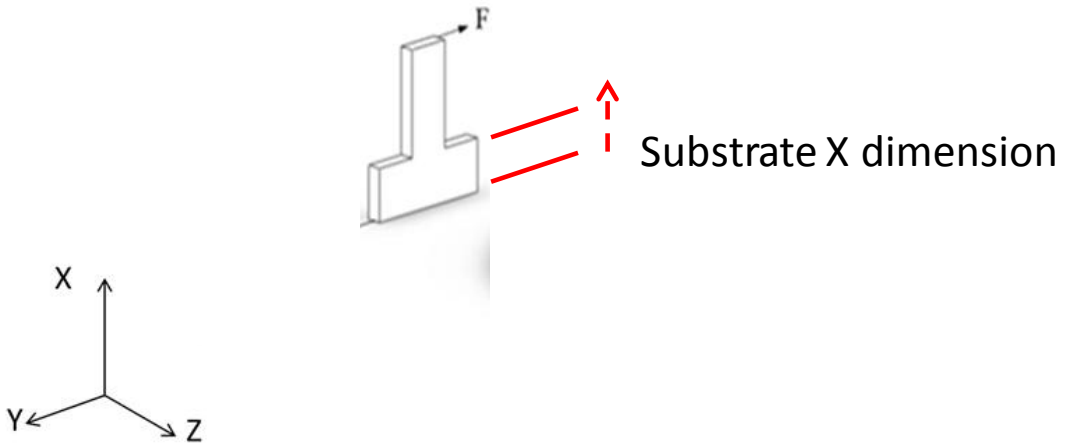

Figure 37: Visualisation of substrate X dimension, sequentially varied in FE models from original O'Donnell design towards BGA designs

As before, the FE calculations were compared to the analytical ones using a ratio, and the results are plotted in Figure 38 as a function of X-ratio. The process was repeated for both the OD Scale long beam and short beam models. The OD Scale model's substrate X-ratio (equal to 3) is shown on Figure 38 as a vertical dotted line and, as expected, there is 100% agreement between FE and Equation (4) for the long beam at this ratio. Reducing the X-ratio (to represent thin substrates) results in an overestimate of rotation by Equation (4), whereas increasing the X-ratio causes an increasing underestimate, which, unlike the Y-ratio, does not saturate for very thick substrates. The short beam changes more rapidly than the long beam at X-ratios above 3 and gives a similar overestimate for thin substrates.

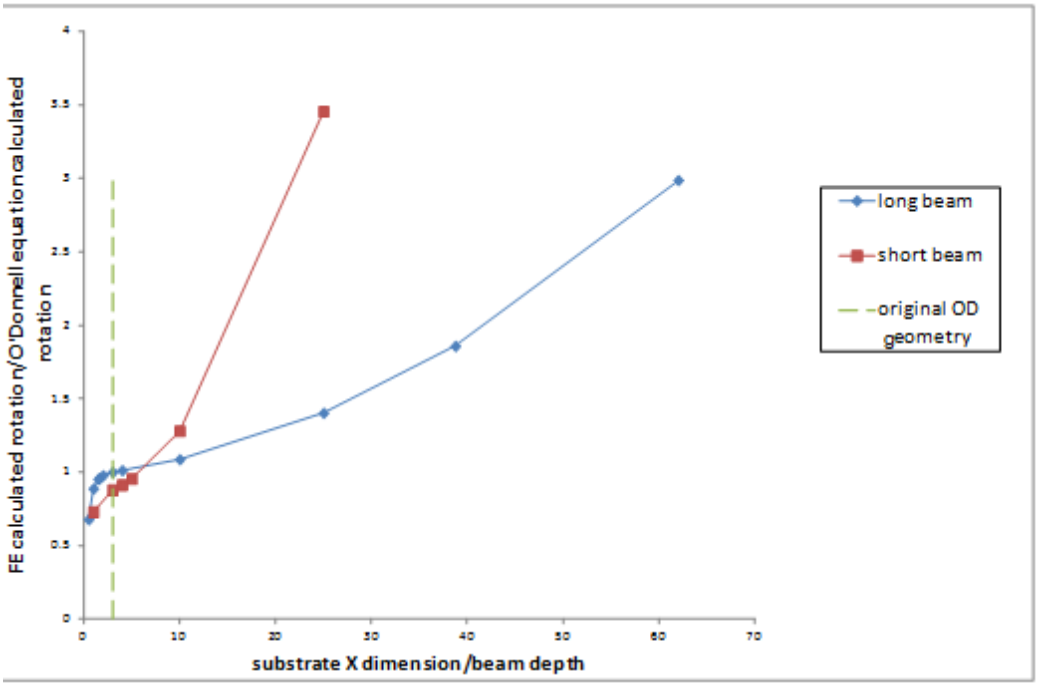

Figure 38: Effect of X-ratio (substrate thickness) on accuracy of Equation (4), Y ratio = 5 throughout

The 4-ball sample equivalent geometry, considered during the current study, has an X-ratio of about 2.3 and commercial BGA PCB substrates thickness can vary greatly, Selex ES [2015]. The Original O'Donnell design and OD scale model dimension X-ratio is 3. Where dimension-ratio values are below 3 the encastré boundary condition dominates beam response, reducing boundary rotation, assuming of course that the substrate itself is attached to a rigid base. If not, the modelling would have to be extended to include additional components, making a simple analytical solution less likely. As the intention here is to provide an analytical solution for shear test samples that are assumed to be rigidly constrained within the test set-up, alternative constraints were not considered.

For X-ratios larger than 3, the substrate itself acts as a beam and contributes its own deflections/rotations (additional to the original boundary rotations, and similar to the effect shown in the above Y-ratio study, Figure 35). An extra Y constraint was added to the FE models, to attempt to isolate the boundary rotation of interest and exclude the

increasing global rotations of the specimen/bulk substrate deflections, keeping the Y-ratio at 5. Figure 39 shows that this additional Y constraint removes the large underestimates associated with large X-ratios, but has little effect on the rotations for X-ratios from 3 downwards. For X-ratios of 2 and above, the FE calculated rotations (long beam) are in agreement with Equation (4) to within 3% and the X-ratio effect saturates (thick substrate limit) at X-ratios of between 5 and 8.

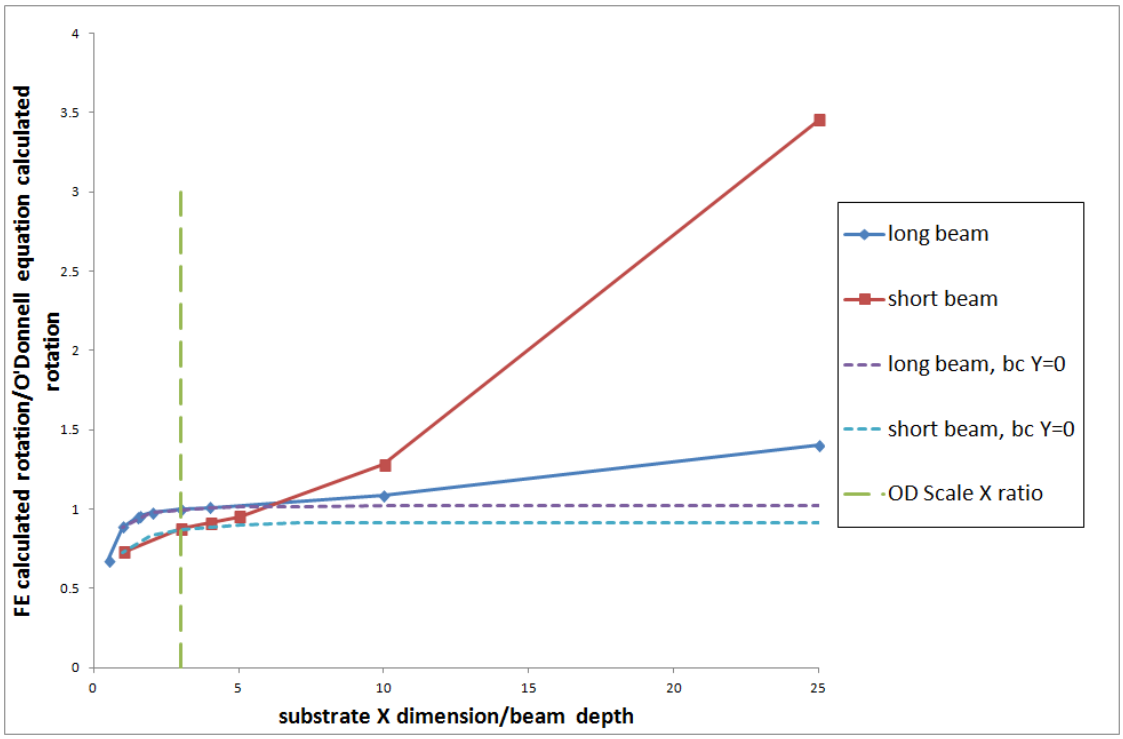

Figure 39: Effect of X-ratio (substrate thickness) on accuracy of Equation (4) modified to remove substrate beam effect. Y ratio = 5 throughout

To determine a substrate X dimension correction factor, Equation (7) was fit to the data shown in Figure 39, with the additional Y constraint, valid for substrate X dimension ratios of 1 to 10 and for the long beam:

$$C_3 = -0.0003x^4 + 0.0072x^3 - 0.0612x^2 + 0.220x + 0.722. \qquad (7)$$

This is also shown in Figure 40, along with the polynomial equation for the short beam. Again, an unusual number of parameter multiplier significant figures have been shown, so that the detail could be used in future independent verification.

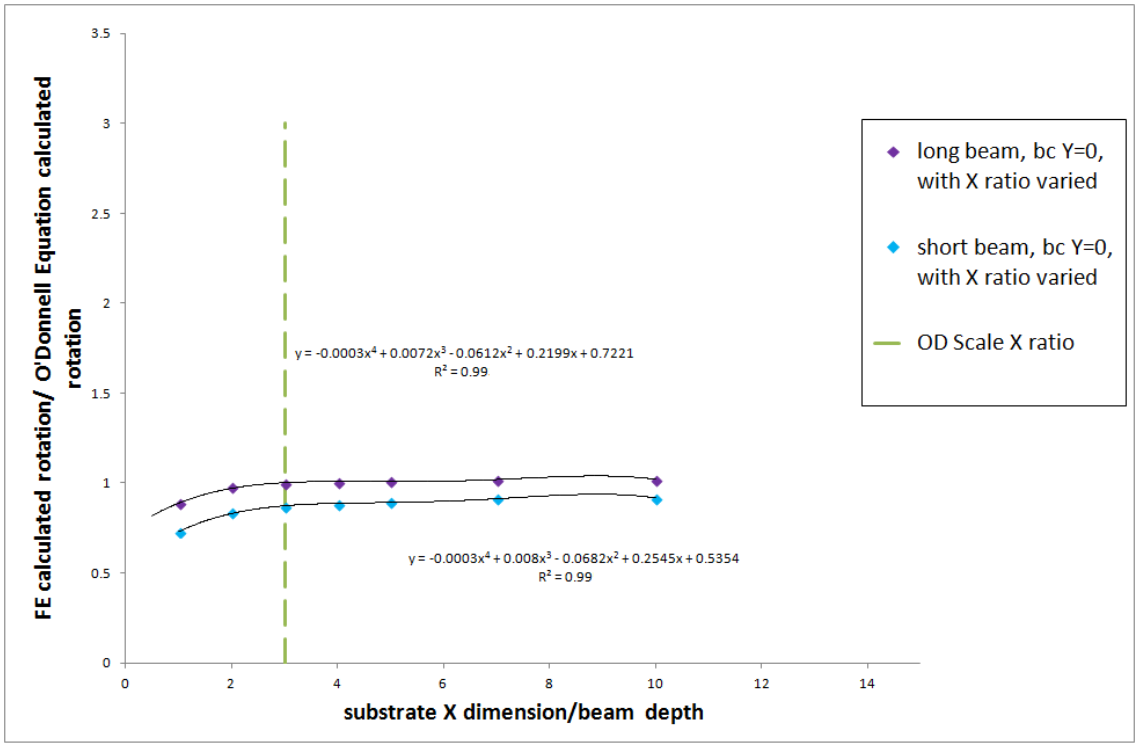

Figure 40: Best-fit polynomial for boundary rotation substrate X ratio correction factor, $C_{3,}$ for long and short beam

4.3.4.3 Substrate Z dimension effect on rotation

The original OD specimen has a uniform thickness over substrate and beam, as shown in Figure 31, left hand side, and Figure 41. The equivalent BGA sample substrate dimension (pitch size) is much larger than the solder joint diameter, Figure 31 left hand side.

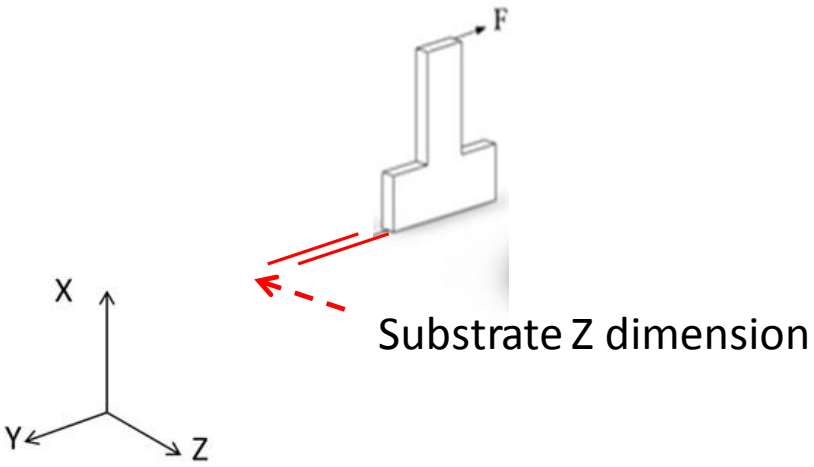

Figure 41: Visualisation of substrate Z dimension, sequentially varied in FE models from original O'Donnell design dimensions towards dimensions of BGA designs

Pitch size can vary widely between individual joints, although, in a commercial BGA it is common for the substrate Z-ratio (BGA pitch/beam width) to be less than 3. To approximate the typical geometry of BGA samples (and to isolate the substrate Z dimension effect on rotation) requires expanding the substrate in the Z direction. Again the global coordinate system shown in Figure 29 and initially the OD Scale, 'long' beam, model was used.

In the FE modelling the substrate Z-ratio (substrate thickness/beam thickness) was sequentially increased from the OD value of unity and the corresponding agreement between Equation (4) again expressed as a ratio, the results being shown in Figure 42. The effect can be seen to saturate at an overestimate of rotation of about 40% with substrate Z ratios of 3.5 and above.

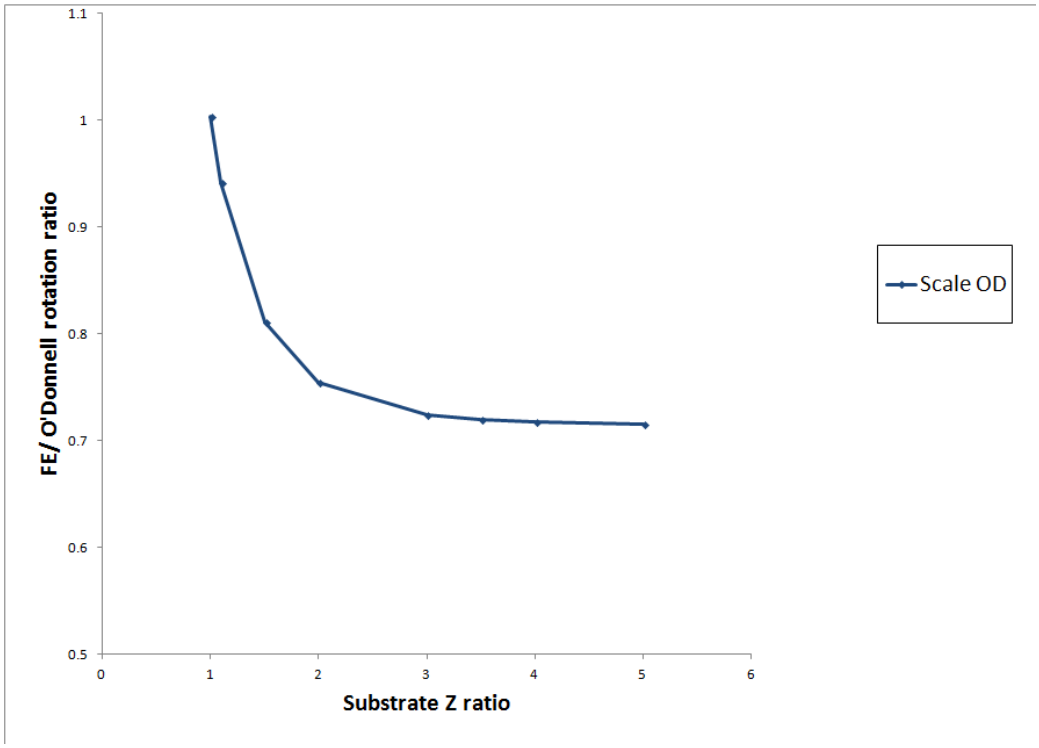

Figure 42: Effect of Z-ratio (substrate thickness) on accuracy of Equation (4) modified to remove substrate beam effect.

The procedure of expanding the Z substrate dimension was repeated, using the short beam model, but here the OD Scale model substrate X and Y dimensions were modified to an X ratio of 7, and Y ratio of 5, i.e. within effect saturation as described above in section 4.3.4.1 and 4.3.4.2, expanding the X ratio to isolate substrate thickness (Z) effect from X ratio effect. Reducing the Y ratio, whilst remaining within effect saturation, reduced required computation effort. Calculations were repeated for both long and short beams. The agreement of FE calculations to Equation (4) with respect to changing Z ratios is shown in *Figure 43*. This X, Y substrate reduction increased the agreement of FEA to (4) by within 1% for the long beam model and by about 10% for the short beam.

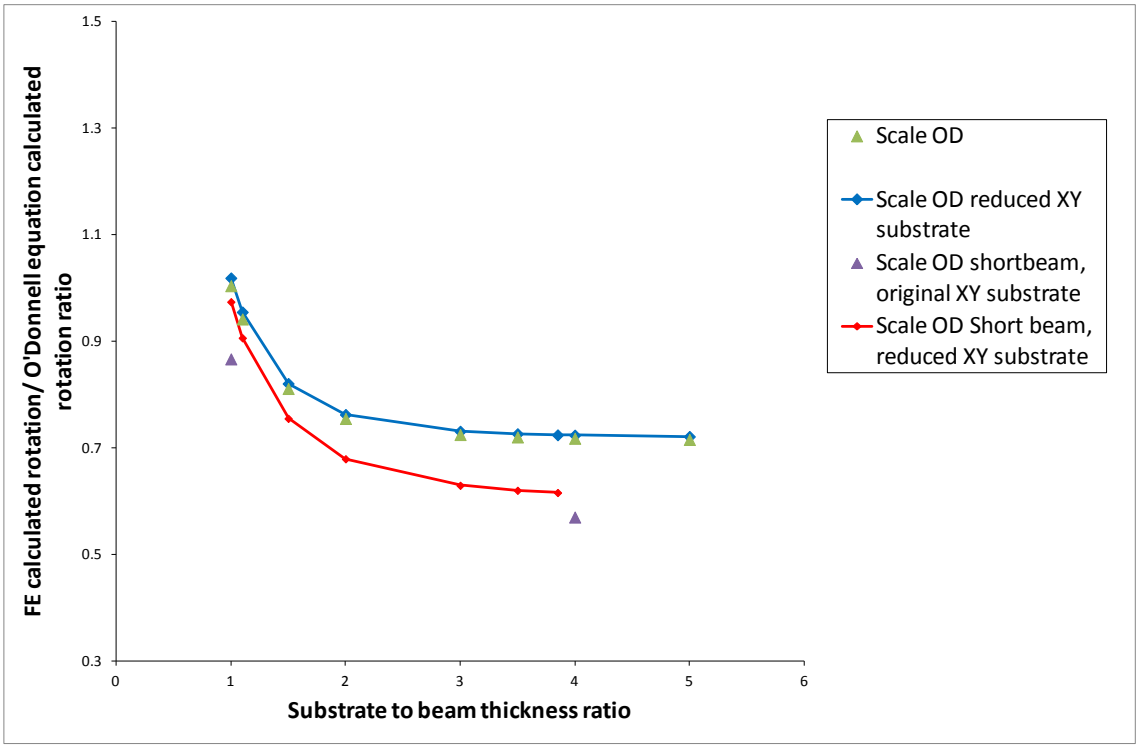

Figure 43: Effect of Z-ratio (substrate thickness) on accuracy of Equation (4) for long and short beams, with and without substrate X and Y ratio's reduced

To determine a substrate thickness correction factor, a polynomial equation was fit to the data, see Figure 44, valid for substrate Z dimension ratios of 1 to 3.85, for the short and long beam. The correction factor for the long beam model is:

$$C_5 = -0.0407x^3 + 0.364x^2 - 1.06x + 1.75. \qquad (8)$$

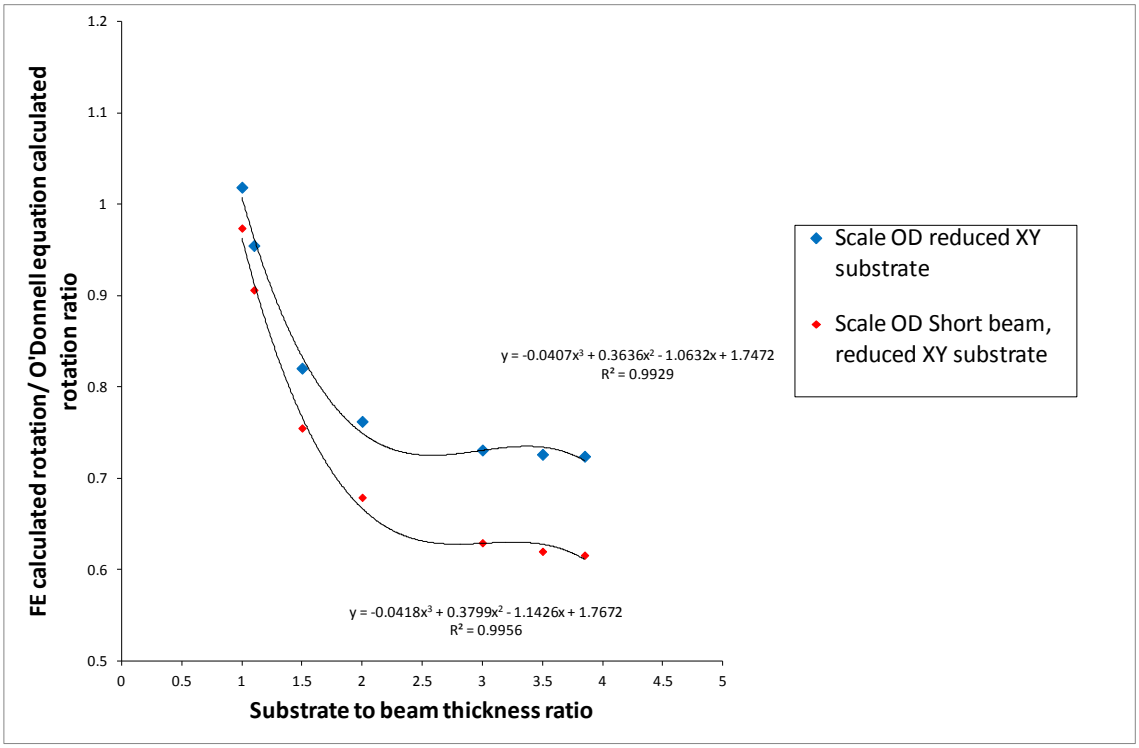

Figure 44: Best-fit polynomial for boundary rotation substrate Z ratio correction factor, $C_{5,}$ for long and short beam

4.3.5 Effect of shape of beam cross-section on rotation

So far, the modifications to the OD Scale model have not addressed the fact that O'Donnell's data was obtained from a beam of rectangular cross section, with width equal to 0.75depth. To investigate the effect of beam shape on FE calculated boundary rotations, models were generated for the following beam cross section shapes; the OD Scale model, circle, square, and rectangle of depth equal to 0.75width. Again, a steel cantilever was considered with a traction load applied to the FE models. To isolate beam shape effect, models with the 'long' beam length only were used (beam length to beam depth ratio of 7.75), and the same boundary conditions are used as in the previous section (X-Encastré, Y=0) were again used.

Comparing FE calculated rotations in beams of the same CSA but different shapes showed considerable scatter. Comparing these rotations with their corresponding *I* value shows improved agreement in the correlation between the different shaped beams,

as could be expected. It is generally understood that, under a given load, beams of different shapes but same CSA produce very different rotations and beams of different shape but the same *I* value are normally expected to give similar results.

Figure 45 shows the calculated boundary rotations with 1N load applied to models of increasing second moment of area (*I*), for each shape. The analytical calculations using Equation (4) are shown alongside as solid lines and the FE calculations are shown as dashed lines. Only one 'shallow wide' rectangle cross-section beam model was run at a CSA equivalent to the 4-ball sample joint, shown as a pint on Figure 45.

When calculating rotation Equation (4) takes into account width and breadth and is therefore able to distinguish between a rectangle and a square of the same *I* value. This is not so with a circular cross section, so an analytical calculation of rotation in a beam of circle cross-section is not possible. The FE predicted rotations were always smaller than the Equation (4) predicted rotations, this being a consequence of using the modified OD Scale model substrate with saturated volume effects (dimension ratio of X is 7, Y is 5, Z is 4).

Comparing calculated rotations, for a specific *I* value larger than 0.025mm^4, whether by FE or by Equation (4), shows negligible difference with respect to beam shape. So beam shape has been shown irrelevant for the purposes of Equation (4) when considering constant second moment of area, *I*, values above 0.025mm^4. For smaller second moment of area values the agreement quickly diverges. It is common for BGA solder connections have *I* values lower than 0.025 mm^4. (this would equate to cylinders of diameter 0.845mm or smaller).

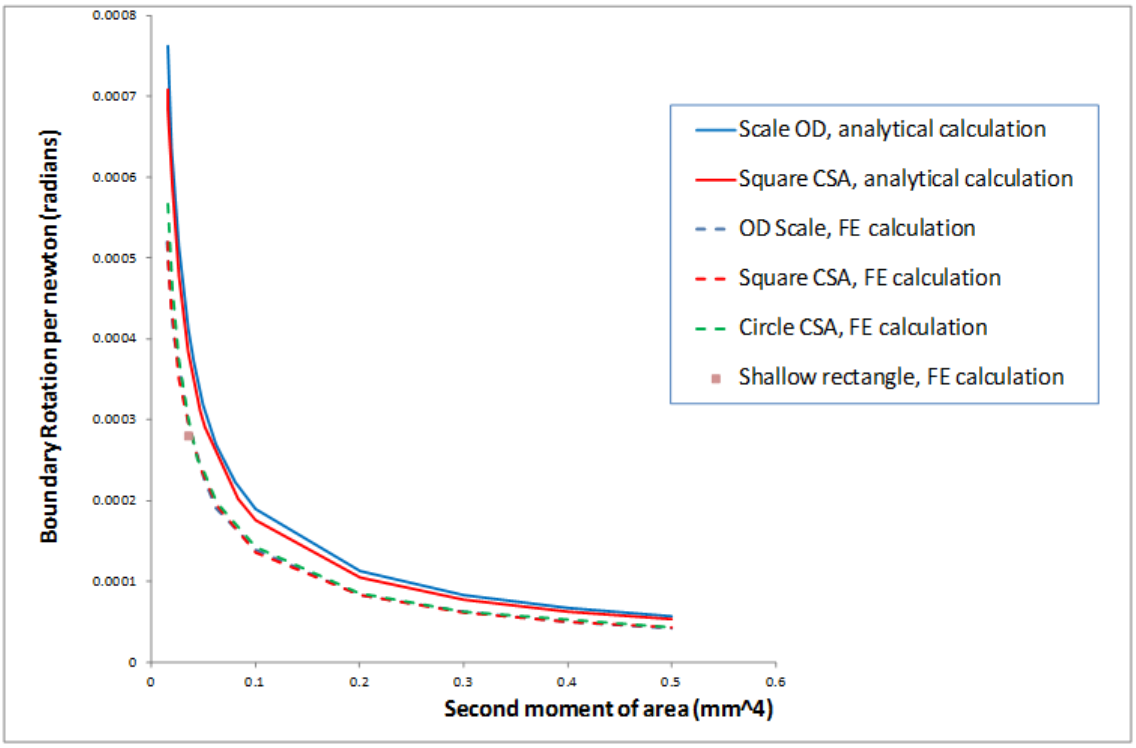

Figure 45: Effect of section shape and second moment of area on rotations calculated using FEA and Equation (4)

Figure 45 shows that FE calculations of Boundary rotation depend on second moment of area not shape as implied by Equation (4), O'Donnell [1960], and the shape effect is negligible for second moment of area, *I*, values larger than 0.025mm^4, for the substrate volume considered.

When applying Equation (4) in cases of circular cross-section, it is sensible to substitute true dimensions for dimensions proportionate to O'Donnell's rectangle cross section (width equal to 0.75depth), preserving the original beam second moment of area value, and for the new width and depth values to be input into Equation (4).

For cases of circular cross-section combined with a very low I value (as in the current problem) a correction factor is required. For example the 4-ball sample, *I*=0.01533 mm^4 and average diameter of connection 0.75mm, Figure 46 which shows that the difference between FE predictions for a circle and scale OD CS is 8.26% (correction

factor =1.083). For a universally applicable BGA constitutive behaviour solution, an accurately determined correction factor for lower I values would be required.

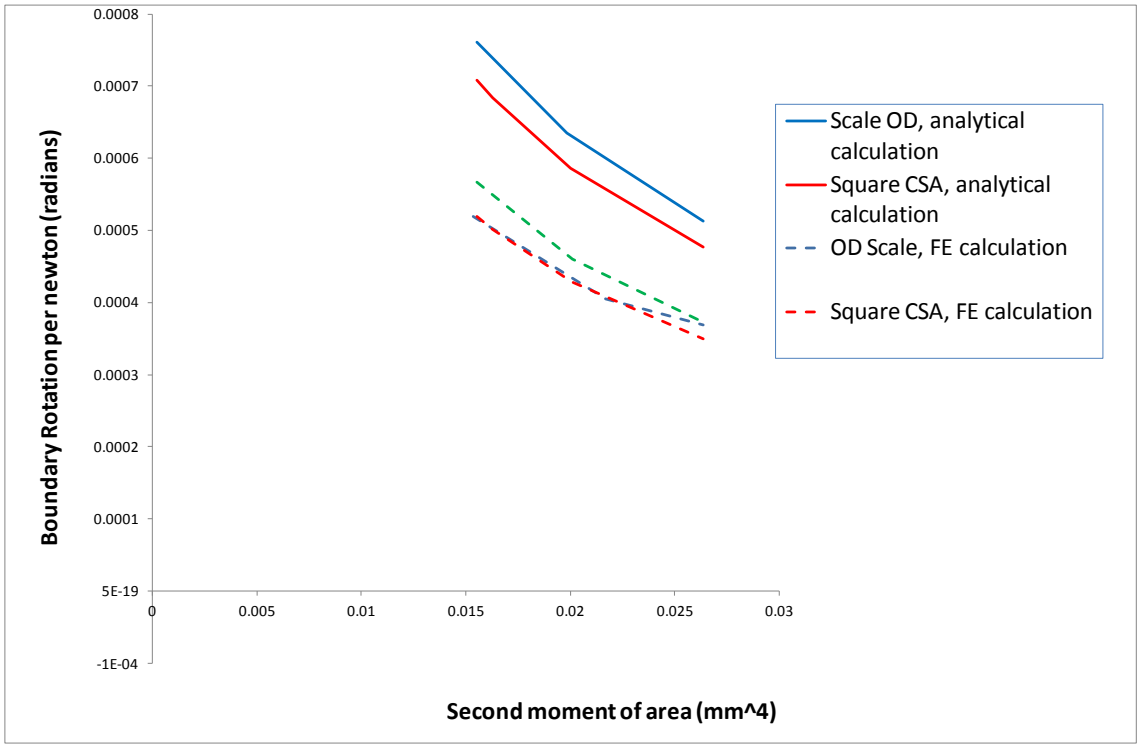

Figure 46: Close up of Figure 45

4.3.6 Effect of mixed materials and determining an effective modulus on rotation

O'Donnell's equation assumes a uniform material, but solder may be used to join many different materials, often in layers, some of which can be very thin. Furthermore, samples used to investigate solder behaviour may similarly use a variety of materials to hold the solder balls in place, including parts of real devices, such as BGAs. To make this investigation manageable, the current focus in on the behaviour of a solder connection (beam) connected to substrates only of FR4 composite, which has a low through thickness modulus relative to the solder.

When using Equation (4) to determine boundary rotations in a system of mixed materials, it was assumed sensible to use the through thickness substrate value of

Young's modulus, *E*, and Poisson's ratio, ν, as equation inputs. This approach was shown to be sensible in the following study.

First Predicted rotations made using Equation (4), with the suggested through thickness substrate value of Young's modulus, *E*, and Poisson's ratio, ν, as equation inputs, were compared to more realistic FEA using a mixed materials system of solder beam and a orthotropic FR4 substrate. Reasonably good agreement was achieved. Next in the FE model the orthotrpic substrate material values were substituted for the same isotropic values used in Equation (4) calculation. The reasonably good agreement was preseved.

After substituting a range of hypothetical isotropic values of *E* and ν, it was shown that Equation (4) with its assumed uniform material set as the substrate modulus, consistantly over estimated the more realistic FE mixed material model, with a stiffer beam than substrate. To account for this effect, a what if command was used in excel to determine an effective modulus for input into Equation (4). This work is described in detail below.

To determine proportionate error in using the substrate through thickness modulus in Equation (4) for a system of mixed materials, rotation in a sample with FR4 composite substrate was calculated using Equation (4) with the proposed through thickness Young's modulus, *Ey*, of 3000MPa (approximately equivalent to the modulus of Epoxy Resin). This calculated rotation showed reasonably good agreement when compared to a corresponding FE model using the suggested orthotropic material properties.

To further isolate the effect of mixed materials in the system in the same FE model the the beam modulus was kept constant as 45,950MPa, as shown in Table 4 to represent the solder material, and a range of isotropic substrate modulus values were substituted as shown in Figure 47. As expected the resonsbly good agreement was preseved, when comparing (4) calculations to corresponding FE modells of a solder joint, with substrate using the proposed FR4 isotropic properties, see Figure 47. Although, the FEA, using the mixed materials system, consistantly predicted higher rotations than Equation (4) that assumes a uniform material across beam and substrate.

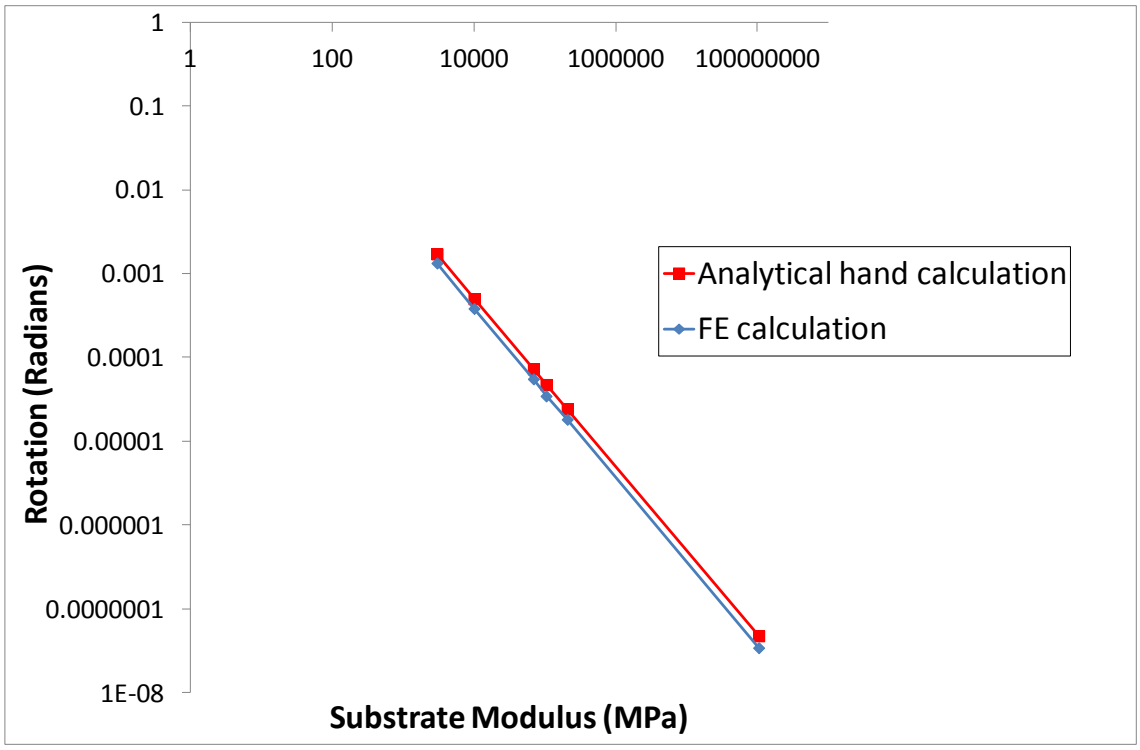

Figure 47: A hypothetical range of isotropic substrate modulus values versus corresponding rotation, calculated analytically and then seperately using FEA

Equation (4) only predicts beam rotation and assumes a uniform material. To simulate what would be the effective system of using E = 3000MPa in Equation (4), i.e. a system of uniform material of modulus E = 3000MPa with several components of deformation under shear, this value was input (for beam and substrate) into an FE model of a single FR4/solder joint based on the 4 ball sample design. The model beam is of diameter 0.75mm and height 0.6mm, with two substrates of XYZ dimensions 1.6, 2.5, 0.75mm (uniform thickness over system). Coordinate system as per Figure 31. 1N lateral load is applied to the top surface which is constrained to move as one in the X direction. When compared to more realistic materials, see Table 12, the low modulus uniform material model showed overall sample deflection increased by factor of 2, increased solder shear and bending by a factor of 10, and a slight increase in rotation. Where, shear and bending in solder is total solder displacement extracted from FE, less displacement due to rotation and less displacement in substrate. The Poisson's ratios used in the FE models were 0.22, 0.4 respectively for materials E=3000MPa and E=45950MPa.

Substrate Modulus (MPa)/ Beam Modulus (MPa)	Maximum lateral displacement of whole sample (µm)	Solder lateral displacement of midline top of joint (µm)	Lateral displacement due to rotation (µm)	Shear in substrate (µm)	Solder shear and bending (µm)
3000/3000	$4.25X10^{-3}$	$3.31X10^{-3}$	$9.64X10^{-4}$	$9.31X10^{-4}$	$1.42X10^{-3}$
3000/45950	$2.65X10^{-3}$	$1.81X10^{-3}$	$8.82X10^{-4}$	$8.34X10^{-4}$	$8.97X10^{-5}$

Table 12: FE calculated constituent displacements for models with different substrate and beam modulus values

When a range of material Young's modulus values were substituted in turn, FE modelling showed that a relatively higher modulus in the beam compared to the substrate reduced predicted rotation when compared to a sample of uniform material of the lower modulus e.g. a SAC387 lead-free solder beam and low substrate modulus, *E*, of 3000MPa, compared to a uniform homologous sample of *E* of 3000MPa.

The model was run with a number of substrate/beam material combinations (material properties equivalent to steel, solder and FR4 through thickness values). Collating the FE data and using a goal seek command in Excel to correlate analytic predictions to FE data, appeared to show Equation (9) could be used describe an effective system modulus (for these conditions).

$$E_{effective} = (0.930 \times E_{substrate}) + (0.043 \times E_{beam}) \qquad (9)$$

When predicted rotations made using Equation (4) with a calculated $E_{effective}$, have been compared to FE calculations, the improved agreement has been shown consistent within 0.5% for a range of material combinations. Using this method, a system $E_{effective}$ of 3329MPa was determined for use in analyses of the Ghaleeh 4 ball sample [2015].

Preliminary FEA showed, for the Ghaleeh sample material/geometry, the mixed materials effect could be considered small when compared to other quantified/identified errors.

The solution proposed requires further verification and suitable validation. Repeating this for cantilever model showed different proportionate effects on shear, bending, and rotation. For use with other materials/geometries/boundary conditions further FE data would be needed to be generated. Poisson's ratio also has an effect and this should be considered in a future study. On consideration of the limited effect of this phenomenon on the current work, it was decided, beyond what is reported here, not to further investigate this effect.

4.3.7 Effect of substrate stiffness on beam deformation

Calculated solder shear and bending based on the average dimentions of the Ghaleeh sample, using Equation (2) and Equation (3), and FEA, have been shown in Figure 48. Analytical shear and bending calculations assume a fixed foundation. Also shown in Figure 48 are the FE calculated predicted rotations for an the same solder column geometry attached to an elastic foundation, the substrate, of isotropic modulus varied as shown.

As the substrate modulus is reduced and rotation is present, FE calculated solder deflection due to shear and bending is reduced when compared to hand calculations. A 9% reduction was observed when comparing the FR4 substrate model of the Ghaleeh sample [2015] to an equivalent model of with no substrate. A modification to the simple analysis suggested may be considered before use as a predictive tool.

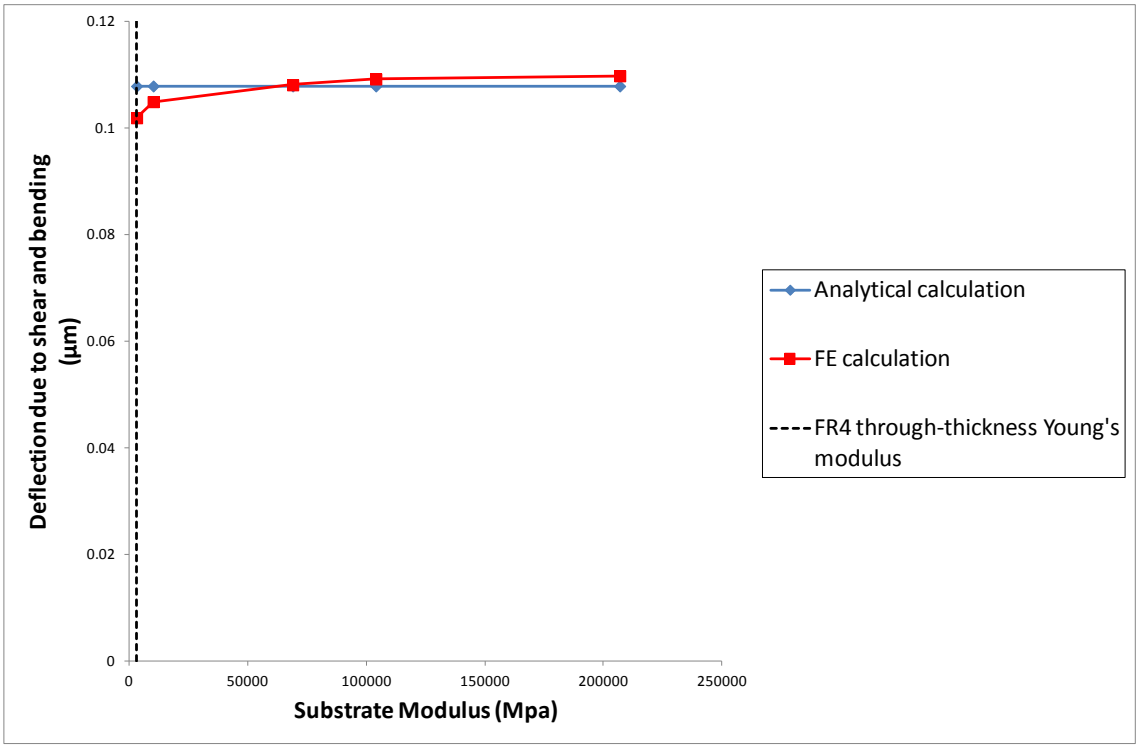

Figure 48: Defection due to shear and bending of the idealised FE (based on Ghaleeh average dimentions), verses correponding substrate modulus

4.3.8 Effect of end condition on rotation

The OD test-piece is a cantilever, whereas BGA sample solder joints examined in the current study are built-in at the both ends and allowed to move only in the direction of the applied shear load. Figure 49 left hand side shows the modified O'Donell specimen, with substrate modified to saturation of substrate effects and right hand side shows Park and Lee BGA with solder material built-in at both ends, as is common in typical BGAs. A correction factor should be used to account for the reduced rotation due to the clamped end condition, in addition to ensuring that the correct moment is entered Equation (4).

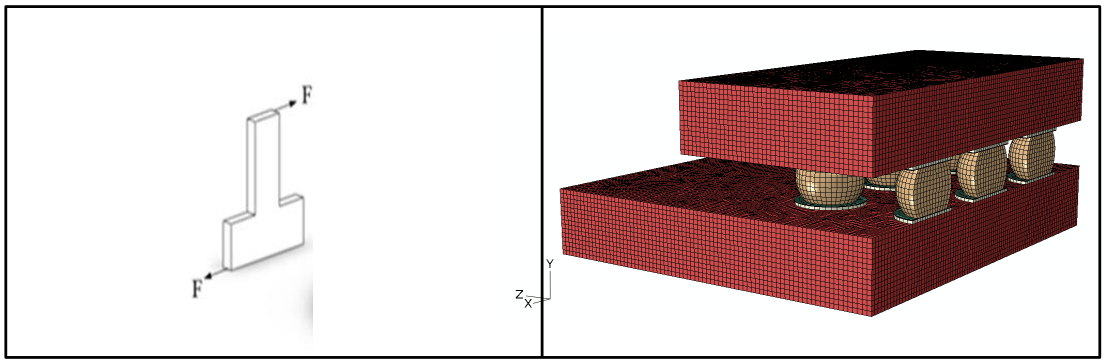

Figure 49: *Left hand side shows geometry of modified O'Donnell cantilever specimen, Right hand side shows to Park and Lee BGA [2005]with solder built-in at both ends*

To determine the required end condition correction factor an FE study, with only depth/length (D/L) and end condition varied, was carried out for the OD Scale model. Both the 4-ball and the Park-Lee (PL) models shown in Table 13 use a OD Scale model geometry but with beam cross sectional area and length equivalent to the original 4-ball and Park-Lee sample designs. These models also differ from the original Ghaleeh, and Park and Lee models in that they consider only one substrate with a Y=0 constraint on other end.

So far all correction factors have been for isolated effects, determined using the original OD geometry with only one parameter changed. It was the intention to use the same approach for the clamped end condition effect, but FE revealed that the combined effect of end condition and length has a greater effect than the product of isolated length and clamped end condition correction factors.

Unlike the other correction factors, the clamped end condition study has also taken account of beam length. Combining these effects in a single correction factor may be problematic for the final calculation of total correction factor. Therefore, as a straightforward but crude rectification, before multiplying through by the other correction factors (including length correction factor), the C_6 correction factors will be divided by C_2, as shown in Table 14.

Beam length representative of sample	Beam depth D (mm)	Beam length L (mm)	D/L	End condition	Agreement to Equation (4) (%)
OD	Original design	Original design	0.129	free	100
OD	Original design	Original design	0.129	clamped	98.6
4 ball, Ghaleeh	0.7605	0.6	1.27	clamped	50.3
PL	0.63268	0.52	1.21	clamped	49.4

Table 13: Effect of stated end condition

Model	C_6	C_2	Value input to calculation for C_6
4 ball, Ghaleeh	0.503	0.886	0.565
PL	0.494	0.884	0.569

Table 14: Clamped end condition factor, C_6, per design

In this section, to liken the OD model to the clamped solder joint, the extreme surface of the OD model cantilever was given a boundary condition to simulate a built-in beam with movement only in the plane the boundary. It was thought that in the real sample. rotation would occur at both substrates, and that discretely altering the original OD sample with a beam end boundary condition was not representative of a sample with

two (elastic) substrates. A combined effect of second substrate and boundary condition was required. This is out with the study objective to isolate discrete effects towards general application of Equation (4),and will not be included in the final calculation.

However for interest, it was decided to use FE to directly fit the effect. This gave a different correction factor of 0.792. This new correction factor reduced agreement to PL rotation FE, by about 25%, and improved agreement to FE 4 ball to about 3%. It is recommended that a future study investigates this combined effect.

4.4 **Application of correction factors to O'Donnell equation for use with BGAs**

The analytical method described in sections 4.1, 4.2, and 4.3 is designed to determine the components of BGA displacement i.e. shear and bending of the solder, shear of the composite and boundary rotation. It is designed to account for a range of design parameters.

To show the effectiveness of the suggested method, in this section the analytical method is applied to the published designs of Park and Lee [2005], and Ghaleeh [2015]. The hand calculated components of displacement are then compared to corresponding FEA and published measurements.

The full calculations of shear and bending of the solder, shear of the composite and boundary rotations are given in **Error! Reference source not found.**.

To apply the O'Donnell boundary rotation calculation to different designs, first the design specific correction factors must be calculated. The unique (non-material) correction factors for the Park-Lee and Ghaleeh samples are determined in **Error! Reference source not found.** and shown in Table 15, where it can be seen that pitch size and the clamped end effect have the dominant effects on rotations and therefore correction factor.

The correction factors shown are specific to the samples under consideration, but correction factors may be derived for a range of geometries using the proposed set of parametric equations.

Correction factor label	**Description**	**Park-Lee sample design correction factor**	**Ghaleeh sample design correction factor**
C_1	Beam shape : circular cross-section combined with very low □ value	1.083	1.083
C_2	Beam length	0.884	0.886
C_3	Substrate *x*-dimension (through-thickness)	0.916	0.982
C_4	Substrate *y*-dimension (pitch)	1.623	1.042
C_5	Substrate *z*-dimension (pitch)	0.734	0.749
C_6	Clamped other end condition	0.569	0.565
C_{total}		0.594	0.416

Table 15: Example correction factors for samples studied in Chapter 3

For the calculation of correction factors, precise values have been used. Where as it is the norm to report values to three significant figures, in this case (the product of multiplying very large number by very small numbers) numerical rounding leads to significant deviation in results. This is particularly important in the calculations to determine very small solder deformations (5%) from much larger whole sample deformations.

4.4.1 Parametric shear equation compared to FEA and measurement: Park and Lee sample

For a single connection from the Park-Lee sample, the behaviour of each material was considered here under 1N shear load, and the parametric equation has been compared to FEA of an 'idealised' linear FE model that approximates the solder as a cylinder of diameter 0.672mm (average diameter of the original Park and Lee solder ball), between two orthotropic FR4 substrates of section 1.27 × 1.27mm (equivalent of the original Park and Lee design pitch size) and original through-thickness dimension, with copper/tin pads intentionally omitted.

Analytical calculations are based on the parameterised and simplified components due to; bending and shear in the solder ($\delta_{b,s}$ and $\delta_{shear,s}$ respectively), rotation of the solder with respect to the FR4 (δ_{rot}) and shear in the FR4 ($\delta_{shear,FR4}$), as summarised in the correction factors given in Table 15. Table 16 compares the lateral displacement per unit lateral force obtained from the FE model with analytical predictions. For comparison with the analytical calculation, 'idealised' FE displacements have been extracted from the sample top surface, on the beam centreline.

	Displacement under a 1N (µm)					
	Shear in solder	Bending in solder	Shear and bending in solder	Rotation	FR4 shear	Total
Analytical Parametric	0.08934	0.02547	0.1148	0.8900	1.4504	2.455
FE	Not available	Not available	0.0974	0.9164	1.4542	2.468
% difference			18	-2.9	-0.3	-0.5

Table 16: Comparison of idealised linear FE with parameteric equations for a single Park-Lee connection

As can be seen, the total displacements from the two methods agree to within 1%, and both methods show that the shear and bending deformation in the solder is a small contribution to the total.

A full description of the analytical calculation of rotation is shown in **Error! Reference source not found.**. When comparing the hand calculations to the idealised FE most of the constituent deflections are in agreement to within 3% or less, with the exception of the solder shear and bending deformation, which differs by almost 18%. The explanation for this is discussed in Section 4.3.7.

4.4.2 Parametric shear equation compared to FEA and measurement: Ghaleeh sample

As for the Park and Lee sample, the parametric equation was used to predict the constituent displacements for the Ghaleeh specimen, and these are compared to calculations from an 'idealised' linear FE model of a single joint of solder height equal to original sample design, and diameter equal to the average of the original design (copper and tin components both omitted). The substrate dimensions are equal to the pitch size and through thickness depth of the original sample. Table 17 shows the results. Again, both analytical and FE calculations show the shear and bending deformation in the solder is a small contribution to the total sample displacement, and agree on total sample displacement to about 7%. For comparison to the analytical prediction, the 'idealised' linear results have been extracted from the top of the centreline of the single joint model. Percentage difference shown is with respect to the FE calculation. Again, for the smallest component of displacement, solder shear and bending deformation, analytical solution significantly over predicts the value.

	Displacement under 1N load (μm)				
	Displacement due to shear and bending of the solder	Displacement due to Rotation	Total Solder	Displacement due to FR4 substrate shear	Total linear deflection
Hand Calculation	0.108	0.593	0.701	1.479	2.180
Idealised FE	0.083	0.807	0.891	1.448	2.339
Difference %	30.1	-26.5	-21.3	2.1	-6.8

Table 17: Hand calculations and idealised FE calculations for the 4-ball sample

For direct comparison to the analytical calculations, FE calculated shear deflections are extracted from the top of the centre line of individual joints. This is not the equivalent of global measurements taken at whole sample extremes. The idealised FE model calculated a global sample deflection of 2.354 μm under 1N load.

4.5 **Array effect**

The preceding sections have investigated the influence of substrate material, loading direction and pitch size on deformation of a discrete solder joint. In reality BGA packages consist of an array of tens or hundreds of joints, in an irregular pattern.

The effect of solder ball array is further investigated here, first using the 4-ball, Ghaleeh sample where there is no excess substrate overhang, i.e. the sample substrate extreme dimensions are equal to pitch size times number of balls in each direction. Followed by the Park and Lee sample where top and bottom substrates are of different sizes and both substrates give the outer rows of solder balls considerable overhang. For these analyses the 'idealised' FE models described in 4.4.1 and 4.4.2 have been used.

4.5.1 Regular array effect

The Ghaleeh 4 ball sample is a design of uniform array without overhang larger than pitch, see Figure 23. To simulate the array (with additional balls in series), appropriate antisymmetry commands were placed on the Idealised FE model described in section 4.4.2. The calculated displacement is shown in Table 18, and compared to the Idealised FE (single joint) calculated values from Table 17. The data shows a negligible reduction in total deflection of 0.5%, solder rotation (-0.6%) and substrate deflection (-1.7%). At the same time there was a 23% increase in solder shear and bending, possibly due to the changed boundary conditions due to the addition of FR4 volume and contemporaneous reduction in FR4 deformation. Difference (%) shown is with respect to the idealised joint.

	Displacement under 1N load (μm)				
	shear and bending	Rotation	Total Solder	FR4 substrate	Total linear displacement at top of joint centreline
Idealised FE (single joint)	0.083	0.807	0.891	1.448	2.339
Idealised FE linear array	0.102	0.802	0.904	1.424	2.328
Difference in FE methods %	+23	-0.6	+1.5	-1.7	-0.5

Table 18: FE calculated constituent displacements for single joints and joints within an array, based on 4-ball sample geometry

Table 19 shows measurement made by Ghaleeh [2015], the values was extracted from original raw data provided in a personal correspondence with Ghaleeh. This is shown alongside predictions from a detailed non-linear FE model (one quarter of the original

design with appropriate symmetry boundary conditions), and predictions from the idealised FE linear array model, and the corresponding linear analytical calculation using the parameterised model for a single joint. An applied whole sample load of 11.55N was chosen for this comparison as it is assumed, from measurements, to be close to the highest load/deflection that is capable of inducing a linear response, Figure 24.

	Displacement under 11.55N global load (μm)						
	Solder, shear and bending	Solder Rotation	Total Solder	Total Copper	Total Tin	FR4 substrate	global
Measured	--	--	--	--	--	--	6.82
'Full' FE, non-linear	0.253	2.720	2.973	0.237	0.094	3.474	6.83
Idealised FE linear array	0.294	2.316	2.610	--	--	4.112	6.72
Parametric calculation	0.312	1.712	2.024	--	--	4.271	6.30

Table 19: Predictions from a non linear model of the 4 ball sample, and measurements

Both FE models show excellent agreement to the global displacement measurement (to about 1%). Comparing the analytical solution to the measurement, the agreement is reduced (about 8%), it should be noted however that this is not a 'like for like' comparison as the single joint calculation is assumed to be on the solder joint centre line, and the full sample global deflection (measurement and calculation) is extracted at the sample extremes. It does however better than confirm that for all three analyses, linear and non-linear, global calculations are in the correct order of magnitude.

All three models show that the majority of the measured deflection is shear in the composite and whole joint displacement due to interface rotation.

As previously described in section 4.3.7, the FE models show a reduction of solder deformation corresponding to the presence of rotation. Both linear idealised models would underestimate global deflections, it is presumed this is partly due to the absence of metallic finish and Cu land.

The measured data was taken at a global load of 11.55N (equivalent to 2.8875N per ball). Linear FE predictions and analytical calculations shown in Table 19 have been suitably scaled up from values in Table 17 and Figure 18, for a scale contrast to the global measurement taken under 11.55N. All linear and non-linear FE model boundary conditions are as stated in their descriptions and are without the adhesive used in 4 ball sample measurements. The values shown in Table 19 for the 'full' non-linear FE model deflections were extracted at 11.5N. In experiments, the global sample response to the applied load of 11.55N was assumed to be linear, see Figure 24, apart from the localised copper plasticity which may be ignored. For comparison with global measurements, FE displacement shown has been extracted at the maximum value (not sum of constituents).

The agreement shown may be a slight 'red herring', given the number of assumptions made in the modelling, however the comparative agreement of all analytical methods to measurements gives credence to the comparative values of the constitutive deflections.

4.5.2 Substrate overhang effect

The Park-Lee sample has a substrate overhang larger than pitch size, see Figure 6. It is reasonable to expect that this will significantly influence solder deformations, in light of the work discussed in 4.3.4 on pitch size. Figure 14 shows excellent agreement between the non-linear FE model of the full Park-Lee 9-ball BGA sample geometry and the measurement. Where measurements were extracted manually from a published plot, Park and Lee [2005], that was subsequently enlarged.

Table 16 shows agreement to within 1% for lateral displacements calculated for a discrete single Park-Lee solder joint, approximated as a solder column bounded at both

ends with FR4 composite substrate, see Figure 13 left hand side. Where the FR4 in-plane dimensions are equal to the original sample pitch size.

Table 20 shows measured global sample displacement under about 20N shear force compared with values calculated using the suggested parametric equation, linear FEA of the corresponding 'idealised' geometry model, and 'full' non-linear FEA of the original sample geometry. This time a sample shear load of 20N was selected for the comparison, as this is expected to initiate a linear response from the assembly see Figure 10 and is a similar load per ball as used in the previous analysis, section 4.5.1. This equates to approximatly 2.22N per ball.

	Global displacement under 20N global load (μm)
Measurement	3.70
'Full' non-linear FE, geoemtry shown in Figure 6	3.84
FE 'idealised' FE single joint, geometry shown in Figure 13 and substrate area equal to pitch size in original design	5.48
Parametric calculation for a single joint, geometry shown in Figure 13 and substrate area equal to pitch size in original design	5.46

Table 20: Calculations based on the Park-Lee sample with measurements

Excellent agreement is shown between the measurement and 'full' nonlinear FE prediction, but both linear single joint models considerably over estimate the global displacement. Showing that the effect of a substrate overhang, in excess of pitch size,

results in different global sample displacement than for an interconnect contained within the regular array of interconnects.

The 'full' nonlinear FE prediction was extracted from a detailed model of one half of the full 9 ball sample with appropriate symmetry and boundary conditions applied, as described in Chapter 3. The linear FE calculation and the analytical calculation are both are both for a single joint, calculated values shown in Table 16, and have been scaled to 2.22N per ball. The comparison with sample global deflections, measured and non-linear FE, and relative displacement of the top and bottom of the single joint centre line, FE 'idealised' FE single joint and parametric equation, is not a like for like comparison, but the comparison does show that excess substrate overhang has a large effect on measured displacement and currently the simple parametric solution cannot account for this design type.

4.6 **Discussion on the parametric equation**

Having used numerical FE modelling to identify the constituents of shear displacement in BGA designs, the overall aim of this chapter was to determine to what extent the discrete constituents could be quantified using simple basic mechanics. Finding an analytical solution for this is complex and has not been found in the literature. The potential benefits of such a parametric analytical solution are threefold; to provide a sensible verification of FEA, it can allow confident interpretation of published empirical fatigue-life data, and a sensible framework for a simple BGA design tool.

The proposed method quantifies the shear deformation in the orthotropic composite material, rotation of the solder material within the elastic composite and finally shear and bending in the solder material. The following technical discussion considers the success of each part of the solution in relative order of contribution to the total deformation of a BGA under shear.

To be clear, the analytical parametric solution proposed predicts the behaviour of a single solder ball (approximated as a cylinder). The Idealised linear FE provides

verification to the suggested simple parametric analytical approximations. The Idealised linear FE has been verified by the detailed, non-linear FE modelling of the Ghalleh [2015] sample which, in turn, gives good agreement to physical measurements for all of the designs considered, providing validation of the method.

4.6.1 Shear deformation of the composite substrate

Using the proposed orthotropic properties, FEA showed that shear deformation in the FR4 composite is the largest contributor to BGA displacement in both the Park and Lee, and the Ghaleeh BGA specimens under shear, see Table 18 and Table 19. FEA also revealed a highly complex stress distribution within the orthotropic substrate above the solder joint, see Figure 26. In practice, the woven glass fibre composite is heterogeneous, the individual laminae being around 0.05mm thick, so the distribution will be even more complex. The Abaqus FE software is capable of modelling the laminate structure in detail but as FE calculations, using the proposed FR4 orthotropic material properties, have shown good agreement with whole sample measurements in Chapter 3, and the focus of interest here is in the solder, it was not felt to be necessary to have a more sophisticated model of the FR4.

Agreement to FE is shown to be about 2% for both designs. It should be remembered that, in section 4.2, the analytical formula for smoothing the complex shear deformation in the FR4 was fitted to the PL FE data. Full verification the analytical solution would require access to other designs, with corresponding empirical data for modelling validation.

The shear calculation correction factor is based on the solder/substrate interface area. It appears to work well in its current form but if further refinement of the calculation is required, it should be straightforward to refine the calculation using a volume calculation to account for substrates of different thickness.

4.6.2 Boundary rotation of the solder joint interface

The original contribution described here is the suggested use of Equation (4), O'Donnell [1960], with suitably determined correction factors, to quantify the previously unreported boundary rotations. O'Donnell's data was obtained from his own unique test-piece design with a single beam. To provide verification of the original solution, a finite element model of the exact material configuration and dimensions modelled by O'Donnell, was run and found to give excellent agreement with the equation.

Section 4.3 describes the procedures developed during the current work, to determine the correction factors required to extend the use of Equation (4) for suitable use with solder joint samples. A total of six non-material effects have been identified and investigated. Based on this, a comprehensive parametric study was carried out, considering beam cross sectional shape, beam and support dimensions, and boundary conditions on the support and at the other end of the beam. FEA was compared with rotations calculated from the equation to devise a series of six correction factors.

Investigating beam shape showed that, for the purpose of input into Equation (4), keeping the value of I constant and transposing the true solder material shape to a geometry of the O'Donnell design (rectangle of width equal to 0.75depth) improved agreement between analytical calculation and FE. Though, in beams of very low I values (typical of approximated BGA solder joints) FEA has been shown to rapidly diverge from agreement to Equation (4) and an additional correction is required (Correction factor 1). Beam length (Correction factor 2) has been shown to affect the severity of rotation and agreement of FE to Equation (4) calculations, and from the study it is clear that even short beams rotate under shear where the support material is not rigid. Shape and size of substrate in X, Y, and Z direction, proportionate to beam volume, each have an effect on boundary rotation and subsequent agreement to Equation (4) (Correction factors 3, 4, and 5). Finally the other end condition (for example free or clamped) has been shown to affect agreement (Correction factor 6).

The O'Donnell specimen consists of a uniform material and so, to account for the effect of mixed materials in a BGA, an effective system modulus has been suggested. The effect on rotation of a system of mixed substrate/beam materials, in this case, was shown to be small but not insignificant and further study is recommended to describe this effect in other solder joint designs under shear, discretely and in combination with other effects particularly with multiple load conditions.

Use of these procedures, and correction factors, has been made to determine the rotations for single solder connections of the Park-Lee and Ghaleeh designs. For other designs with different end conditions, load direction, geometries and/or materials, different to the problem in hand different correction factors would be need to be generated. The proposed equations can be used for this.

The proposed analytical approximation is considered sufficient for the current purpose of verifying the current FE calculations. The rotation correction factors suggested are qualitative, they not intended to be exhaustive and further refinement is recommended. The correction factors could be refined by incorporating more FE data, however use of beam theory, to predict the behaviour of such complex 3D problems, will always have a limited accuracy. Also, given the current resolution of physical measurements, empirical validation of further modelling refinement would be a challenge.

Preliminary work showed rotation effects such as substrate shape and end condition (of other end) have a disproportionately greater effect on short beams (particularly beams of Length to depth ratios of less than one). Therefore in future the length effect could be combined within each of the discrete effects, substrate shape and other end, and not be shown separately in the final equation. Length should still be reflected in the moment entered into calculations. Isolating the individual effects on rotation is somewhat artificial, however it has served to identify and describe these effects towards quantifying BGA rotations. A future study may further investigate the combined length effect with other effects.

Figure 47 shows analytical rotation calculations against FE predictions (entering beam diameter, as both width and depth, into O'Donnell's solution), with respect to substrate

modulus. The disagreement appears to be large but consistent over a range of substrate moduli. Future studies may weigh the improved results of using the proposed method against use of the original equation, in conjunction with appropriate FE, assuming a large but consistent error could be determined for each design/test set up. It should be noted that Figure 47 is a ln-ln plot and the error varies from 22 to 28%.

This study of rotation considers a model of only one substrate with a command for the other end of the beam to act as one in the Y-plane. In reality rotation would occur at both sample beam/substrate interfaces. In loading and rotation of a short wide beam, Sant-Venant's principle may need to be considered.

4.6.3 Solder deformation

Classical mechanics theory of shear and bending were used to quantify the solder deformation. These calculated values are much smaller than measured BGA specimen shear displacements. Both beam theory and FEA showed that the proportion of the total sample deformation that is solder deformation is very small (less than 5 %, as shown in Table 16 and Table 17) and is highly sensitive to whole sample design.

When comparing the proposed parametric solution to FEA, a large percentage error is in the cylinder of solder (the simplest element of the model), see Table 16, Table 17, and Table 19. This is expected because classical analytical calculations of shear and bending consider discrete beam material rigidly clamped at both ends, and there is far better agreement with FE calculations for such an arrangement. Similarly Bending solutions are intended for limited use with a minimum depth to length ratio (although as before with a fixed boundary the errors are small). FEA showed for models without rotation we expect the agreement in shear and bending of a short beam to be within 5%.

The work revealed that solder shear and bending is reduced where the substrate modulus is low and rotation is present, see Figure 48. In the case in hand, where the composite substrate through thickness modulus, used with Equation (4) is around 3000MPa (proposed value of FR4 through thickness Young's modulus), this overestimate of solder deformation has been shown to be around 9% by comparison to the idealised linear FE using the proposed orthotropic FR4 properties.

Moreover, when an FE model of uniform array is compared to a single joint model, the relative proportion of displacement due to solder deformation is increased (but is still very small compared to total sample deflection) and deformation of the FR4 composite reduced, see Table 18, this must be the restraint associated with increased substrate area. These linear model findings are consistent with the 'Full' non-linear FE results shown in Table 19.

In the current simple strength of materials solution, beam shape has been simplified. To capture the true stress distribution within a beam of changing cross-section would require a sophisticated elasticity solution. Given the range of possible solder profiles, even within a single BGA component, this hugely time consuming approach would likely be impractical.

4.6.4 Comparing analytical calculations to FEA and measurements

Detailed non-linear FEA has shown very good agreement with measurements for the Park and Lee, and Ghaleeh BGA specimens under shear. The proposed analytical constitutive solution is intended to proportionately describe each of the mechanical phenomenon occurring within a single idealised solder joint. In a like for like comparison, the analytical calculations correlate well with specimen shear deflections extracted from single joint linear FE models (extracted at top of centreline of joint) for several quite different sample designs (Park-Lee and Ghaleeh, shown here, and Pang amd Xiong [2005] shown in Annex C). Agreement between analytical calculation and linear FE; is shown in 4.6.3.

FE has shown that, where rotation is present, the classical analytical calculation over predicts the solder deformation (by almost 25% in the Ghaleeh specimen, when compared to non-linear FEA, Table 17). The predicted deflection due to rotation also shows some disagreement, and it is thought the agreement could be improved through additional refinement of the rotation correction factors (this could be achieved by increasing FE data points). Although, as the hand calculation is a simplified attempt to isolate each of the identified discrete rotation parameter effects, where as the true effect of this large number of parameterised effects is co-dependent on each of the other

parameters, possibly too complex for a simple hand calculation to be determined. However, as in the Park and Lee, and Ghaleeh sample analyses have shown, the amount of constituent deflections predicted using the proposed analytical method and the linear idealised single joint FEA are in relative agreement.

Future recommendations have been made here to refine the proposed solution, however the problematic use of classical theory (beam theory etc) to describe other mechanical constituent behaviours and the numerical errors intrinsic to the product of a large number of factors of very small value, limits the accuracy of any refined solution.

Global sample deflection values are of course different from discrete joint centre line deflections. The effect of inclusion in a regular array was studied and when compared to calculations for a single beam, negligible effect was shown on total combined deflections. The Ghaleeh sample, of regular array, showed good agreement between parametric analytical calculations, measurements, and FE predictions (both idealised-linear and detailed non-linear, Table 19). Validating the methodology for this regular array. However closer inspection showed this agreement to be a combination of a small reduction in the FR4 shear and boundary rotations, negated by a (proportionally larger) deformation of the solder material, again see Table 19. This is assumed to be due to the increased substrate area and corresponding increase in restraint.

For the Park-Lee whole sample, with substrates of different sizes, a different mechanical response was shown when comparing single joint linear calculations to the equivalent non-linear FEA and measurements, see Table 20. Preliminary FE modelling (not reported here) showed inclusion in an irregular array had a greater effect, prohibiting the application of the analytical solution proposed here. Another correction factor is needed to account for the array effect, but this is more complicated and may not be described with a simple analytical calculation.

As a first attempt to quantify the rotation, each of the discrete rotation effects were initially considered in isolation. FEA showed the severity of combined rotation effects is more complex than a straight forward accumulation. A future study could investigate

an expanded combined FE-analytical parametric 'trend fit' correction factor formulae with respect to substrate volume, for example a combined length and shape or *I* effect.

The work has been compared to empirical data, as is expected in validation of any analytical or numerical modelling. Access to raw measurement data for the 4-ball Ghaleeh sample showed force-displacement measurements were not smooth curves (displacement measurements fluctuate at each load point), and measurements varied from sample to sample. For example, under 4 N load per sample, measured whole displacement was between 2 and 2.4μm. From personal experience and personal correspondence with experimentalists, this is not an uncommon problem and publications often report measurements in terms of an average value. Without access to original raw measurements and all test parameter details, where the range of scatter within results is unknown, it may not be possible to determine the accuracy of any validation provided to FEA.

Chapter 5 **Discussion and Conclusions**

The work has contributed towards the requirement, identified from the literature, for a better understanding of the components of deflection in a BGA test-piece. To this end methods of determining, and the effect of using, correct mechanical properties in solder joint analysis have been investigated. A simple analytical solution, based on classical mechanics theory, has been proposed to approximate the various components of deformation for a range of BGA sample designs under shear. A detailed technical discussion is presented in Chapter 3, Chapter 4 and **Error! Reference source not found.***, respectively, for each of the three technical areas investigated; Selection of appropriate mechanical properties for a simple FE model, Parameterisation of the components of shear, and modelling of time dependent behaviour. The following discussion considers the impact of the work, with respect to current knowledge on material characterisation, analysis of solder joint structures, and advice for design. A summary of the main conclusions, contributions to the current state of the knowledge on BGA behaviour, and recommendations for future work are also given.*

5.1 **Material Characterisation**

For many of the materials commonly used in micro-electronic assemblies (component, solder, substrate) constitutive behaviour with strain rate, temperature and time is not fully quantified. Other authors have measured the mechanical behaviour of unique BGA assemblies and unique bulk solder sample designs under different load ranges and conditions (monotonic, creep, fatigue, tensile, compressive, shear and bending). This has led to a disappointingly wide range of reported material properties and behaviour equation parameters that is problematic to correlate. This section of the discussion is intended to compare conventions in mechanical testing with current attempts to characterise solder material.

5.1.1 Mechanical testing of bulk solder

Material property values are generally considered to be universally applicable but, as discussed in Chapter 2, this is where the bulk material has been characterised according to a recognised standard. It is of great concern that there are no commonly adhered to solder mechanical characterisation test standards for bulk solder material or solder joint assemblies such as BGAs. Although the current measurement work fell into the expected range, see **Error! Reference source not found.**, it did not advance this area of the knowledge.

5.1.2 Mechanical testing of BGAs

It is of equal concern that BGAs and other solder joint assemblies are used to characterise solder properties. Consider the case in hand where the solder deformation was found to be about 5% of measured sample deformation, for different sample designs. This shows that without a better understanding of the components of deformation, BGA specimens should not be used for solder material characterisation.

It is clear that some BGA structural design tests will be needed to simulate solder joint behaviour under specified load conditions, given the widely different response of the bulk solder material and a solder joint assembly. It is not uncommon in any industry sector to conduct design behaviour tests. These are useful but the purpose and meaning is limited to the design and load conditions used in the evaluation.

For example, although BGA fatigue life is assumed to correlate to plastic strain in the solder, many workers have correlated a force and overall deflection of solder joint specimens to obtain fatigue-life data, Kim *et al.* [2013], Xu *et al.* [2012], Park and Lee [2005], Darveaux [2005], Andersson *et al*. [2005], Pang *et al.* [2003].

Loads and deflections can be correlated to local stress-strain behaviour but this requires assumptions about internal behaviours of complex specimens, and this method is known to be limited to the specific structure under similar load ranges, Darveaux and Banerji [1991], Xie and Wang [1998], Lee *et al.* [2000] and Lau *et al*. [2014], as discussed in section 2.2.4**.** It is difficult to directly measure the solder deformation, and no previous

attempt to analytically isolate or quantify each of the discrete components of total BGA sample deformation could be found in the literature.

The current FE modelling showed that the relative amount of solder deformation is design sensitive. The global sample measurements do not reflect this, which is a concern for correlating similar tests designed to characterise a joint assembly fatigue life based on assumed solder deformation. For these tests, before utilising the data, the components of deformation in the solder and other assembled materials should be quantified using a similar approach to the one suggested here.

5.1.3 Characterisation of the composites used in microelectronic assemblies

If solder has proved difficult to quantify, then the composites provide their own challenge and this is reflected in the data. In structural applications, composites make use of specific properties such as high stiffness and strength in fibre direction, which is well documented with many examples from aerospace, e.g. Airbus A350 XWB, and Formula 1 racing. In contrast the work has shown that critical composite properties in BGA behaviour are secondary properties which are not seriously measured, except in exceptional circumstances.

There are no published standards for characterising through thickness composite properties, however FE numerical modelling has been shown here to be a useful research tool in determining these difficult to measure properties, though comparison with empirical data.

Commercial PCB designs tend to be more complex than the plain FR4 substrates considered here, and characterising these materials may not be as straightforward. The lay-ups of these boards may be un-symmetrical and consist of several highly dissimilar materials, including large quantities of copper in non-continuous arrangements. The boards may also contain non-uniform arrays of perforations of various dimensions. Considering the relative size of the solder joint and the PCB, it is likely that the position of the fibre weave and corresponding resin rich areas will be significant. In the development of future mechanical characterisation standards careful consideration is needed to suitably capture the overall response of these boards in three directions, and

to determine if the resolution of available mechanical tests can usefully account for localised variations in these boards.

5.2 **Implications of the work on predicting BGA behaviour**

The following section discusses the effect of using the derived FR4 material properties in the FE modelling, and in the light of the current work with respect to published analyses, considers guidelines for good practice in BGA modelling.

Any prediction (or measurement) of initial elastic behaviour under mono-tonic loading is unlikely to be representative of long-term behaviour of solder joints. Just as in modelling of the time independent behaviour, the literature has reported difficulty in correlating creep data from one source to another. **Error! Reference source not found.** suggests a sensible methodology for solder creep modelling, and the implications for this are also discussed here.

5.2.1 Implications of the work for time independent modelling

Inputting the proposed orthotropic FR4 properties in the FE modelling not only gives good agreement with measurements but also reveals the deformation of each of the discrete materials and a previously unreported rotation of the solder/composite interface. The rotation significantly contributes to the measured deflection.

Using the proposed orthotropic properties also reveals that the crucial solder deflection is much smaller than measured total BGA deflection and is design specific. Therefore a big change in solder deflection between two specimens will result in a small change in BGA deflection. It is likely that such a difference in solder deflection would be undetected in specimen measurements.

The work here shows the extreme effect of using sensible material properties in determining constituents of deformation. The uncertainty in the material data is likely to be the biggest challenge to modelling of BGAs. If these material properties are known then the current work has shown that the problem can be modelled.

Numerical modelling is an expensive, time consuming approach and, in addition to suitable material properties, also relies heavily on the operator's wider knowledge of many inter-dependent factors, such as classical mechanics theory, strength of materials, and materials science to ensure that the model is appropriate and the results are sensible. The current literature offers much advice on possible methodologies for numerical analyses of solder joints, however the reports often lack the model detail that would allow independent verification. The source of material properties can be unclear and in some cases the material values used can be illogical, when considering the fundamental nature of the material in question. For example the interface rotation shown in the current work, is not observed when isotropic properties are used, see Kim *et al*. [2013], but isotropic composite substrate properties are often used in published analyses of BGAs. Without appropriate model detail, substantiated material properties, empirical validation and where possible rigorous verification from first principles of strength of materials theory, FE calculated data cannot be used by others with confidence.

5.2.2 Implications of the work for time dependent modelling

To know where to start modelling time dependent behaviour, first the time independent behaviour must be known. Given the state of time independent material characterisation and modelling, reliable creep modelling is difficult. The constant load creep modelling work shown in **Error! Reference source not found.**, again highlights the importance of using appropriate material behaviour parameters, and yet, again as in time dependent characterisation, there are is plethora of non-standard test piece designs and test conditions. The current state of understanding of published time dependent solder behaviour is just as confusing as in the time dependent data. The work suggests a FE based methodology, supported by empirical data, to determine if a particular creep law and corresponding parameters are suitable.

Although most Authors have considered only steady-state creep behaviour, it is reasonable to expect under practical service conditions that transient creep and stress relaxation would be highly significant. It is still to be shown that a single steady-state creep law could describe the constitutive response of the solder.

5.3 **Implications of the work on BGA design advice**

Isolating the constitutive behaviour of the solder joint material is a basic requirement of Coffin-Manson type fatigue failure predictions, and therefore accurate determination of the solder deformation should be critical in the design process. To describe the relative magnitudes of the individual components of deflection, within limits, of a non-design specific BGA under shear, an analytical parametric solution is suggested in Chapter 4. The following section discusses how such simple basic mechanics solutions can be used to inform design advice.

5.3.1 Meeting current industry requirements for simple design tools

In practice industry has a need for quick reliable solutions. These could be provided by the methodology used here whereby a relatively simple solution is developed from first principles, using strength of materials theory, and supported by FE analysis and physical testing. The FE analysis can be used to provide basic verification and can provide a deeper understanding to address issues such as complex geometry, variations in material composition and non-linear responses. Where required, the FE modelling can be taken further to model the micro-mechanics such as fibre weave pattern, resin rich areas, and variations in microstructure.

Where possible, input from standardised testing should be incorporated into the modelling, e.g. bulk tests to provide material properties and component tests to validate the analyses, before committing to full production of expensive systems. If required the modelling can also be used to interpret physical data, particularly where the measurement is non-standard, for example it has been shown that the modelling may be used to extract sensible material properties from empirical data, provided sufficient data from independent tests were available.

The approach used here to isolate solder deflection could be applied to all common solder joint types; BGA, QFN, Gull wing, Plastic balls and S-joint, under different loading conditions. This knowledge could be used to enable correlation from one source to another, leading to generally applicable solder fatigue parameters, which could be confidently used in design advice. Improved understanding of legacy

empirical data could also reduce the requirement for costly future testing. If it is shown that the accuracy of the solution is less than ideal, the method may still offer a useful approximation to compare one design to another. Given the surprisingly large number of micro-electronic design variables, these analytical solutions will prove useful in determining which are the variables and/or properties of most influence.

5.4 **Conclusions**

The findings of the work are presented here on each of the three technical areas investigated, followed by the main conclusions.

5.4.1 Findings on the influence of material properties to sample behaviour

FE Modelling of the Park and Lee [2005] 9 ball BGA sample under monotonic loading in shear and tension showed that overall sample stiffness is extremely sensitive to the elastic properties of the FR4 composite substrate. In particular the analysis showed that the FR4 through thickness Young's modulus, *E*, and through thickness shear modulus, *G*, dominate the elastic behaviour of the BGA sample. No previous acknowledgement of the significance of shear properties with respect to BGA assemblies could be found.

Applying this knowledge highlighted the discrete constitutive mechanical phenomena which contribute to total sample deformation under loading at different angles, including considerable deformation of the composite, and revealed a previously unreported rotation of the solder joint at the composite/joint interface.

It is common for published analyses to use isotropic composite properties and the rotation is not present under such conditions, see Kim *et al*. [2013], and this must, in part, account for the absence of solder rotation from BGA shear test publications.

It was shown that FE software could be used as a research tool to refine the FR4 through thickness properties, and comparison to Park and Lee's published load-displacement data, in tension (0°) and shear (90°), allowed appropriate values of *E* and *G* to be derived by fitting to the empirical data. These values, shown in Table 7, were

corroborated using further Park and Lee test data (45°), and original data from a shear test of a different BGA geometry, Ghaleeh [2015]. The intension was to use several similar published BGA examples for full validation. Unfortunately, no further examples of FR4 on FR4 specimens could be found with sufficient detail of sample design, test procedure and empirical constitutive data. The suggested values have found some agreement to published material properties, Chandran *et al.* [2000].

Current modelling also showed that the calculated stiffness, for each of the designs, was not particularly sensitive to the solder modulus value (within bounds of typical published values).

5.4.2 Findings on the parameterisation of the components of shear

The unified parametric analytical solution suggested here is intended to determine the time independent mechanical deformation in a single solder joint assembly, under a mechanical shear load. Within the specified limits, the proposed solution may be applied to a range of designs. Each of the components of the solution have been shown to be suitable using one or more of the following methods; classical mechanics theory, linear FEA, and empirical measurements.

Although substrate material is known to influence the constitutive behaviour of BGA samples, as previously discussed in section 2.2.4, Darveaux and Banerji [1991], Xie and Wang [1998], and Lau *et al*. [2014], no previous attempt to quantify the relationship under mechanical load could be found**.**

The proposed parametric analytical solution is capable of quantifying the elastic response of each of the identified deformation mechanisms within a BGA joint assembly. The solution has been verified against FE calculations for a range of designs.

The solution includes calculations for the previously unreported rotation of the solder joint and a sensible approximation of the orthotropic composite substrate through thickness shear. Fundamental to the suitability of the solution was use of the validated FR4 through thickness properties, E and G, determined in Chapter 3. Although a lack of original measurements has prevented conclusive validation and refinement of the

proposed method, when using this simple analytical calculation excellent agreement between analytical and FE calculations has been shown, for a range of designs and loading arrangement.

As intended, the analytical solution suitably accounts for a wide range of design variables but the analytical solution cannot account for the effect of array design and edge effects. FEA confirmed the sensitivity of solder joint deformation and rotation to array design, and/or a substrate overhang larger than pitch. The effect of joint inclusion in a regular array has been shown to be small but not zero. For effects such as substrate overhang larger than pitch size, FE Analysis is still needed.

To allow a published rotation solution, O'Donnell [1969], to be applied to a wider (but still limited) range of designs including BGAs, an exhaustive parametric study was conducted to determine a total of six correction factors. The proposed correction factors address discrete geometric variables with respect to joint height, clamped ends, substrate thickness, pitch size and approximate cross section shape. This is to identify the proportion of the whole sample deflection attributable to solder rotation.

FEA has shown where there is elasticity in the supports and solder rotation occurs, there is reduced shear and bending deformation of the solder material, compared to a rigidly supported beam under shear load. The classical simple mechanics solutions cannot account for this.

Excellent agreement between analytical and FE calculations has been shown using the proposed simple analytical calculation, for a range of designs and loading arrangement, however a lack of original measurements has prevented conclusive validation and refinement of the solution.

5.4.3 Findings on the time dependent modelling

A range of material creep parameters were found in the literature for essentially Sn3.8Ag0.7Cu. In **Error! Reference source not found.** analytical calculations using a number of these parameter sets, showed an equally wide range of calculated strains, this corroborated reported difficulty in the general application of empirical creep

parameters. Closer inspection of publications revealed that the accuracy of individual creep parameter sets varies even over the original range of test conditions, temperature and stress.

The accuracy of calculations made with any analytical constitutive creep relationship has been shown to be highly dependent on the suitability of the associated model parameters. Published empirical parameter sets describe creep strain rates under a prescribed range of temperatures and stress. Currently, to usefully correlate empirical creep data, it must be ascertained that measurements are from the same material composition and preparation, and test conditions.

A study was made into the suitability of a number of creep laws for the modelling of creep strain in lead free solder, in particular those available in the Abaqus FE software. The work here describes bulk solder samples under monotonic load, this is to allow comparison with published empirical data. Good agreement was shown when comparing current calculations, from both analytical and FE, with original steady state strain rate measurements (using a single steady-state creep law, *CREEP command in Abaqus with a hypersine model and published creep parameters determined from the corresponding measurements).

The *CREEP time hardening and strain hardening models' sensitivity to the time order parameter, *m*, was shown, as was the time order parameter's temperature dependence. Values of *m* appear to be interchangeable between the time hardening and strain hardening models.

The two-layer model, recommended by Abaqus for use in creep analysis with fluctuating load, requires a number of creep parameters including *m* and *f* (a code specific non-standard parameter). No published values for creep parameters *m* and *f* with respect to Sn3.8Ag0.7Cu or any other unleaded solder material could be found. Suitably validated values of two-layer creep model parameters, *m* and *f* , have been suggested.

When modelling creep under cyclic load frequencies commonly used in BGA tests, basic analytical calculations showed the potential significance of omitting a transient

creep term. None of the creep models commonly used in FE and considered here address transient creep (too late for the current work, the inclusion of a transient creep model in the Abaqus software has been announced [2014]).

5.4.4 Main Conclusions

The current work has achieved the original objective of using FEA to provide a more detailed understanding of the response of Sn3.8Ag0.7Cu under specified mechanical and thermal mechanical load, for different BGA designs. FE calculations have been validated against global BGA sample measurements.

A simple, normalised, generally applicable relationship between empirical data of overall BGA sample deflection and solder deformation cannot be assumed. FEA of several designs confirmed inherent solder strain sensitivity to sample design.

Solder deformation accounts for only about 5% of the measured total sample displacement in the Park and Lee and Ghaleeh BGA samples, as confirmed by classical mechanics theory and FE calculations. The majority of measured whole sample displacement in FR4 on FR4, BGA solder joint samples is contributed by shear deformation of the composite and rotation of the solder ball.

In order to accurately isolate the solder joint strain from measurements, before apply any strain based fatigue-life relationship, the work has highlighted the importance of correct material properties, and a sound understanding of structural analytical analysis. The work also illustrates why measured overall BGA deflections, from different designs, cannot be directly correlated.

5.5 **Contributions to numerical and analytical modelling of BGA assemblies under a mechanical shear and over time.**

This work has led to a better understanding of the whole sample behaviour of FR4 on FR4 solder joints. The main original contributions are;

- the identification of rotation at the solder/FR4 interface.
- the identification of the relatively small contribution of the solder deformation to the total sample deformation.
- the identification that overall BGA sample behaviour is relatively insensitive to the solder modulus value, within the bounds of typical published values and for all of the sample designs considered.
- the identification of the significant contribution of shear deformation of the composite to the overall deformation.
- the identification of the significant effect of the composite through thickness properties.
- the development of a simple analytical method to quantify these individual components of deformation, for a range of sample design.

5.6 **Future work**

It is hoped that the original knowledge reported here will assist in unlocking a legacy of confusing empirical data. The author in her new role will soon have access to a specialised mechanical testing laboratory and the intention is to design a rigorous test plan to characterise solder joint behaviour, with respect to the effect of specific current commercial manufacturing procedures and reliability requirements. This will be supported by numerical modelling and analysis techniques developed throughout the PhD.

It is suggested that the future work widens the investigation, to include ceramic, plastic, or other, components on FR4, solder joints and joints of increasingly diverse geometry, e.g. non-balled. It is for future work to determine if the mechanical deformation phenomena described here, also occur in commercial micro-electronic assemblies under thermal and/or vibration load only.

Also it is hoped that the work included here, using FEA with the proposed orthotropic FR4 properties in determining array boundary influence on solder strain, could be applied to an improved understanding of edge effects such as location of critical solder joints and localised composite failure (cratering).

Further refinement of the analytical model might lead to some improvement in predictions but there will always be a limit to the accuracy and the range of application of a simple strength of materials/statics solution. The availability of powerful numerical analysis allows very sophisticated analysis to be carried out on desktop computers, yet commercial manufacturing has a keen demand for simple design tables to readily approximate this complex behaviour. Pragmatic use of detailed mechanical modelling supported by relatively simple analysis provides the best route to understanding the behaviour of what is a complex mechanical structure under complex loading.

References

Abaqus Release Notes 6.14 (2014) 6.2 Enhancements to creep models, http://www.3ds.com/products-services/simulia/portfolio/abaqus/abaqus-portfolio/abaquscae/

Abaqus Regional Users Meeting (2013), personal communication with Abaqus technical staff, Crewe, UK

Abaqus Technology Brief (2011) TB-07-CALFS-3 , Revised: November 2011, Last checked May 2015, http://www.3ds.com/fileadmin/PRODUCTS/SIMULIA/PDF/tech-briefs/HT-Creep-Analysis-of-Lead-Free-Solders-Undergoing-11.pdf

Abaqus Analysis Users Manual 6.9-EF (2009a) 20.2.11 Two-layer Viscoplasticity

Abaqus Analysis Users Manual 6.9-EF (2009b) 20.2.4 Rate dependent plasticity and swelling

An T, Qin F (2014) Effects of the intermetallic compound microstructure on the tensile behavior of Sn3.0Ag0.5Cu/Cu solder joint under various strain rates, Microelectronics Reliability 54: 932–938

Andersson C, Lai Z, Liu J, Jiang H, Yu Y, (2005) Comparison of isothermal mechanical fatigue properties of lead-free solder joints and bulk solders, Materials Science and Engineering, A 394: 20-27

Andersson C, Sun P, Liu J; (2008) Tensile properties of microstructural characterization of Sn-0.7Cu-0.4Co, Review, Journal of alloys and compounds 457: 97-105

Agarwala BN (1985) Thermal Fatigue Damage in Pb-In Solder Interconnections, International Reliability Physics Symposium, Orlando, Florida, USA: 198-205.

Bertheau J, Hodaj F, Hotellier N, Charbonnier J (2014) Effect of intermetallic compound thickness on shear strength of 25 mm diameter Cu-pillars, Intermetallics 51: 37-47

Bhatti PK, Pei M, Fan X (2006) Reliability Analysis of SnPb and SnAgCu Solder Joints in FC-BGA Packages with Thermal Enabling Preload, IEEE 56th Electronic Components and Technology Conference, San Diego, CA; United States: 601-606

Bhate D, Chan D, Subbarayan G, Chiu TC (2006) Solder interconnection specimen design and test control procedure for valid constitutive modelling of solder alloys, Thermomechanical Phenomena in Electronic Systems, proceedings of the 10th Intersociety Conference, San Diego, CA: 977-983

Bhate D, Chan D, Subbarayan G, Chiu TC, Gupta V, Edwards DR, (2008) Constitutive behaviour of Sn3.8Ag0.7Cu and Sn1.0Ag0.5Cu alloys at creep and low strain rates, IEEE transactions on components and packaging technologies **31 (**3) 977-983

Bhatti PK, Pei M, Fan X (2006) Reliability Analysis of SnPb and SnAgCu Solder Joints in FC-BGA Packages with Thermal Enabling Preload, 2006 Electronic Components and Technology Conference, San Diego, CA: 601-606

Böhme T and W H Müller (2007) Theoretical and experimental investigations of microstructural changes in lead-free solders, Computational Materials Science **43**: 221–228

Broughton WR, Gower MRL, Lodeiro MJ, Shaw RM (2001) Through thickness testing of polymer matrix composites, NPL report MATC (MN) 06

BS EN 62137-1-1:2007. Surface mounting technology. Environmental and endurance test methods for surface mount solder joint. Pull strength test, BSI 978 0 580 55335 6

BS EN 62137-1-2:2007. Surface mounting technology. Environmental and endurance test methods for surface mount solder joint. Shear strength test, BSI 978 0 580 55357 8

BS EN 62137-1-3:2009 Surface mounting technology. Environmental and endurance test methods for surface mount solder joint. Cyclic drop test, BSI 978 0 580 57386 6

BS EN 62137-1-4:2009 Surface mounting technology. Environmental and endurance test methods for surface mount solder joint. Cyclic bending test, BSI 978 0 580 59252 2

BS EN 62137-1-5:2009 Surface mounting technology. Environmental and endurance test methods for surface mount solder joints. Mechanical shear fatigue test, BSI 978 0 580 59253 9

BS EN 62137-4:2014 Electronics assembly technology. Endurance test methods for solder joint of area array type package surface mount devices, BSI 978 0 580 89842 6

BS EN 60749-25:2003 Semiconductor devices. Mechanical and climatic test methods. Temperature cycling, BSI 0 580 42859 1

Chai F, Osterman M, Pecht M, (2014) Strain-range-based solder life predictions under temperature cycling with varying amplitude and mean, IEEE Transactions on Device and Materials Reliability **14** (1): 351-357

Chaillot A, Massiot G, Munier C, Lombaërt-Valot I, Bousquet S, Chastanet C, Plouseau D, Munier E, Maron D, Raynal P, Villard S, Dumonteil R (2007) Finite Element Modelling (FEM) of Green Electronics in Aeronautical and Military Communication Systems (GEAMCOS), EuroSime 2007: International Conference on Thermal, Mechanical and Multi-Physics Simulation Experiments in Microelectronics and Micro-Systems, London: 1-8

Chandran B, Goyal D, Thomas J (2000) Effect of package design and layout on BGA solder joint reliability of an organic C4 package, 50th Electronic Components and Technology Conference, Las Vegas, Nevada, USA: 1205-1214

Che FX, Pang JHL (2013) Fatigue Reliability Analysis of Sn–Ag–Cu Solder Joints Subject to Thermal Cycling, IEEE Transactions on Device and Materials Reliability **13** (1) 36-48

Che FX, Pang JHL, Xiong BS, Xu L, Low TH (2005) Lead Free Solder Joint Reliability Characterization for PBGA, PQFP and TSSOP Assemblies, 55th Electronic Components and Technology Conference, Lake Buena Vista, Florida, USA: 916-921

Chen G, Chen X (2006) Finite element analysis of fleXBGA reliability, Soldering and Surface Mount Technology **18** (2) 46 - 53

Chen H, Yan B, Yang M, Ma X, Mingyu L, (2013) Effect of grain orientation on mechanical properties and thermomechanical response of Sn-based solder interconnects, Materials Characterization **85**: 64-72

Chen H, Han J, Li J, Li M (2012) Inhomogeneous deformation and microstructure evolution of Sn-Ag-based solder connects during thermal cycling and shear testing, Microelectronics Reliability **52**: 1112-1120

Chen X, Zhou J, Xue F, Bai J, Yao Y (2015) Microstructure and mechanical properties of Sn-0.1Ag-0.7Cu (Co, Ni and Nd) lead-free solders, Journal of Electronic Materials 44 (2)

Cheng Y-W, and Siewert TA (2003) Predicting tensile properties of the bulk 96.5Sn-3.5Ag lead-free solder, Journal of Electronic Materials, **32** (6) 535-540

Clech, http://www.metallurgy.nist.gov/solder/clech/Sn-Ag-Cu_Main.htm

Clech J-P (2005) An extension of the omega method to primary and tertiary creep of lead-free solders, 55th Electronic Components and Technology Conference, Lake Buena Vista, Florida, USA **3**: 1261-1271

Clough R W (1980) The Finite Element Method after twenty-five years: a personal view, Computers and Structures 12: 361-370

Coffin LF (1973) Fatigue at high temperature. In fatigue at elevated temperatures, special technical publication 520, as detailed in Deiter [1981]

Cook RD, Malkus D-S , Plesha ME (1989) Concepts and Applications of finite element analysis, third edition, John Wiley and Sons

Cottrell, A. (1980) An introduction to metallurgy

D. S. M. R D Cook, M E Plesha, Ed., *Concepts and Applications of Finite Element Analysis*. John Wiley and Sons, 1989.

Darveaux R, Norton L, Carney F (1995) Temperature Dependent Mechanical Behavior of Plastic Packaging Materials, IEEE

Darveaux R, Banerji K, (1991) Fatigue analysis of flip chip assemblies using thermal stress simulations and a Coffin-Manson relation, Proceedings 41st Electronic Components & Technology Conference 1991, 797-805, IEEE

Darveaux R, Banerji K (1992) Constitutive relations for tin-based solder joints. IEEE Trans Component Hybrids Manufacturing Technology, **15** (6): 1013-1024

Darveaux R, Heckman J, Syed A, Mawer A, (2000) Solder joint fatigue life of one pitch BGA's ± impact of design and materials choices, Microelectronics reliability **40**: 1117-1127

Darveaux R (2005) Shear Deformation of Lead Free Solder Joints, Proceedings IEEE Electronic Components & Technology, 2005. ECTC '05, 2005, 882-882

Dauksher W (2008) A second-level SAC solder-joint fatigue-life prediction methodology, IEEE Transactions on Device Materials Reliability 8 (1) 168–173

Déplanque S, Nüchter W, Spraul M, Wunderle B, Dudek R, Michel B (2005) Relevance of primary creep in thermo-mechanical cycling for life-time predictions in Sn-based solders, 6th International conference on thermal mechanical simulation and experiments in micro-electronics and micro-systems, EuroSimE

Dieter GE (1988) Mechanical metallurgy (SI Metric Edition) ISBN 0-07-100406-8

Dudek R, Doering R, Bombach C, Michel B (2009) Simulation based analysis of secondary effects on solder fatigue, Microelectronics Reliability 49: 839–845

Dušek M, Hunt CP (2006) Test approach to isothermal fatigue measurements for lead-free solders, NPL report DEPC-MPR 048

Dušek M, Nottay J, Hunt C, Lu H, Bailey C (2001) An experimental validation of modelling for Pb-free solder joint reliability, NPL report MATC (A) 11

Erinç M (2007) Thermomechanical fatigue failure of interfaces in lead free solders, PhD Thesis, Eindhoven University of Technology, the Netherlands, , ISBN 978-90-386-1149-5

Ferguson RF, Hinton M J, Hiley MJ (1998) Determining the through-thickness properties of FRP materials, Composites Science and Technology **58**: 1411-1420

Fink M, Fabing TH, Scheerer M, Semerad E, Dunn B, (2008) Measurement of mechanical properties of electronic materials at temperatures down to 4.2K, Cryogenics **48**: 497-510

Garafolo F (1960), Properties of crystalline solids, ASTM Spec. Tech. Publ. 283 p.82, cited by Dieter [1988].

Gao F, Nishikawa H, Takemoto T, Qu J [2009] Mechanical properties versus temperature relation of individual phases in Sn-3.0Ag-0.5Cu lead-free solder alloy, Microelectronics Reliability 49: 296-302

Ghaleeh M (2015) The durability of solder joints under-thermo mechanical loading; application to Sn-37Pb and Sn-3.8Ag-0.7Cu lead free replacement alloy, PhD thesis, Heriot-Watt University

Gere and Timoshenko (1997) Mechanics of materials, PWS publishing, fourth edition, p315, ISBN 0-534-93429-3

Goldman LS (1969) Geometric optimization of controlled collapse interconnections, IBM Journal of Research and Development **13** (3), as cited by Dauksher [2008]

Gong J, Liu C, Conway PP, Silberschmidt, VV (2007) Micromechanical modelling of SnAgCu solder joint under cyclic loading: effect of grain orientation, Computational Materials Science **39**: 187-197

Graham C (2013) Daphne Jackson Fellowship final technical report, unpublished

Grivas D, Murty KL, Moms JW Jr. (1979) Deformation of Pb-Sn eutectic alloys at relatively high strain rates, Acta Metallurgica, 27: 731-737, as detailed by Déplanque *et al*. [2005]

He M, Chen Z, Qi GJ (2005) Mechanical Strength of Thermally Aged Sn-3.5Ag/Ni-P Solder Joints, Metallurgical and Materials Transactions A, **36A**: 65-75

Hearn EJ (1997) 'Mechanics of materials 1. An introduction to the mechanics of elastic and plastic deformation of solids and structural materials' Butterworth-Heinemann, 3rd Edition: 146, ISBN 0-7506-3265-8

Henkel safety data sheet SDS No.: 153908 V003.3 Revision: 06.05.2014, last checked 27/06/15;http://mymsds.henkel.com/mymsds/0006.589908.0160.en.MSDS_UT_GB.12470282.0.GB.pdf

Herkommer D, Punch J, Reid M, (2010) A reliability model for SAC solder covering isothermal mechanical cycling and thermal cycling conditions, Microelectronics Reliability **50:** 116-26

Herakovich, CT (1984) Composite Laminates with negative through-the-thickness Poisson's ratios, Journal of Composite Materials **18:**447-455

Huang Z, Kumar P, Dutta I, Pang JHL, Sidhu R, Renavikar M, and Mahajan R (2012) Fracture of Sn-Ag-Cu Solder Joints on Cu Substrates: I. Effects of Loading and Processing Conditions, Journal of Electronic Materials **41** (2)

Jalar A, Majlis BY, Ahmad I, Leng EP (2007) Mechanical Properties of Sn3.5Ag and Sn3.8Ag0.7Cu Solder Balls for BGA Package, International Journal of Engineering and Technology **4** (2): 221-227

Kanda Y, Kariya Y (2012) Evaluation of creep properties for Sn–Ag–Cu micro solder joint by multi-temperature stress relaxation test, Microelectronics Reliability **52**: 1435–1440

Kanda Y, Yoshiharu K, and Oto Y (2012) Influence of cyclic strain-hardening exponent on fatigue ductility exponent for a Sn-Ag-Cu Micro-Solder Joint, Journal of Electronic Materials **41** (3)

Kariya Y, Hosoi T, Kimura T, Terashima S (2004) Fatigue life enhancement of low silver content Sn-Ag-Cu flip-chip interconnects by Ni addition, 2004 Inter society conference on thermal phenomena, 0-7803-8357-5/04 IEEE

Keller J, Baither D, Wilke U, Schmitz G (2011) Mechanical properties of Pb-free SnAg solder joints, Acta Materialia **59**: 2731-2741

Khatibi G, Lederer M, Byrne E, Kotas B, Weiss B, Ipser H (2013) Characterization of Stress–Strain Response of Lead-Free Solder Joints Using a Digital Image Correlation Technique and Finite-Element Modelling, Journal of Electronic Materials **42** (2)

Kim I, Lee S-B (2007) Fatigue life evaluation of lead-free solder under thermal and mechanical loads, 57th Electronic components and technology conference, Reno, Nevada, USA: 95-104

Kim KS, Huh SH Suganuma K (2002) Effects of cooling speed on microstructure and tensile properties of Sn–Ag–Cu alloys Materials, Science and Engineering A333: 106–114

Kim SB, Yu J (2010) Effects of solder ball geometry on lap shear creep rate, Journal of Electronic Materials **39** (3) 326- 332

Kim YK (2007) Viscoelastic effect of FR-4 material on packaging stress development, IEEE Transactions on Advanced Packaging, **30** (3) 411

Kim YK, Hwang DS (2015) PBGA packaging reliability assessments under random vibrations for space applications, Microelectronics Reliability 55 (2015) 172–179

Kovačević IF, Drofenik U, and Kolar JW (2010) New Physical Model for Lifetime estimation of power modules, IEEE International Power Electronics conference, 978-1-4244-5393-1/10/

Kumar P, Huang Z, Chavali SC, Chan DK, Dutta I, Subbarayan G, Gupta V (2012) Microstructurally adaptive model for primary and secondary creep of Sn-Ag-based solders IEEE transactions on components, packaging and manufacturing technology **2** (2)

Lau C-S, Abdullah MZ, Ani FC (2012) Effect of solder joint arrangements on BGA lead-free reliability during cooling stage of reflow soldering process, IEEE Transactions on Components, Packaging and Manufacturing Technology **2** (12)

Lau C-S, Abdullah M Z, Mujeebu MA, Yusop NMD (2014) Finite element analysis on the effect of solder joint geometry for the reliability of ball grid array assembly with flexible and rigid PCBs', Journal of Engineering Science and Technology, **9** (1) 47-63

Lau JH (2001) Elastic, elastic-plastic and creep analysis of wafer level chip scale package solder joints on microvia build-up printed circuit boards, Circuit World **27**: 20-31

Lau J, Dauksliei W, and Vianco P (2003) Acceleration models, constitutive equations, and reliability of lead-free solders and joints, Electronic Components and Technology Conference: 229-236

Lee K-O, Morris Jr JW, Hua F (2013) Mechanisms of creep deformation in pure solder joints, Journal of Electronic Materials 42 (3)516-525

Lee T-K, Kim C-U, Bieler T R (2014) Influence of High-G mechanical shock and thermal cycling on localised recrystallization in Sn-Ag-Cu solder interconnects, Journal of Electronic Materials 43 (1) 69-79

Lee WW, Nguyen LT, Selvaduray GS (2000) Solder joint fatigue models: review and applicability of chip scale packages, Microelectronics Reliability **40**: 231-244

Li X, Wang Z (2007) Thermo-fatigue life evaluation of SnAgCu solder joints in flip chip assemblies, Journal of Materials Processing Technology **183** (1) 6-12

Liu F, Liang L, Liu Y, (2009) An improved substructure method for prediction of solder joint reliability in thermal cycle, International Conference on Electronic Packaging Technology and High Density Packaging (ICEPT-HDP)

Lopez EP, Vianco PT, Rejent JA, George C, Kilgo A (2010) Compression stress-strain behavior of Sn-Ag-Cu solders, Journal of Electronic Materials **39** (1)

Ma H, Lee T-K (2013) Effects of board design variations on the reliability of lead-free solder joints, IEEE Transactions on Components, Packaging and Manufacturing Technology 3 (1)

Ma H, Suhling JC (2009) A review of mechanical properties of lead-free solders for electronic packaging, Journal of Material Science **44**: 1141-1158

Ma H, Ahmad M, Liu K-C (2011) Reliability of Lead-Free Solder Joints Under a Wide Range of Thermal Cycling Conditions, IEEE Transactions on Components, Packaging and Manufacturing Technology, 1 (12)

Maio DD, Thomas O, Dusek M, Hunt C (2011) Novel testing instrument for lead-free solder characterization, IEEE Transactions on Instrumentation and Measurement, **60** (10)

Metasch R, Boareto JC, Roellig S, Wiese S, Wolter, K-J (2009) Primary and tertiary creep properties of eutectic SnAg3.8Cu0.7 in bulk specimens, 10th Int. conf. on thermal, mechanical and multiphysics simulation and experiments in micro-electronics and micro-systems, EuroSimE

Modi M, McCormack C, Armendariz N (2005) New insights in critical solder joint location, 2005 Electronic Components and Technology Conference

Moon K-W and Boettinger WJ (2004) Accurately determining eutectic compositions: the Si-Ag-Cu ternary eutectic, The Journal of The Minerals, Metals & Materials Society 56 (4) 22-7

Morris Jr. JW, Song HG and Hua F (2003) Creep Properties of Sn-rich Solder Joints, Electronic Component Technology Conference

Müller WH, Worrack H, Sterthaus J, (2010) Experimental setup for the determination of mechanical solder materials properties at elevated temperatures, Materials Science Forum **638-642:** 3793-3798

Munday AJ, Farrar RA (1989) MacMillan Education ltd 0-333-25829-0

Murai H, Takeda Y, Takano N, Ikeda K (2000) Halogen-free materials for PWB and advanced package substrate, The International Symposium and Exhibition on Advanced Packaging Materials Processes, Properties and Interfaces, Braselton, GA, USA: 221-226.

Hellen TK and Becker AA (2013) Finite Element Analysis for Engineers - A Primer, NAFEMS, ISBN 978-1-874376-98-9, 12.11 Elenent shapes and distorsions 241-244

National Physical Laboratory, Kaye and Laby, tables of physical and chemical constants http://www.kayelaby.npl.co.uk/general_physics/2_2/2_2_2.html, last checked 01/10/2014

Nguyen VL, Kim H-K (2015) Effect of Thermal Aging on the Mechanical Properties of Sn3.0Ag0.5Cu/Cu Solder Joints Under High Strain Rate Conditions, Journal of Electronic Materials 44 (7)

Nguyen TT, Yu D, Park SB (2011) Characterizing the Mechanical Properties of Actual SAC105, SAC305, and SAC405 Solder Joints by Digital Image Correlation, Journal of Electronic Materials **40** (6)

Norris KC, Landzberg AH (1969) Reliability of controlled collapse interconnections, IBM Journal of Research and Development **13** (3) 266–271, as cited by Dauksher [2008]

Nose H, Sakane M, Tsukada Y, Nishimura H (2003) Temperature and strain rate effects on tensile strength and inelastic constitutive relationship of Sn-Pb solders, Journal of electronic packaging, **125**: 59-66

Nottay J, Dusek M, Hunt C, Bailey C, Lu H (2001) Creep properties of SnAgCu solder in surface mount assemblies, National Physical Laboratory (NPL) report MATC(A)51

O'Donnell WJ (1960) The additional deflection of a cantilever due to the elasticity of the support' Transactions of the ASME journal of applied mechanics: 461-464

Pang JHL, Tan KH, Shi XQ and Wang ZP (2001) Microstructure and intermetallic growth effects on shear and fatigue strength of solder joints subjected to thermal cycling aging, Material Science and Engineering A **307**: 42-50

Pang JHL, Wang YP, Shi XQ, Wang ZP (1998) Sensitivity Study Of Temperature And Strain Rate Dependent Properties On Solder Joint Fatigue Life, 2nd Electronics Packaging Technology Conference, Singapore:184-189

Pang JHL, Xiong BS, Neo CC, Bang XR, Low TH (2003) Bulk Solder and Solder Joint Properties for Lead Free 95.5Sn-3.8Ag-0.7Cu Solder Alloy, 2003 Electronic Components and Technology Conference, IEEE

Pang JHL, Xiong BS, Low TH (2004) Creep and fatigue characterization of lead free 95.5Sn-3.8Ag-0.7Cu, 2004 Electronic Components and Technology Conference

Pang JHL, Xiong BS (2005) Mechanical Properties for 95.5Sn-3.8Ag-0.7Cu lead-free alloy', IEEE transactions on components and packaging technologies, IEEE Transactions on Components and Packaging Technologies, **28** (4)

Park J-Y, Kim C-U, Carper T, and Puligandla V (2003) Phase equilibria studies of Sn-Ag-Cu eutectic solder using differential cooling of Sn-3.8Ag-0.7Cu alloys, Journal of electronic materials, **32** (11)

Park S, Dhakal R, Lehman L, Cotts E (2007) Measurement of deformations in SnAgCu solder interconnects under in situ thermal loading, Acta Materialia **55**: 3253–3260

Park T-S and Lee S-B (2002) Isothermal Low Cycle Fatigue Tests of Sn/3.5Ag/0.75Cu and 63Sn/37Pb Solder Joints under Mixed-Mode Loading Cases, 2002 Electronic Components and Technology Conference, IEEE

Park T-S, Lee S-B (2005) Low cycle fatigue testing of ball grid array solder joints under mixed-mode loading conditions, Journal of electronic packaging, **127**: 237-244

Park T-S (2012) a personal communication

Puttlitz KJ, Stalter KA (2004) Handbook of lead-free solder technology for microelectronic assemblies, CRC press ISBN: 978-0-8247-4870-8

Qi Y, Ghorbani HR, Spelt JK (2006) Thermal Fatigue of SnPb and SAC Resistor Joints: Analysis of Stress-Strain as a Function of Cycle Parameters, IEEE Transactions on Advanced Packaging **29** (4)

Qin HB, Li WY, Zhou MB, Zhang XP (2014b) Low cycle fatigue performance of ball grid array structure Cu/Sn–3.0Ag–0.5Cu/Cu solder joints Microelectronics Reliability 54: 2911–2921

Qin HB, Zhang XP, Zhou MB, Li XP, Mai Y-W (2015) Geometry effect on mechanical performance and fracture behavior of micro-scale ball grid array structure Cu/Sn–3.0Ag–0.5Cu/Cu solder joints, Microelectronics Reliability xxx (2015) xxx–xxx, in press , corrected proof - note to users

Qin HB, Zhang XP, Zhou ZB, Zeng JB, Mai Y-W (2014a) Size and constraint effects on mechanical and fracture behavior of micro-scale Ni/Sn3.0Ag0.5Cu/Ni solder joints, Materials Science & Engineering A617: 14–23

Ratle A, Lagacé M, Pandelfellii V, Allaire C, Rigaud M (1996) A simple method for evaluating elastic modulus of refractories at high temperature, Journal of Canadian ceramic society **65** (3)

Ridout S, Dusek M, Bailey C, Hunt C, (2006) Assessing the performance of crack detection tests for solder joints, Microelectronics Reliability, **46** (12) 2122-2130

Rodgers B, Punch J, et al. (2004) Experimental and numerical evaluation of SnAgCu and SnPb Solders using a microBGA under accelerated temperature cycling conditions,

American Society of Mechanical Engineers, Electronic and Photonic Packaging **4**:153-159

(RoHS) Directive 2002/95/EC of the European Parliament and of the Council of 27 January 2003 on the restriction of the use of certain hazardous substances in electrical equipment

Rosenthal Y, Stern A, Cohen SR, Eliezer D (2010) Nanoindentation measurements and mechanical testing of as-soldered and aged Sn–0.7Cu lead-free miniature jointsMaterials Science and Engineering A 527: 4014–4020

Sabri MFM, Shnawah DA, Badruddin IA, Said SBM (2014) Effects of aging on Sn–1Ag–0.5Cu solder alloys containing 0.1 wt.% and 0.5 wt.% Al, Journal of Alloys and Compounds 582: 437–446

Schubert A, Dudek R, Auerswald E, Gollbardt A, Michel B, Reichl H (2003) Fatigue Life Models for SnAgCu and SnPb Solder Joints Evaluated by Experiments and Simulation, Proceeding of the 53rd electronic components and technology conference: 603–610

Selex-ES (2015) commercial product information gathered during the authors new role

Shi XQ, Pang HLJ, Zhou W and Wang ZP (1999) A modified energy-based low cycle fatigue model for eutectic solder alloy, Scripta Materialia **41** (3) 289-296

Shin SW and Yu J (2005) Creep deformation of Sn-3.5Ag-xCu and Sn-3.5Ag-xBi solder joints, Journal of Electronic Materials **34** (2) 188-195

Shirley DR, Ghorbani HR, Spelt JK (2008) Effect of primary creep and plasticity in the modelling of thermal fatigue of SnPb and SnAgCu solder joints, Microelectronics Reliability **48**: 455–470

Shirley DR and Spelt JK (2009a) Primary creep in Sn3.8Ag0.7Cu solder. Part I: theory, experiments, and data reduction' Jounal of Electronic materials, **38 (**11) 2376-2387

Shirley DR and Spelt JK (2009b) Primary creep in Sn-3.8Ag-0.7Cu solder, part II: constitutive creep model development and finite element analysis' Jounal of Electronic materials, **38** (11) 2388-2397

Shrotriya P, and Sottos NR (1998) Creep and relaxation behaviour of woven glass substrates for multilayer circuit board applications, Polymer Composites, **19** (5)

Schubert A, Dudek R, Auerswald E, Gollhardt A, Michel B, Reichl H (2003) Fatigue life models for SnAgCu and SnPb solder joints evaluated by experiments and simulation, 53rd Electronic Components and Technology Conference

Sidhu RS, Deng X, and Chawla N (2008) Microstructure characterization and creep behavior of Pb-free Sn-Rich solder alloys: Part II. creep behavior of bulk solder and solder/copper joints, Metallurgical and Materials Transactions **39A**: 349-362

Suhling JC, Johnson RW, White JD, Matthai KW, Knight RW (1994) Solder Joint Reliability of Surface Mount Chip Resistors/Capacitors on Insulated Metal Substrates, Proceedings 44th Electronic Components & Technology Conference, 465-473, 9. IEEE.

Sun P, Andersson C, Wei X, Cao L, Cheng Z, Liu J (2005) Low cycle fatigue testing and simulation of Sn-8Zn-3Bi and Sn-37Pb solder joints, Soldering and Surface Mount Technology **17** (4) 38-45

Sun CT, Li S (1988) Three dimensional effective elastic constants for thick laminates, Journal of Composite Materials **22**: 629-639

Sundelin J, Nurmib ST, Lepistö TO, Ristolainen EO (2006) Mechanical and microstructural properties of SnAgCu solder joints, Materials Science and Engineering, A 420: 55-62

Svetley A, University of Ausberg, personal communication (2014)

Tee TY, Ng HS, Yap D, Zhong Z (2003) Comprehensive board-level solder joint reliability modelling and testing of QFN and Power QFN packages, Microelectronics Reliability **43**: 1329–1338

Tsai M-Y, Hsu CHJ, Wang CTO (2004) Investigation of thermomechanical behaviors of flip chip BGA packages during manufacturing process and thermal cycling, Transactions on Components and Packaging Technologies 27 (3) 568-576

Ubachs RLJM, Schreurs PJG, Geers MGD (2007) Elasto-Viscoplastic nonlocal damage modelling of thermal fatigue in anisotropic lead-free solder Mechanics of materials **39** (7) 685-701

Vaynman S (1989) Effect of strain rate on fatigue of low-tin lead-base solder, 39th Electronic Components Conference, Houston, Texas, USA: 273-276.

Vianco P; and **J** Rejent (2002) Compression deformation response of 95.5Sn-3.9Ag-0.6Cu Solder, UCLA Lead-Free Workshop**,** as detailed by Lau *et al.* (2003)

Vianco PT, Rejent JA, Kilgo A (2003) Time-independent mechanical and physical properties of the ternary 95.5Sn-3.9Ag-0.6Cu solder, Journal of Electronic Materials, **32** (3) 142-151, Regular issue paper

Wang X-S, Jia S, Ren H-H, Pan P (2014) Effects of solder ball and arrays on the failure behaviours in package on package structure, Microelectronic Reliability **54**: 633-640

Wang X-S, Li X-D, Ren H-H, Zhao H-Y, Murai R (2011) SEM in situ study on high cycle fatigue of SnPb solder joint in the electronic packaging, microelectronic reliability **51**: 1377-1384 - nonBGA SEM imaging measurement of crack growth

Wang Q, Gail W, Johnson RW, Mechanical Properties and Microstructure Investigation of lead free solder, 2005

http://www.eng.auburn.edu/department/ee/leap/files/Mechanical_Properties_of_Lead_Free_Solder_Alloys.pdf, last checked 17/11/14.

(WEEE) Waste Electrical and Electronic equipment regulations, UK 2006 No.3289

Wickham M, Nottay J, Hunt C (2001) A review of mechanical test method standards for lead-free solders, NPL report MATC (A) 69

Wiese S, Roellig M, Mueller M, Wolter K-J (2008) The effect of downscaling the dimensions of solder interconnects on their creep properties Microelectronics Reliability 48: 843–850

Wiese S, Wolter K-J (2007) Creep of thermally aged SnAgCu-solder joints' Microelectronics reliability **47**: 223-232

Williams C, Tan KE, Pang JHL (2010) Thermal cycling fatigue analysis of SAC387 solder joints, 978-1-4244-5343-6/10 IEEE

Xiao Q, and Armstrong WD, (2005) Tensile creep and microstructural characterization of bulk Sn3.9Ag0.6Cu lead-free solder' Journal of electronic materials, **34** (2) 196-211

Xiaoyan N, Xuefeng S (2010) Characterization of the creep constitutive behavior of SnAgCu solder in flip-chip joints from the indentation creep testing, 11th international conference on Electronic Packaging Technology and High Density Packaging, Xidian University, Xi'an, China

Xie DJ, Wang ZP (1998) Process capability study and thermal fatigue life prediction of ceramic BGA solder joints, Finite Elements in Analysis and Design **30**: 31-45

Xu L, Tan KE, Pang JHL (2010) Intermediate strain rate dependant mechanical properties for lead-free solders, IEEE

Yaofeng S, Pang JHL (2007) Digital image correlation for solder joint fatigue reliability in microelectronic packages" microelectronics reliability

Young WC, Budynas RG. (2002) Roark's formulas for stress and strain, McGraw-Hill, 7th edition, [a] 153, [b]167

Zhang L, Han J-G, He C-W, Guo Y-H (2013) Reliability behavior of lead-free solder joints in electronic components, Journal of Material Science: Materials in Electronics 24: 172–190

Zhang L, Han J-G, Guo Y-H, Sun L (2014) Reliability of SnAgCu/SnAgCuCe solder joints with different heights for electronic packaging, Journal Material Science Mater Electron **25**: 4489–4494

Zhang Q, Dasgupta, Haswell P (2004) Partitioned viscoplastic-constitutive properties of the Pb-free Sn3.9Ag0.6Cu solder, Journal of Electronic materials, **33** (11) 1338 regular issue paper

Zhang QK, Zou HF, Zhang ZF (2009) Tensile and fatigue behaviors of aged Cu/Sn-4Ag Solder Joints, Journal of ELECTRONIC MATERIALS, **38** (6)

Zhang QK, Zhang ZF (2011) In situ observations on creep fatigue fracture behavior of Sn–4Ag/Cu solder joints, Acta Materialia 59: 6017–6028

Zhang Y, Cai Z, Mustafa M, Suhling JC, Lall P, Bozack MJ (2010) The influence of aging on the stress-strain and creep behaviour of SAC solder alloys; 12th IEEE intersociety conference on thermal and thermo-mechanical phenomena in electronic systems (ITherm)

Zhang Y, Zhu H, Fujiwara M, Xu J, Dao M (2013) Low temperature creep of SnPb and SnAgCu solder alloys and reliability prediction in electronic packaging modules, Scripta Materialia 68:607-610